NASA TECHNICAL NOTE

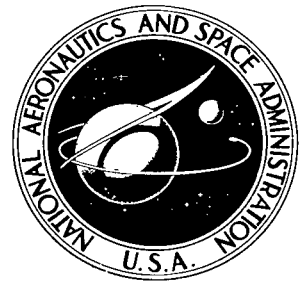

NASA TN D-6080

NASA TN D-6080

ACOUSTIC AND AERODYNAMIC PERFORMANCE OF A 6-FOOT-DIAMETER FAN FOR TURBOFAN ENGINES

II - Performance of QF-1 Fan in Nacelle Without Acoustic Suppression

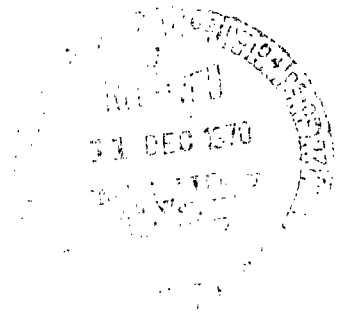

by Arthur W. Goldstein, James G. Lucas, and Joseph R. Balombin

Lewis Research Center
Cleveland, Ohio 44135

NATIONAL AERONAUTICS AND SPACE ADMINISTRATION • WASHINGTON, D. C. • NOVEMBER 1970

1. Report No. NASA TN D-6080	2. Government Accession No.	3. Rec
4. Title and Subtitle ACOUSTIC AND AERODYNAMIC PERFORMANCE OF A 6-FOOT-DIAMETER FAN FOP TURBOFAN ENGINES II - PERFORMANCE OF QF-1 FAN IN NACELLE WITHOUT ACOUSTIC SUPPRESSION		5. Report Date November 1970 6. Performing Organization Code
7. Author(s) Arthur W. Goldstein, James G. Lucas, and Joseph R. Balombin		8. Performing Organization Report No. E-5757
9. Performing Organization Name and Address Lewis Research Center National Aeronautics and Space Administration Cleveland, Ohio 44135		10. Work Unit No. 737-52 11. Contract or Grant No.
12. Sponsoring Agency Name and Address National Aeronautics and Space Administration Washington, D.C. 20546		13. Type of Report and Period Covered Technical Note 14. Sponsoring Agency Code
15. Supplementary Notes		

16. Abstract

This fan, designed for low-noise output, produced significantly less perceived noise at take-off and approach conditions than fans in current use. Measured broad-band noise varied with speed but not with aerodynamic blade loading. Multiple pure-tone noise was present at 80 percent of design speed and above and at 90 percent of design speed was strongly dependent on loading. Blade-passing tone noise contributed substantially to noise radiation in front of the fan, but very little rearwards. At 90 percent of design speed this noise component varied strongly with loading in a manner opposite to the loading variation of the multiple pure tones.

17. Key Words (Suggested by Author(s)) Fan acoustics Noise	18. Distribution Statement Unclassified - unlimited		
19. Security Classif. (of this report) Unclassified	20. Security Classif. (of this page) Unclassified	21. No. of Pages 91	22. Price* $3.00

*For sale by the Clearinghouse for Federal Scientific and Technical Information
Springfield, Virginia 22151

ACOUSTIC AND AERODYNAMIC PERFORMANCE OF A 6-FOOT-DIAMETER FAN FOR TURBOFAN ENGINES

II - PERFORMANCE OF QF-1 FAN IN NACELLE WITHOUT ACOUSTIC SUPPRESSION

by Arthur W. Goldstein, James G. Lucas, and Joseph R. Balombin

Lewis Research Center

SUMMARY

The QF-1 fan was designed to be representative of the high-bypass, low-noise fans to be considered for the NASA quiet-engine project. The tests were performed to determine its acoustic and related aerodynamic performance characteristics with no sound-absorption treatment on the internal flow surfaces.

The tests were made at speeds from 60 to 90 percent of design speed and at each speed the aerodynamic loading was varied by changing the exhaust nozzle area in three steps from 97 to 124 percent of design.

The calculated perceived noise levels for the fan alone were 100 and 99 perceived noise decibels (PNdB) at approach and take-off conditions, respectively. Both values were well below those for typical currently operating turbofan engines of equivalent cruise thrust and lower bypass ratio.

Spectrograms showed broad-band noise with superimposed blade passing tones and harmonics at all speeds, with the addition of multiple pure tones at speeds of 80 percent of design and higher.

Broad-band noise was about equal in the front and rear quadrants and was independent of aerodynamic loading of fan blades. Blade-passing tones were directed primarily frontwards at a level that was lower than the broad band there at speeds below 80 percent of design. Blade-passing noise in the front quadrant was approximately equal to the broad-band noise at speeds of 80 percent of design and higher. Multiple pure tones were much lower than other noise components except for fan operation at 90 percent of design speed with the 110 percent of design area exhaust nozzle with the short inlet cowl.

Broad-band noise correlated with rotor speed to the exponent 4.5 to 5.7. Blade-passing tone depended on rotor blade loading; at low speeds the speed correlation exponent was 8 to 9 with the smallest nozzle and 6.5 to 7 with the two larger nozzles.

INTRODUCTION

The QF-1 fan was built and tested at Lewis as part of the support program for the NASA Quiet Engine Project, the object of which is to build an experimental jet engine with 98 000-newton (22 000 lbf) thrust at take-off. Additional details of the project are given by McBride (ref. 1) and Kramer (ref. 2). The Quiet Engine is expected to produce less noise than turbojet engines because it is a high-bypass turbofan engine with a specially designed low-noise fan. Power for driving the fan is extracted from the core engine exhaust by a power turbine, thereby reducing the velocity of the core engine jet and making up the thrust by moving a large mass of relatively low-velocity air through the fan. A bypass ratio of five has been selected, and a goal of 15 to 20 PNdB less noise is expected to be achieved from the reduced noise generation and the sound suppression treatment to be applied to the engine nacelle.

The expected effect of the bypass fan on noise output was partially confirmed in a study by Marsh and McPike (ref. 3) by comparing the JT3C-6 turbojet and JT3D-1 turbofan engines of Pratt & Whitney. The study is not directly applicable to the Quiet Engine study because the JT3D-1 uses a two-stage fan with a comparatively low bypass ratio of 1.5 and because of the presence of inlet guide vanes for the fan. The fan engine achieved a much lower perceived noise level at full rated power, but its noise was dominated by the blade-passing tones of the fan. At low engine power, the fan tones resulted in comparable PNdB levels for the two engines. Another valuable contribution to the prediction of engine noise was a study of the noise output of the fan component and core engine compressor component of the turbofan engine made by Smith and House (ref. 5), who obtained correlations of experimental data of the noise of small fans and engine compressors. These correlations can be used to estimate engine noise.

The tests reported here also provide full-scale fan data to add to that of the Smith and House paper. The effects of blade loading and rotor speed are shown on the broadband noise and blade-passing tone, as well as on the multiple pure-tone system not considered by Smith and House.

The objective of the tests reported here is to provide detailed data on the far-field noise generated by the QF-1 alone as a full-scale component of a high bypass fan engine designed for subsonic transport. The present experiment will provide noise data uncontaminated by the noise from the core engine and the high-speed exhaust jet of the engine. The noise produced in the exhaust jet discharged by the fan cannot always be separated from that produced in the fan itself.

SYMBOLS

A	area
B	number of rotor blades
D	diffusion factor for constant radius, $1 - \frac{V_{out}}{V_{in}} + \frac{\Delta V_\theta}{2\sigma V_{in}}$
M	Mach number
m	number of periods distributed around axis for oscillation of gas in an annular duct
n	harmonic number of wake disturbance
P	pressure (static unless otherwise noted by subscript T)
s	integer used in acoustic analysis of stator-rotor interaction
T	temperature (static unless otherwise noted by subscript T)
U_p	rotational phase velocity
U_t	rotor rotational tip speed
V	velocity
V_c	velocity corrected to NACA sea-level standard atmospheric conditions
V_{in}	velocity of gas relative to blade row (at inlet)
V_{out}	velocity of gas relative to blade row (at exit)
ΔV_θ	change in gas rotational velocity, through a row of blades
v	number of stator vanes
W_c	weight flow, corrected to NACA sea-level standard atmospheric conditions
w	weighting factor
γ	ratio of specific heats
η	adiabatic temperature rise efficiency $\left[\left(\frac{P_{T,2}}{P_{T,0}}\right)^{(\gamma-1)/\gamma} - 1\right] \Big/ \left(\frac{T_{T,2}}{T_{T,0}} - 1\right)$
σ	solidity of blade row (ratio of blade chord to pitch spacing)

Subscripts:

i	particular pressure or temperature reading identification
S	NACA standard sea-level atmospheric condition
T	stagnation condition

0 axial station ahead of inlet bellmouth

1 axial station inside cowl for mass-flow measurement

2 axial station just downstream of stator vane row

3 axial station at exhaust nozzle discharge

APPARATUS AND DATA ACQUISITION

The test facility and fan are described in detail in part I (ref. 4) of this series of reports, but for convenience, some salient features will be noted here.

Fan Design

A cutaway view of the fan is shown in figure 1. The following table gives pertinent design values:

Rotor tip diameter, in.; m	71.81; 1.824
Rotor tip speed (cruise design corrected value), ft/sec; m/sec	1107; 337.4
Assumed shaft speed at takeoff, percent of design	90
Assumed shaft speed at approach, percent of design	60
Design pressure ratio of fan	1.50
Design corrected weight flow, lbm/sec; kg/sec	873; 396
Rotor hub to tip radius ratio (inflow face)	0.50
Axial spacing, rotor trailing edge to stator leading edge, in.; m	20; 0.51
Number of rotor blades	53
Rotor blade chord, in.; m	5.5; 0.140
Number of stator vanes	112
Stator blade chord, in.; m	2.69; 0.068
Stator blade hub radius, in.; m	20.07; 0.510
Stator blade tip radius, in.; m	33.97; 0.863

The corrected values of speed and weight flow referred to in the table are calculated on the basis of operation at NACA standard sea-level atmospheric conditions of P_S = 29.92 inches of 0° C mercury and $T_S = 59^\circ$ F with internal flow Mach numbers unchanged.

To provide a quiet fan, several features were incorporated into the design. Axial spacing between the rotor and stator was made large, so that rotor wakes would have enough distance to dissipate; noise generated by impact of the wakes on the stator blades

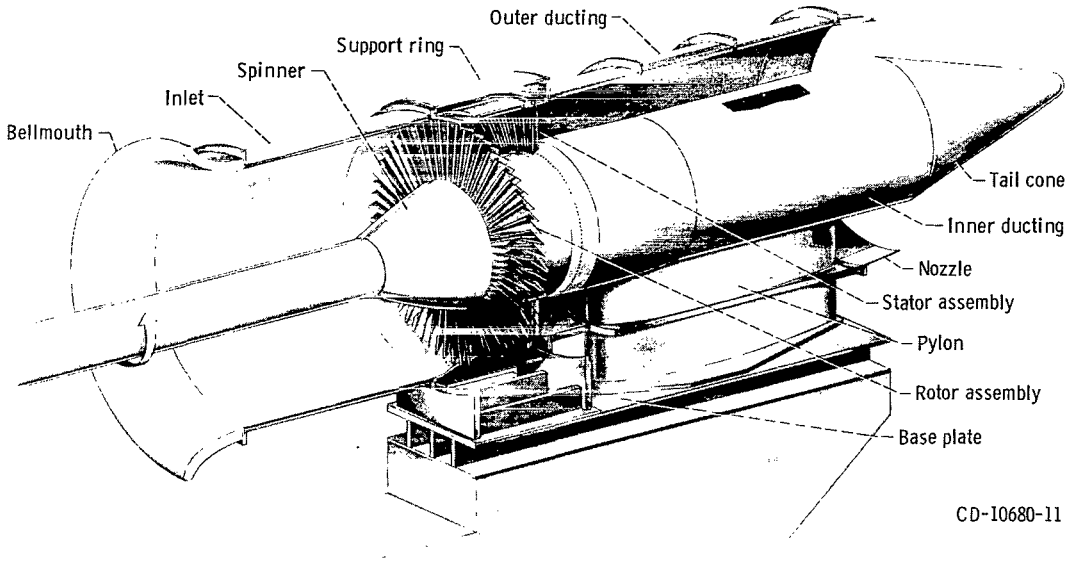

Figure 1. - Quiet fan nacelle assembly.

would thereby be reduced. In addition, the generation of broad-band noise by the rotor was to be substantially reduced by designing the fan for a minimum rotor speed; subsonic and low supersonic relative velocities would reduce the noise generated by shock waves. To reduce noise transmission in the ducting fore and aft of the fan, the number of stator blades was selected to obtain natural spinning modes of duct air oscillation, which, the theory indicated, would not propagate well in the duct. These modes are discussed by Tyler and Sofrin (ref. 6) and by Morfey (ref. 7) and Lowson (ref. 8). In the present case, the large axial spacing insures that the fundamental period (n = 1) of the wake disturbance predominates in the region near the leading edges of the stator blades. For the fundamental period of stator reaction (s = -1), the number of periods m of the interaction mode distributed around the shaft is

$$m = nB + sv = -59$$

where B is the number of rotor blades and v number of stator vanes.

The rotational phase velocity of the mode U_p is

$$U_p = \frac{nB}{m} U_t = -\frac{53}{59} U_t$$

where U_t is the rotor tip speed. For the take-off condition (the highest speed tested)

$$U_{t(\text{take-off})} = 0.9\, U_{t(\text{design})}$$

where

$$U_{t(\text{design})} \sim \text{sonic speed}$$

Therefore, the phase velocity is 0.8 of the sonic speed and is below cutoff speed. The theory shows that the interaction noise will not propagate. Also, the pressure pattern on the rotor rotating at 0.9 of sonic speed will not propagate in the duct either.

The operating condition of the fan could be altered by changing the exhaust nozzle area. Three nozzle areas were available: one of 1895 square inches (1.22 m^2) or 97 percent of the design area, one of 110 percent of the design area, and one of the 124 percent of design area. Also tested were a short inlet cowl measuring 86 inches (2.18 m) from the rotor face to the cowl front face and a long one of 127 inches (3.23 m) length. Variation of nozzle discharge area permitted changing the fan airflow and pressure ratio (blade loading) at a fixed speed. The long cowl was made available to increase the amount of acoustic treatment. These cowls differed only in the length of the cylindrical sections, and data reported here are for untreated cowls.

Test Facility

The fan was mounted on the end of a concrete viaduct with the shaft centerline 19 feet (5.79 m) above the grade level. It was driven from the air intake end by a shaft connecting the fan and stepup gear box which, in turn, was driven by a shaft to the drive motors of the 10- by 10-Foot Supersonic Wind Tunnel (see fig. 2). The distance of the front end of the fan rotor from the building was 47 feet (14.33 m). The wall of the motor building was covered with sound absorbing material and was shown by tests to reduce reflections to an adequately low level for frequencies above 500 hertz.

The microphones were placed on poles at the same elevation as the fan shaft on an arc 100 feet (30.5 m) from the face of the fan rotor if the building did not interfere;

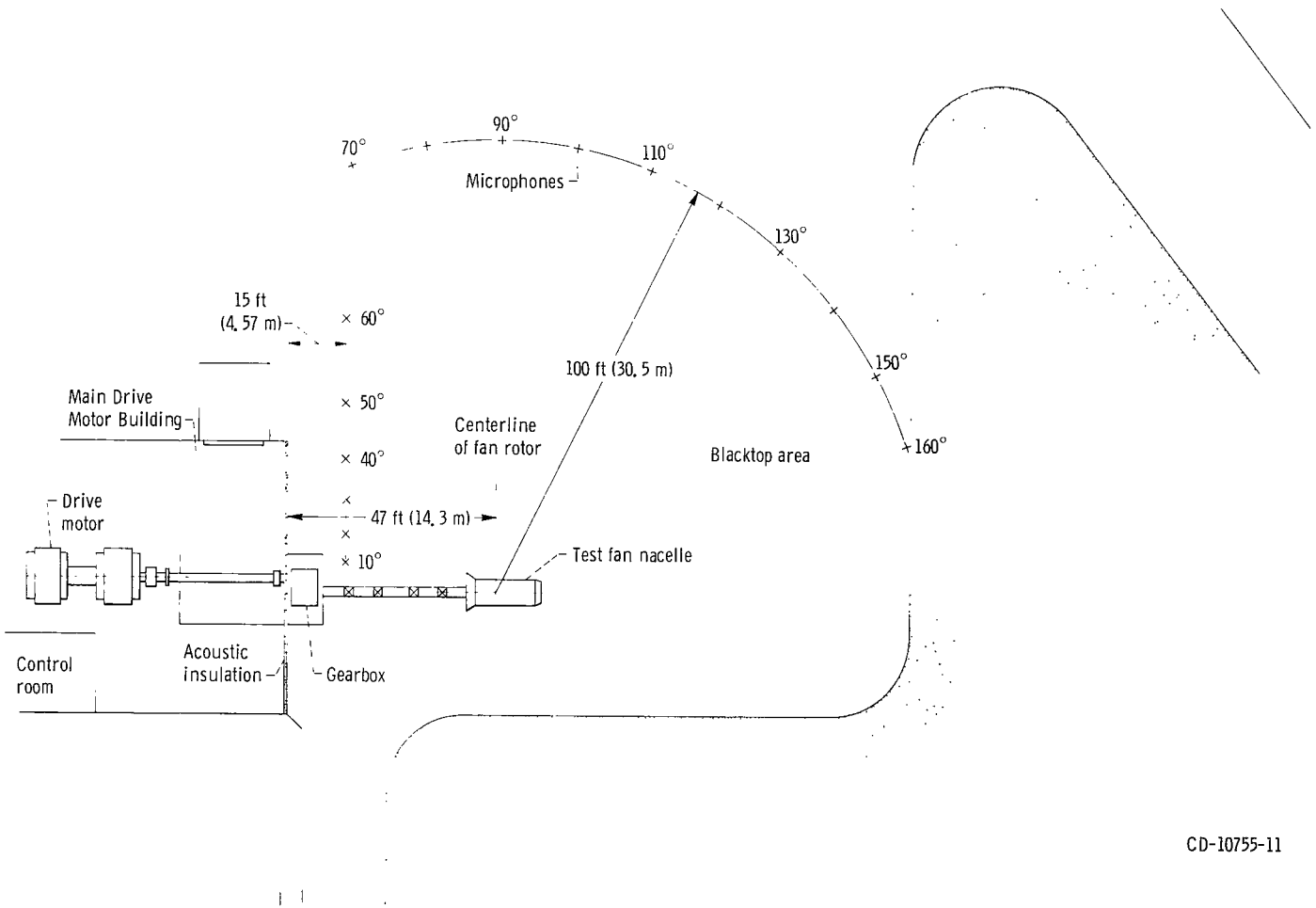

Figure 2. - Plan view of quiet fan facility area with microphone locations. Microphones at fan shaft elevation, 19 feet (5.8 m) above ground. (Scale: 1 in. = 20 ft; 1 cm = 2.4 m).

otherwise, microphones were placed 15 feet (4.6 m) from the building wall). The array of microphones was centered at the rotor face and placed at 10^{o} intervals from 10^{o} to 160^{o}, measured from the shaft centerline (see fig. 2).

Aerodynamic Measurements

Measurements of aerodynamic characteristics of the fan were performed by the following instrumentation:

Station (0): In front of the cowl, four thermocouples measure the ambient temperature, T_{T0}.

Station (1): Inside the cowl, 18 inches (0.46 m) into the cylindrical section, six wall taps, at uniform circumferential intervals, measure static pressure P_1. This pressure was used with the ambient pressure to calculate corrected mass flow. The location was selected as a result of previous calculations that indicated a uniform flow distribution there.

Station (2): About 13 inches (0.33 m) downstream of the discharge stator ring, four rakes with nine thermocouples and 10 total-pressure tubes each were used in conjunction with six static-pressure wall taps to find the state of the gas discharged from the fan.

Other rakes were set into the entrance to the exhaust nozzle and the nozzle discharge to measure the internal drag effects of the acoustic treatment when that is installed.

Data at station (2) were mass averaged by means of the equations

$$P_{T,av} = \frac{\sum_i P_{T,i} w_i}{\sum w_i}$$

$$T_{T,av} = \frac{\sum_i T_{T,i} w_i}{\sum w_i}$$

$$w_i = A_i \sqrt{\frac{P_i (P_{T,i} - P_i)}{T_i}}$$

where w_i is the weighting factor of the reading and is proportional to local flow rate, the subscript i identifies the particular reading, and A_i is the area element in which each sensor is centered.

Shaft speeds were held to within 0.2 percent of the desired value. The standard deviation, calculated from repeated measurements of the pressure, was found to be about 1/2 percent. The pressure rise ratio is the pressure ratio minus 1.0:

$$\frac{P_{T,2} - P_{T,1}}{P_{T,1}} = \frac{P_{T,2}}{P_{T,1}} - 1$$

The efficiency is approximately proportional to the pressure rise ratio for pressure ratios in the range of our tests. For a low pressure rise, the pressure ratio error would cause an undesirably large error in the efficiency. For sufficiently high pressure rises, an average of three data points would give acceptable errors within ±2 percent.

Weight flows measured at the entrance (station 1) and fan discharge (station 2) showed discrepancies mostly within 1 percent; a few were as high as 3 percent. The flow conditions at station 2 were nonuniform and therefore less reliable for weight-flow measurements than station 1, where the measured static pressures at the cowl were very uniform. Temperatures were obtained with adequate accuracy for determination of sonic speeds, but they were inadequate for determining the efficiency. At the take-off condition, the air passing through the fan experiences a temperature rise of about 57 F^O (32 C^O) and, at fan speed for approach, a rise of about 25 F^O (14 C^O). During the entire course of the tests, the problem of obtaining temperatures to within an adequately small fraction of these temperature rises was not solved. Therefore, no efficiency data are presented in this report.

Acoustic Measurements

Acoustic data were obtained by omnidirectional microphones in locations previously described. Data were recorded on multichannel tape recorders. Microphones and tape recorders were calibrated at the beginning of each day. From the tapes 1/3 octave bandpass data of sound pressure levels were prepared for each microphone and from which overall power levels and perceived noise levels were computed. Analysis of selected microphone outputs were obtained with continuous narrow-band analyzers.

Data acquisition was limited to periods when wind velocity was less than 10 knots (5.1 m/sec) with the exception of data obtained in the configuration of the long cowl and 124-percent exhaust nozzle area, when 13-knot (6.7-m/sec) gusts occurred. During the course of operation, substantial fluctuations in sound level could be heard. Such variations are illustrated in figure 3 which shows a strip chart trace of the overall sound pressure level of a single microphone as a function of time. This signal is, of course, heavily conditioned by the dynamics of the pen, but the large fluctuations of 8.5 decibels

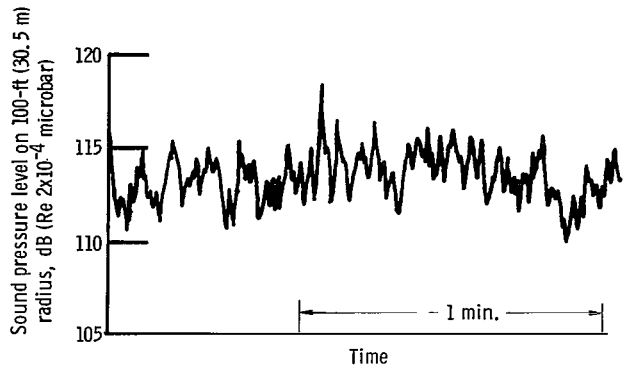

Figure 3. - Sample variation with time of overall sound pressure level of one microphone.

indicate that an accurate average can be obtained only by continuing the averaging process over an ample time period. The acoustic data analysis equipment used had a time constant of about 1/2 second. Figure 3 indicates that a longer time constant would have been desirable to provide more reliable and repeatible average readings.

Error estimates. - In order to judge the adequacy of the present system and the accuracy of the time averaged sound meter readings, data obtained at different times under equivalent fan operating conditions may be compared. Three different, but comparable, data samples were obtained in the normal course of data acquisition. An estimate of the error may be found on the following manner. From the data of three observations of any single microphone and single 1/3 octave band, an average may be found. From the three samples and their average, a sound pressure level deviation may be found for each sample. A standard deviation prepared from only three samples will not be reliable, but if one assumes that all the microphones will record similar random fluctuation of output with time, then one may form the standard deviation for all the microphones and for each frequency band by averaging the squared deviations. Some trend was seen for the average standard deviation to depend on frequency, but the higher deviations at low frequencies have little importance because of the low sound level at low frequency for most of the data. These were therefore averaged in with the remainder of the data, which they affected only slightly. The overall average for the standard deviation of a population of single readings was then found to be about 1.4 decibels. For a population of three-sample averages, the standard deviation was then found by dividing by the square root of 3; the value is 0.8 decibel. If one assumes a normal population, the probable error of a single three-sample average is about 0.6 decibel, and one three-sample average in 20 will be in error by as much as 1.7 decibels. Three-sample averages only are used in this report.

Operation. - Because three samples of the acoustic data were obtained for each operating state, the aerodynamic data were also acquired three times. The operational

procedure was to take a single set of data at each desired speed, in sequence, starting at the lowest speed and increasing to the highest. Then, two data samples were then taken at each speed as the speed was lowered from the highest to the lowest value. The discharge nozzle was then changed and, on another day, data were obtained with the new nozzle. The three different nozzles used altered the fan air flow and pressure ratio, thereby permitting the noise to be obtained under different conditions of aerodynamic loading of the fan blading. Two different inlet cowl lengths were used so that six fan configurations in all were tested.

RESULTS

Aerodynamic Characteristics of Fan

Because the QF-1 fan is a possible candidate for the Quiet Engine, its aerodynamic characteristics are of interest; they are also related to the acoustic performance of the fan. Figure 4 displays the fan pressure ratio $P_{T,2}/P_{T,0}$ as a function of the corrected weight flow W_c for various fixed values of the corrected shaft speed. (The data for the 100 percent of design area nozzle with the short inlet cowl are not shown; these data were obtained, but were discarded because of errors in some of the recorded values.)

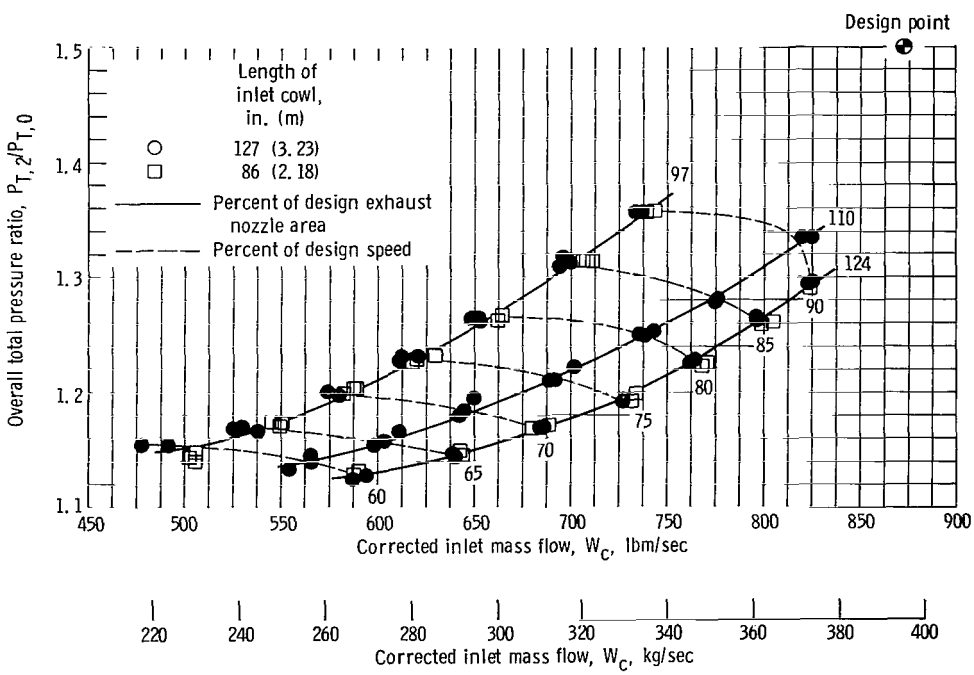

Figure 4. - Fan overall aerodynamic performance characteristics.

The range of speeds is from 60 percent of design value (assumed approach speed) to 90 percent of design value (assumed take-off speed).

It was mentioned previously, that the efficiency of the fan is not presented because of the unsatisfactory accuracy of the air temperature rise data. An estimate of the actual efficiency of the fan may be made according to the following procedure: The expected efficiency η at design speed was 85 percent, with a pressure ratio of 1.5 (ref. 4). The expected temperature rise ratio at design speed is

$$\frac{T_{T,2} - T_{T,0}}{T_{T,0}} = 0.145$$

If one assumes that the fan will develop approximately the expected rise in stagnation temperature and that this rise varies as the square of the rotor speed, then at 90 percent of design speed the temperature rise ratio is

$$(0.9)^2 \times 0.145 = 0.1175$$

From this estimate of temperature rise ratio and the measured pressure ratio of 1.355 at the 90 percent speed condition (fig. 4), the efficiency is estimated as 77 percent.

Low efficiency generally signifies separated flows, with broad wakes and high turbulence levels. The impact of rotor wakes on stator blades and the turbulence will give rise to noise. One may therefore expect a reduced noise level from a more efficient fan. Aside from the condition at the very innermost radius of the stator blades, the diffusion factors D at design conditions are all less than 0.53. These values are not excessive according to usual practice. The low efficiency indicates a need for reevaluation of the design technique to provide more reliable loss predictions for this type of design. It is not necessary that a fan such as this one shall incur high losses. There is a very similar NASA fan (ref. 9) which develops a stage efficiency of 88 percent at 90 percent speed; it is designed for a pressure ratio of 1.5 at a tip speed of 1000 feet per second (305 m/sec), has an inflow hub to tip radius ratio of 0.4, and has a rotor blade aspect ratio of 1.9 as compared with the value of 3.5 for the present rotor. It is not presently known what is the cause of the large difference in efficiency between the two fans.

The effect of the longer inlet cowl on the overall pressure ratio, as compared with the shorter, is negligible, but there appears to be a slight consistent reduction in the mass flow as compared with the shorter inlet. This is probably a displacement effect of the thicker boundary layer.

The weight flow is rather close to the value estimated from the design process. At 90 percent of design speed the predicted value is 90 percent of the design value of 873

pounds per second (396 kg/sec), namely, 787 pounds per second (356 kg/sec). The ratio of weight flow at 90 percent speed to the estimated value is shown for the various exhaust nozzles:

Nozzle area ratio, percent	Airflow ratio, percent
97	94
110	104
124	105

These figures indicate that a discharge nozzle with some intermediate area ratio will produce the desired flow. At design speed, choking of the flow between the rotor blades rather than the discharge nozzle may provide a more severe upper limit to the flow.

Noise generation in the fan depends on internal aerodynamics, several aerodynamic parameters are therefore plotted that have a bearing on the noise output. Figure 5 shows the velocity of the gas, relative to the rotor, just upstream of the blades at two

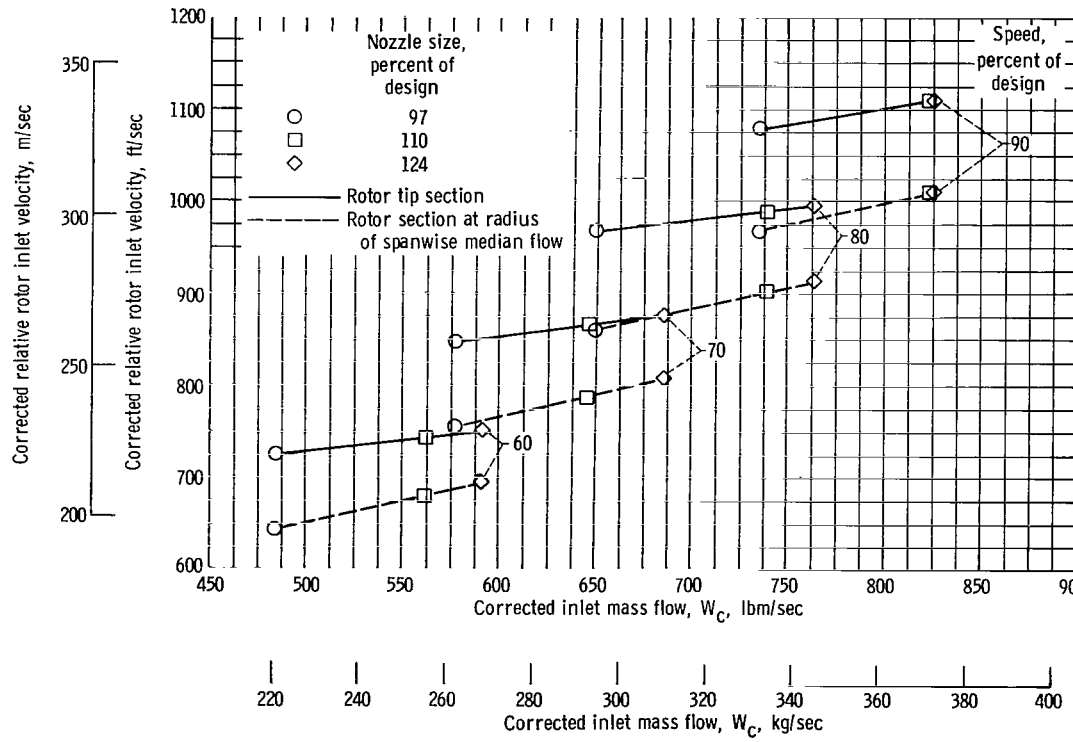

Figure 5. - Rotor inlet relative velocity over fan operating range. Design point radial distribution of flow assumed fixed over full range.

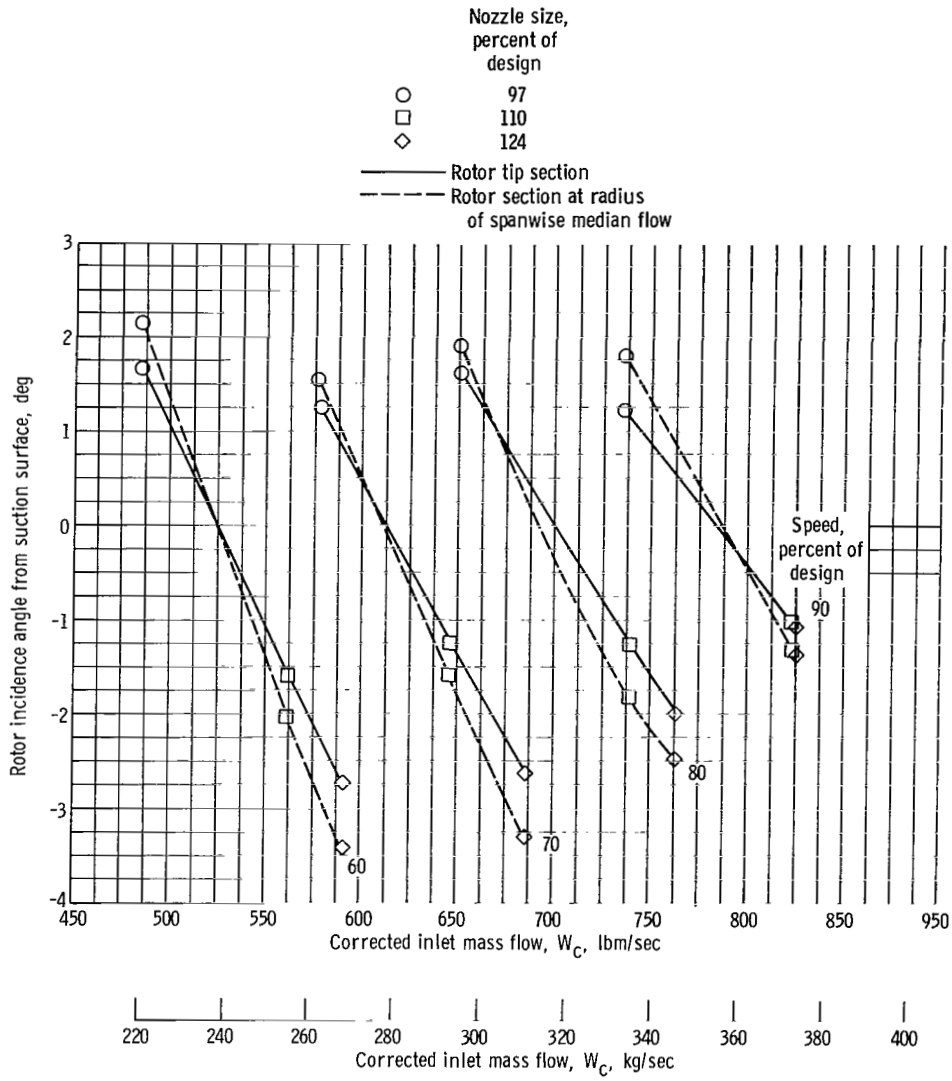

Figure 6. - Rotor incidence angle variation over fan operating range. Design point radial distribution of flow assumed fixed over full range.

radial stations: one station at the very tip of the blade and the other at the radius which divides the flow equally into an inner and outer flow. Figure 6 shows the corresponding incidence angles. These results were obtained from the measured weight flows that were used to scale the calculated axial velocity distribution at the design condition. The important region of noise radiation from the rotor blades is between those two radial positions.

The nozzle discharge velocity is important in determining the fan jet noise. This is

shown in figure 7 for various operating conditions of the fan with the long inlet. The values are given corrected to standard atmospheric conditions; that is,

$$V_{c,3} = \frac{V_3}{\sqrt{\frac{T_0}{T_S}}} = 1116\ M_3 \frac{\sqrt{\frac{T_{T,3}}{T_0}}}{\sqrt{1 + \frac{\gamma - 1}{2} M_3^2}}$$

Values of M_3 were determined from the total pressures and static pressures measured at station 3.

Acoustic Data

The noise picked up by the instrumentation is modified somewhat by the testing facility. Reflection from the building has some effect below 400 to 500 hertz (ref. 4),

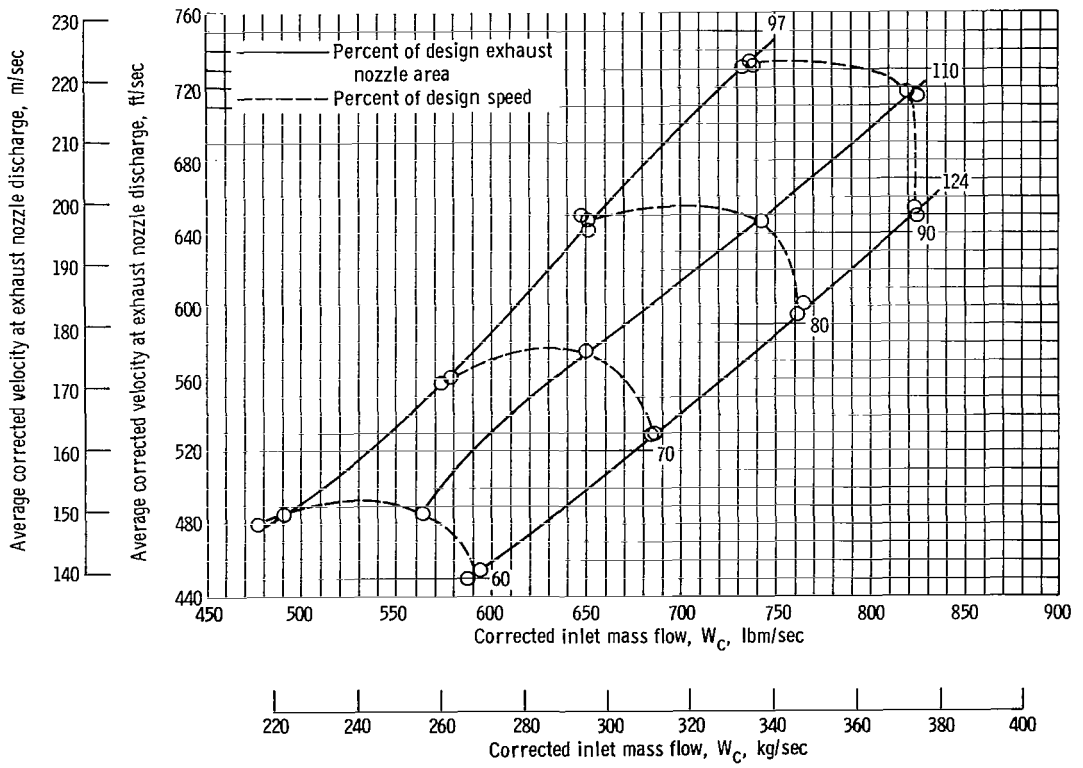

Figure 7. - Average fan exhaust nozzle discharge velocity with 127-inch (3.23-m) inlet cowl length.

and ground reflection has an unknown effect. An additional effect results from a slightly nonuniform inflow condition described in detail in reference 4. A survey was made of the total pressure distribution in the inlet, and there was found a maximum discrepancy of 2 percent of the dynamic pressure when the short cowl was mounted and 5 percent with the long. The extent of this pressure depression was not accurately determined, but it is less than 4 inches (0.10 m) wide and 9 inches (0.25 m) high. This low-energy region was clearly displayed when a vortex of condensing water vapor was observed. The vortex was anchored on the viaduct supporting the fan and extended along the bottom of the inlet cowl toward the fan. It is possible that because of the effect of this vortex, the rotor may have generated a substantial tone at the blade-passing frequency.

One-third octave band data. - The spectrum of the noise radiation intensity of each fan configuration is displayed in figures 17 to 22 (bound at back) for each microphone position and selected fan speed for 1/3 octave bands. The 1/3-octave-band spectrum of the acoustic power for each configuration and speed is shown in figure 23 (also at the back). All data are corrected for atmospheric attenuation by the SAE method (ref. 10) and to a distance of 100 feet (30.5 m) from the center of the fan face.

The question of the relative magnitudes of the noise radiated from the fan and that from the fan jet noise calculation proposed by the SAE (ref. 11) was applied to the data of figure 7 but was modified by extrapolation of the noise curve to velocities below 1000 feet per second (0.305 m/sec). This conservative estimate of the noise level provided very large overestimates of the low-frequency jet noise as compared with measured values. Maximum spectral output would have occurred at 37 hertz for the 90-percent speed operation, but this characteristic spectral distribution is not evident in the experimental spectra. Those spectra obtained close to the jet axis (angles of 140°, 150°, and 160°) indicate a maximum output at about 120 hertz, which corresponds to a Strouhal number of 0.65. This value differs widely from that for a circular jet because of the annular shape of the nozzle. There is no indication of this type of spectrum from the microphones located from 10° to 130°. The high level of low-frequency broad-band noise component is picked up only at the microphones located at 140°, 150°, and 160°. These three microphones cover about 15 percent of the total radiation area and therefore have only a slight influence on the measurement of the power level of the broad-band fan noise.

There is present in all of these 1/3 octave spectra, a strong tone of the blade-passing frequency, which is 53 (number of rotor blades) times the shaft rotational rate. The tone at twice the blade-passing frequency is also evident at all the speeds. At 80 percent of design speed there is a slight energy concentration in a band centered near half the blade-passing frequency; at 90 percent of design speed there is apparent a large energy content in this band from 1250 to 1600 hertz. This spectrum characteristic is accompanied by an audible change in the character of the noise, in that the fan begins to sound like a circular saw cutting lumber. This sound is typical of the multiple pure

tones which are known to occur with supersonic fans. (See Ehrich, ref. 12.) It is when this fan achieves local supersonic flow on a region of the rotor blades that this noise becomes evident. This fan is designed with a 1.45 maximum relative Mach number on the blade surface; the corresponding Mach number is 1.3 at 90 percent speed and 1.16 at 80 percent speed. (Corresponding relative approach Mach numbers are 1.12, 1.01, and 0.90.) This correlation of relative velocity and multiple pure tones shows that such tones can arise as a consequence of a supersonic flow phenomenon in the fan, rather than supersonic rotor speed as deduced by Ehrich (ref. 12) and as described by Kester and Slaiby (ref. 13).

Narrow-band data. - The output of the microphone at the 40° location was analyzed with a continuous narrow-band analyzer of 10-cycle bandwidth under several operating conditions; these spectra are displayed in figure 8. They show clearly the blade passing frequency tone which has a broad structure, indicating an unsteady generation process which produces a range of frequencies. The random fluctuations are also shown in the irregularities of the broad-band noise spectra. The double frequency tone and sometimes the triple are discernible, but most of the energy is in the fundamental and the first harmonic.

In the sequence of figures 8(a) to (c), the fan speed is increased. At the 80 percent speed a cluster of multiple pure tones may be seen first, and it develops into a major noise component at 90 percent of design speed. The individual tones differ in frequency by integral multiples of the shaft speed. Some of these tones may be seen near the blade-passing frequency and at higher frequencies, but practically all the energy is concentrated in the subharmonic region, which shows up in the 1/3-octave band data as a subharmonic maximum. A rough estimate of the energy involved in these multiple pure tones may be obtained by consideration of the extension of this protuberance above the local broad-band level.

The effect of blade loading on the multiple pure tones is demonstrated in figures 8(c) to (e). The greatest output of multiple pure tones is with the 110 percent nozzle; the 124 and the 97 percent exhaust nozzles cause the fan to produce a small amount of multiple pure-tone noise.

Resolution of noise components. - The fan noise output was subdivided into three components by processing the 1/3-octave band spectra: (1) blade-passing tone and its harmonics, (2) broad-band noise, and (3) multiple pure tones. A broad-band noise base or substratum was faired below each maximum resulting from a blade-passing tone or its harmonic, and the maximum was corrected for the broad-band base level to obtain the amplitude of the blade-passing tone alone. A similar procedure was applied to the subharmonic maximum which represented the combination cluster of multiple pure tones. The remainder, after subtraction of these two components from the overall noise, was designated as the broad-band noise. The present procedure of calculating the level of

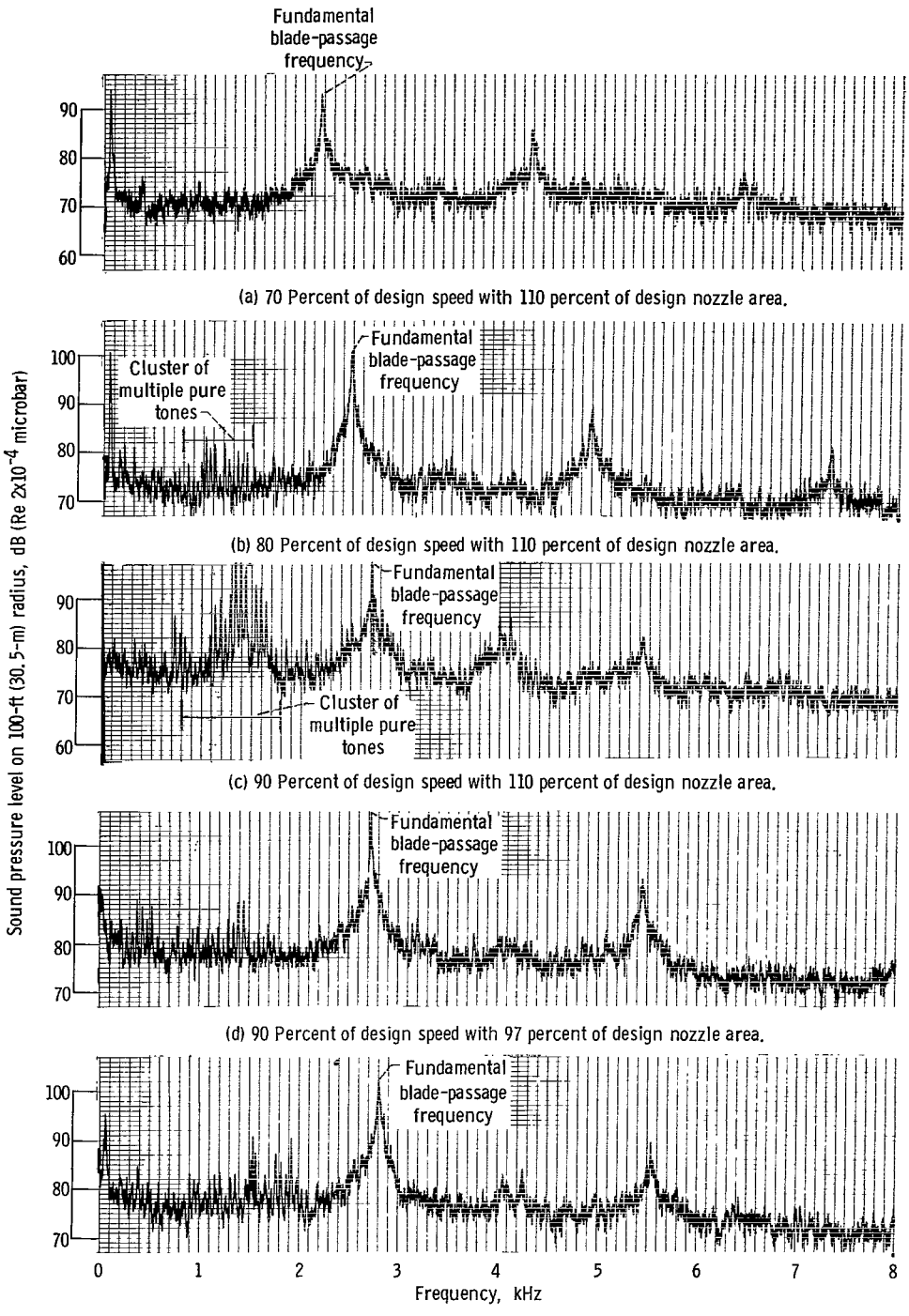

Figure 8. - Ten-Hertz constant band width spectrum of sound pressure level at 40° from inlet of fan with 86-inch (2.18-m) inlet cowl length.

multiple pure-tone noise is believed to provide a rough but adequate level of accuracy for the application.

Blade-passing frequency tones. - Amplitude of the blade-passing frequency tone and its harmonics is shown in figure 9 as a function of angular position. All the sound pressure level distributions of the blade-passing frequency noise have maxima in the front region and relatively low values near the rear axis. This distribution is typical with the 97 and 124 percent exhaust nozzles for all operating speeds.

The circumstances of the noise radiation suggest that this noise is radiated from the forward-facing portion of the rotor blades rather than the rear part or from the stator by the following considerations: The rotor is of high solidity (ratio of blade chord to spacing) with a value of 1.34 at the tip and 2.57 at the root. Thus, any noise radiating upstream from the stator must interact with the rotor blades before passing upstream and out of the front end of the fan. Since this noise is reradiated from the rotor, it must propagate in the relative velocity field rather than in the absolute velocity field. The internal flow is such that, for operation at 90 percent of design speed, the channels between the blades of the rotor have a flow that is very close to choking over most of the blade span. The blades are formed from multiple circular arc sections with a suction surface curvature that increases the relative velocity flowing into the interblade channel to a value greater than the upstream value. At 90 percent speed this channel entrance average Mach number is 1.16 at the blade tip and is supersonic over the outer two-thirds of the blade span - a region that carries 85 percent of the mass flow. Such a flow condition in the rotor flow channels will reflect forward-progressing sonic disturbances downstream again, and most of the noise originating on the stator or the aft sections of the rotor blades should show up in the aft quadrant of the field. This blockage of the forward propagation by inlet guide vanes was shown by Chestnutt and Crigler (ref. 14). The data at 90 percent design speed with the 97 and 124 percent of design area nozzles show the opposite distribution - most of the blade-passing frequency noise is radiated forward - which implies that the origin of this noise is in the forward part of the rotor blades. For operation with the 110 percent of design area nozzle, there is a lower level of blade-passing tone noise in the front at 80 and 90 percent of the design speed than with the other nozzles and a reduction in front-end radiation relative to rearward at 90 percent speed. Since this noise is believed to have been generated on the rotor, the local aerodynamic conditions at the rotor might account for this change. Figure 6 shows that the computed angle of incidence is the same for the 110 and 124 percent of design area nozzle at 90 percent of design speed. Hence, some other aerodynamic factor must account for the differences in generation of the blade-passing tone in this fan.

Comparison of the measured blade-passing tone noise with the values estimated by the method of Smith and House (ref. 5) was made by converting the data from the 40° and 110° locations (locations for peak sideline values) to 100-foot (30.5 m) sideline values. The input data were a relative velocity of 1105 feet per second (337 m/sec) at the blade

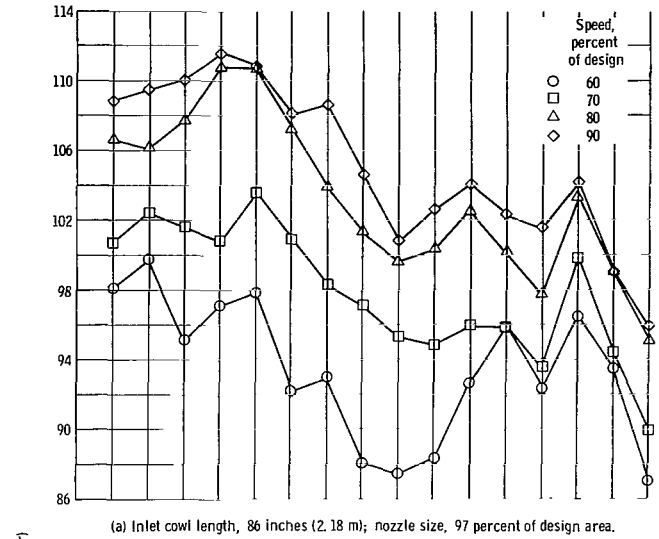

(a) Inlet cowl length, 86 inches (2.18 m); nozzle size, 97 percent of design area.

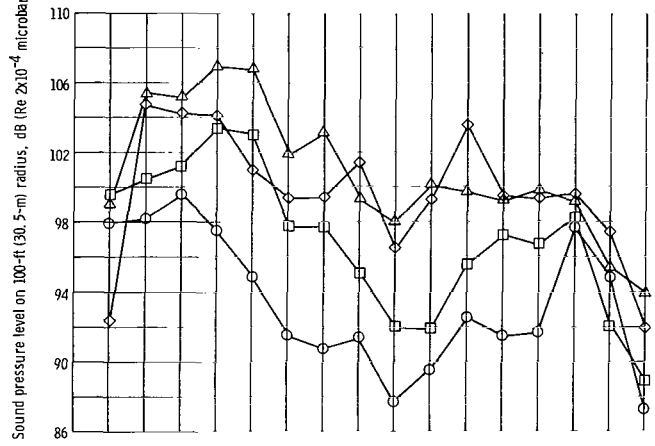

(b) Inlet cowl length, 86 inches (2.18 m); nozzle size, 110 percent of design area.

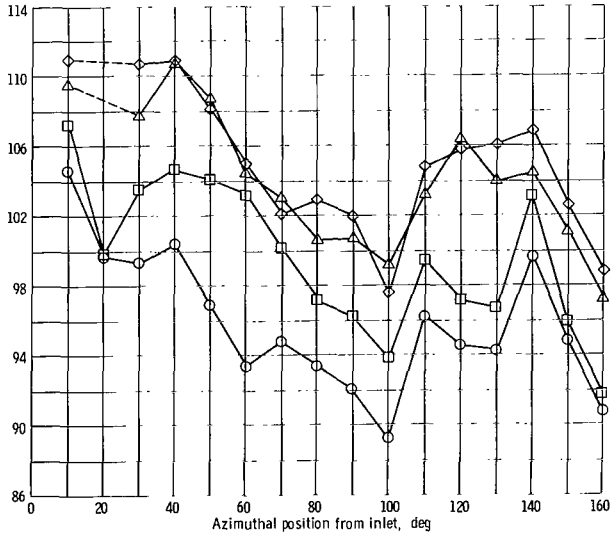

(c) Inlet cowl length, 86 inches (2.18 m); nozzle size, 124 percent of design area.

Figure 9. - Azimuthal distribution of discrete tones on 100-foot (30.5-m) radius.

tips when the fan is operating at 90 percent of design speed, a mass flow of 820 pounds per second (372 kg/sec), an axial chord at the tip of 3.3 inches (0.084 m), a rotor-stator spacing of 20 inches (0.51 m), and a radius ratio of 0.5. Comparison with results for the short cowl configurations are shown in the following table:

Type of data	Nozzle size, percent of design	Microphone location, deg	
		40	110
		Blade passing tone noise, dB	
Calculated	--	90.5	103.5
Experimental	97	107.8	103.5
	110	100.2	103.0
	124	107.0	104.4

The accuracy of the prediction for the rear quadrant indicates that this noise probably originates in the same aerodynamic processes as the noise upon which the correlation of Smith and House is based; the front quadrant noise is probably of different origin. The mere fact that most of the sound appears in the front disagrees with the calculation scheme. It seems possible, in view of the large spacing (20 in.; 0.51 m), that the noise does not depend on blade row interaction but results, instead, from rotor reaction to the nonuniform inflow described previously. (The interaction noise should not propagate in any case because the rotative speed is much lower than sonic velocity.) Noise from such a source would propagate freely through the duct as a nonrotating wave. Therefore, the large blade-passing frequency tone propagated forward from the fan does not contradict the Tyler and Sofrin (ref. 6) theory of spiralling waves which predicts suppression of the interaction tones and also tones originating in the rotor's rotating pressure field.

Broad-band noise. - Angular distribution of broad-band noise is displayed in figure 10. Here, the increase of amplitude with speed is fairly uniform; the angular distribution is similar for the various speeds and shows an angular variation of from 5 to 8 decibels. There is no consistent trend in the effect of blade loading on broad-band noise output.

Comparison is shown in the following table of the measured broad-band sound pressure level and the estimates of Smith and House (ref. 5). The measured data were for 90 percent speed values taken at the 50° and 120° locations (locations for peak sideline values) and corrected to 100-foot (30.5-m) sideline values. The Smith and House estimates were modified from the peak 1/3-octave level to overall spectrum level using the typical spectrum of reference 5.

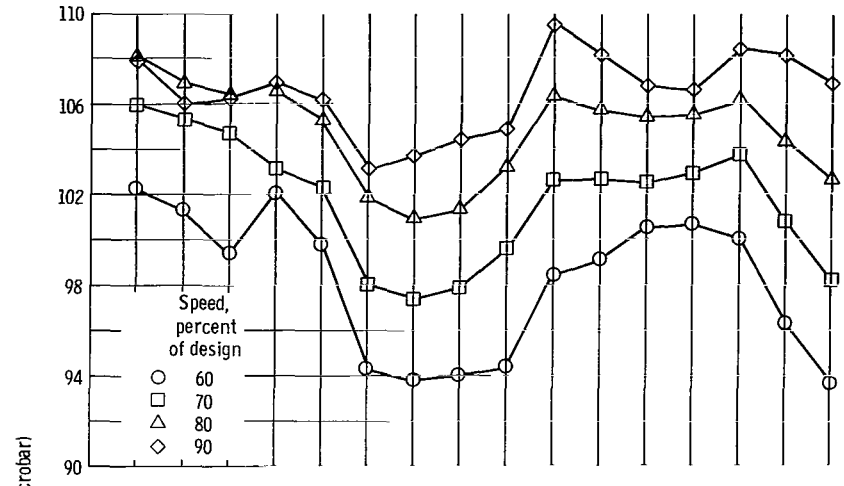

(a) Inlet cowl length, 86 inches (21.8 m); nozzle size, 97 percent of design area.

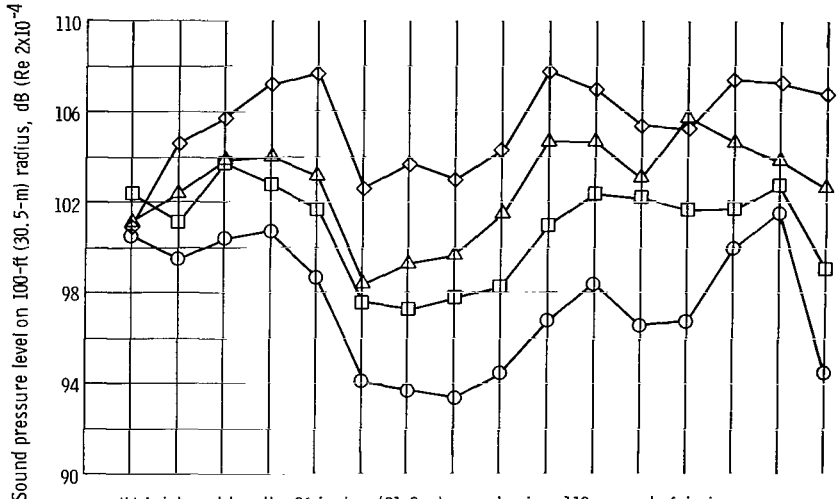

(b) Inlet cowl length, 86 inches (21.8 m); nozzle size, 110 percent of design area.

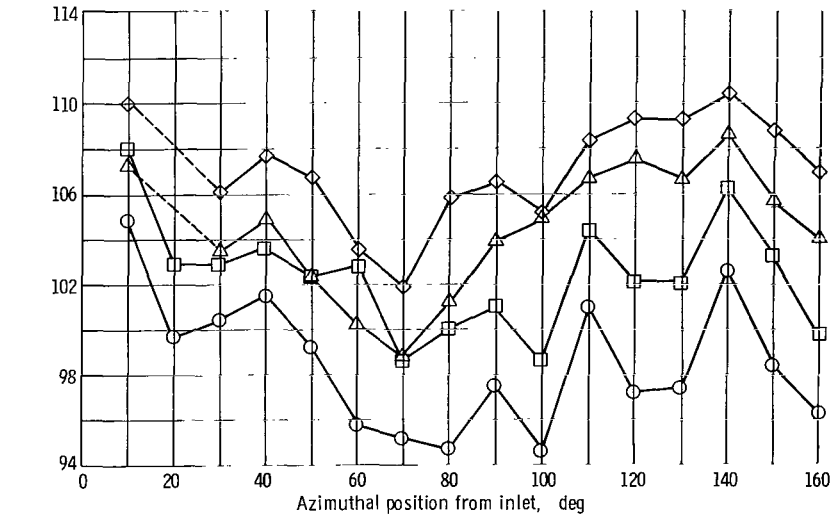

(c) Inlet cowl length, 86 inches (2.18 m); nozzle size, 124 percent of design area.

Figure 10. - Azimuthal distribution of broad-band noise on 100-foot (30.5-m) radius.

Type of data	Nozzle size, percent of design	Microphone location, deg	
		50	120
		Broad-band sideline sound pressure level, dB	
Estimated	--	103.9	116.9
Experimental	97	103.9	105.6
	110	105.3	104.2
	124	104.4	108.1

The method appears adequate for the estimation of the front quadrant broad-band noise, but it overestimates the rear quadrant noise. Actually, the reliability of the front quadrant noise estimate has not been demonstrated by these data. The flow factor correction is -10 decibels because of the near critical flow near the blades. When the correction is this large, it is bound to be very sensitive to slight flow variations and to details in the between-blade channel flows. These factors are not taken into account in the simple correlation procedure. Therefore, one may not regard the apparent agreement with the front end noise as confirmation of this estimating procedure. An additional calculation was made for the broad-band noise data for a fan speed of 60 percent of the design value in order to reduce the noise blocking effect of the flow in the rotor. The results, corrected to 100 feet (30.5 m) sideline, are

Type of data	Nozzle size, percent of design area	Microphone position, deg	
		50	120
		Broad-band sideline sound pressure level, dB	
Calculated	--	101.1	107.1
Experimental	97	97.5	99.3
	110	96.4	95.4
	124	96.9	96.0

The estimated noise is too high by 4 decibels in the front, which substantiates that the agreement at 90 percent of design speed in the front quadrant was not so good as indicated by the data. Some possible causes for this discrepancy are that (1) the Smith and House data may have been obtained under conditions (engine, fan speed, etc.) different from those data obtained with the QF-1 fan and (2) it is possible that details of the fan design (such as solidity, blade loading, stage pressure coefficient, blade shapes, etc.) have an important effect on noise production. Correlations of this type could not be expected to have general validity if this were true.

Multiple pure tones. - Multiple pure tones were observed on narrow band analysis to be present at 80, 85, and 90 percent speed. The tones were most prominent with the 110 percent nozzle. The angular distribution of this noise as calculated from 1/3-octave analysis as shown in figure 11. The multiple pure tone is concluded to have originated on the rotor, because it is almost entirely propagated out of the front of the fan and is most prominent at the highest speed.

The fan radiated, with the largest nozzle, only a small amount of multiple pure tone and, with the smallest nozzle, produced no noticeable multiple pure tones. This noise is therefore very sensitive to blade loading, and the details of patterns of the shock waves and expansion waves originating on the blading should, consequently, be sus-

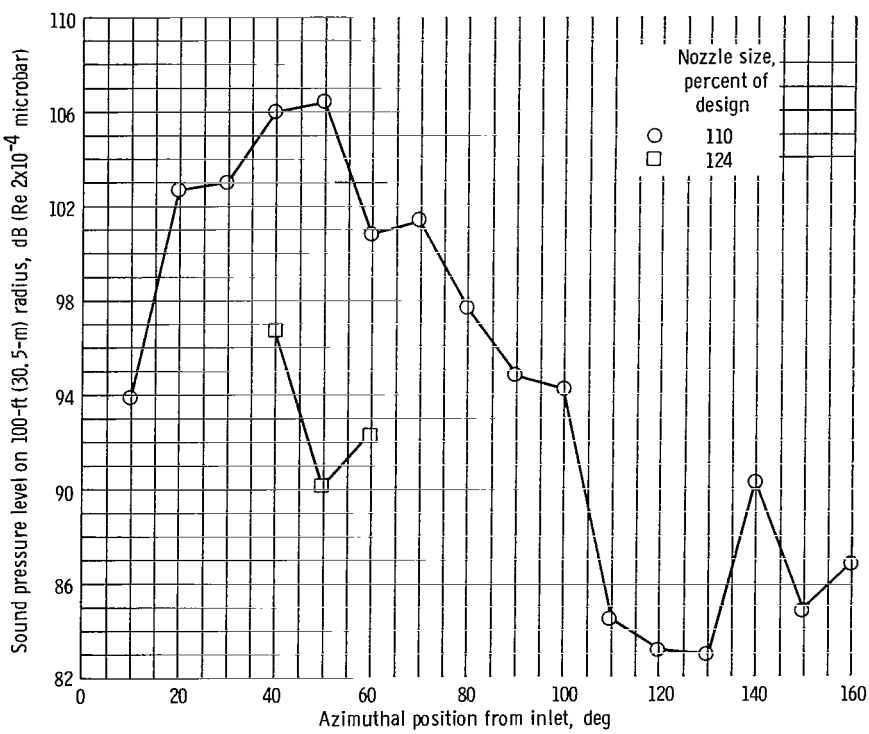

Figure 11. - Azimuthal distribution of multiple pure-tone noise on 100-foot (30.5-m) radius at 90 percent of design speed. Inlet cowl length, 86 inches (2.18 m).

ceptible to control in the aerodynamic design process.

Acoustic power. - The dependence of the amplitude of broad-band noise, blade passing tone, and multiple pure tone on rotor speed is of interest, particularly in the phase of fan design when a decision on fan speed is to be made. Plots of radiated power against rotor speed are displayed in figure 12 with breakdown into blade passing tone, multiple pure tones, and broad-band noise. There is also shown a separate grouping of the front quadrant microphone outputs plus one-half that of the 90° microphone, and the rear quadrant microphone outputs plus one-half that of the 90° microphone. The entire hemispherical radiation of each acoustic component is shown in figure 13. The blade passage tone can be approximated by a simple power law in the range from 60 to 80 percent of design speed, but for higher speeds the output does not always increase with speed at the same rate. At the low speed range, the exponent depends on the blade loading (nozzle area); with the short inlet cowl the exponent is about 9 with the small nozzle and about 6.7 with the larger ones. These values are somewhat larger than the sixth power found in the literature for correlating this type of data. With the longer cowl the exponent varies from about 8 to 6.5.

Variation with speed of the blade passing tone output in the higher speed range from 80 to 90 percent of design speed is not simple. In all cases the total high-speed output is less than the extrapolated low-speed curve, but the amount varies. For the short cowl with the 110 percent of design area nozzle the noise level actually decreases when the speed is increased. This case is accompanied by the loudest multiple pure tone and probably results from appearance of a certain parcel of energy in the form of multiple pure tones rather than blade-passage tones. The quantitative support of this theory is lacking because of the rough estimate of the energy involved in the multiple tones. The dependence of the amplitude of the multiple pure tones on the blade loading may be simply explained as resulting from the establishment of variations of the pressure distribution from one blade to the next; this variation may be expected to depend on fan pressure ratio and weight flow. Under the circumstances of nonequal loading, the fundamental period is the shaft revolution, and each blade acts somewhat independently of the others as an isolated source. When the blade pressure distributions are precisely equal, the propagation waves of the multiple pure tones will precisely cancel each other, and only the blade-passing frequency will remain.

Broad-band noise is the major component of the acoustic power radiation of the fan. It cannot be directly determined by the methods of the present investigation because of the inclusion of fan jet noise in the measurements. The jet noise is evident in the spectrographs of the noise picked up by the microphones located at 140°, 150°, and 160° as a dominant low-frequency noise. The effect of the jet noise on broad-band power level is small because most of the jet noise is picked up by these three microphones involving only 15 percent of the hemispherical surface at the 100-foot (30.5-m) radius and because

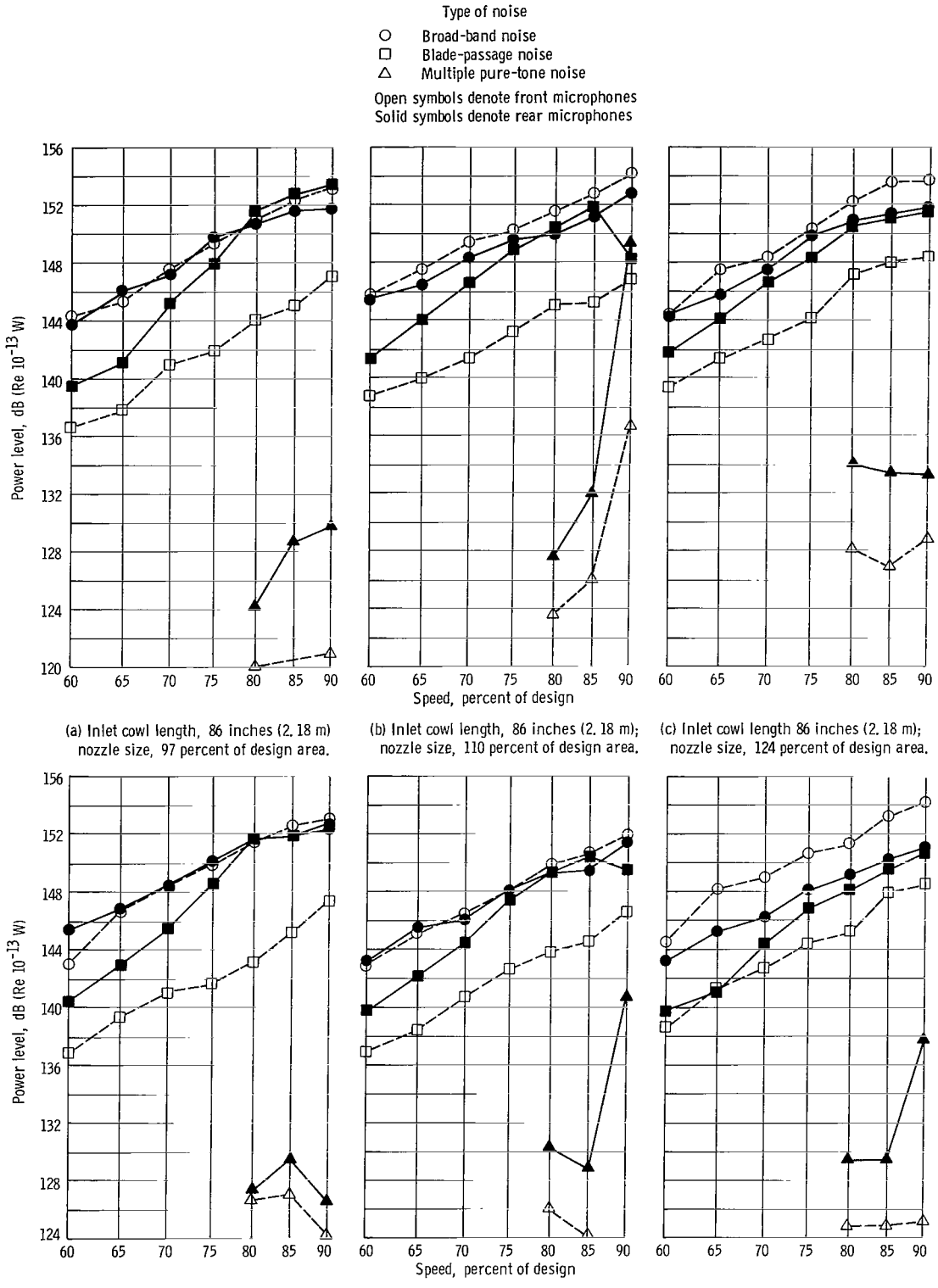

(a) Inlet cowl length, 86 inches (2.18 m) nozzle size, 97 percent of design area.

(b) Inlet cowl length, 86 inches (2.18 m); nozzle size, 110 percent of design area.

(c) Inlet cowl length 86 inches (2.18 m); nozzle size, 124 percent of design area.

(d) Inlet cowl length, 127 inches (3.23 m); nozzle area, 97 percent of design.

(e) Inlet cowl length, 127 inches (3.23 m); nozzle size, 110 percent of design area.

(f) Inlet cowl length, 127 inches (3.23 m); nozzle size, 124 percent of design area.

Figure 12. - Front and rear split of components of overall fan noise.

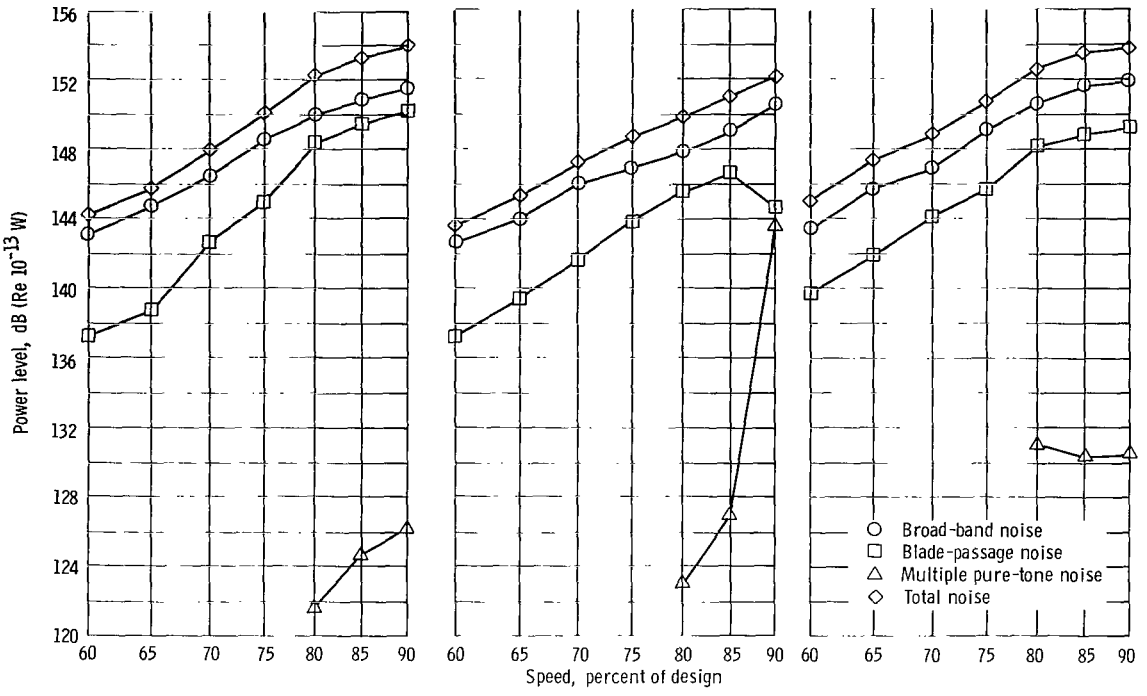

(a) Inlet cowl length, 86 inches (2.18 m); nozzle size, 97 percent of design area.

(b) Inlet cowl length, 86 inches (2.18 m); nozzle size, 110 percent of design area.

(c) Inlet cowl length, 86 inches (2.18 m); nozzle size, 124 percent of design area.

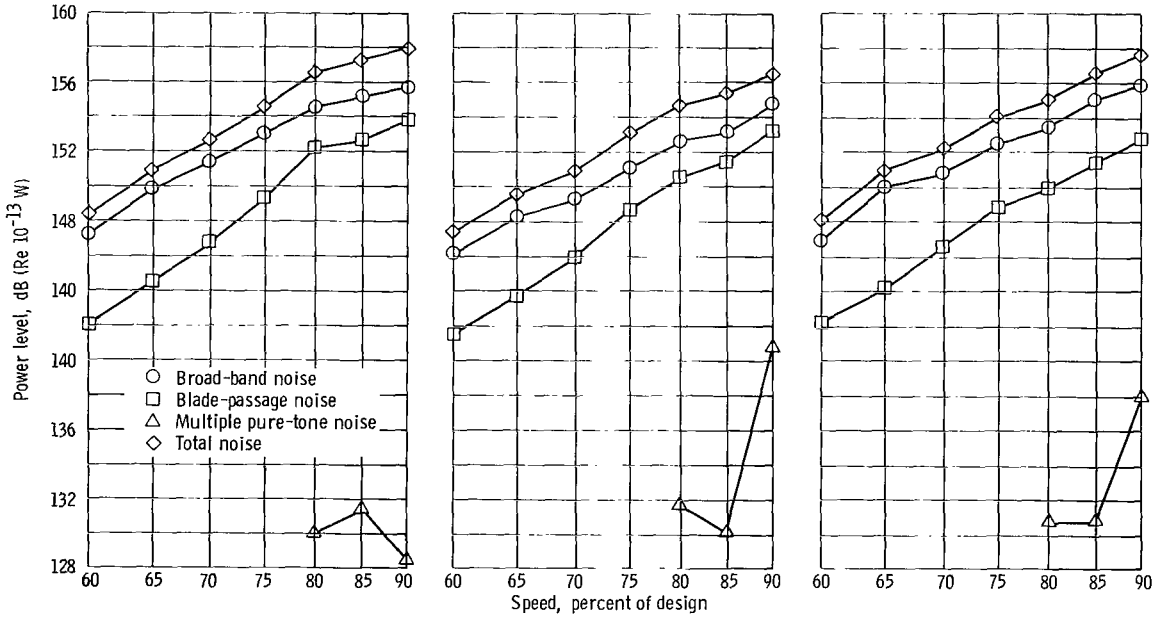

(d) Inlet cowl length, 127 inches (3.33 m); nozzle size, 97 percent of design area.

(e) Inlet cowl length, 127 inches (3.33 m); nozzle size, 110 percent of design area.

(f) Inlet cowl length, 127 inches (3.33 m); nozzle size, 124 percent of design area.

Figure 13. - Measured overall fan noise and its components.

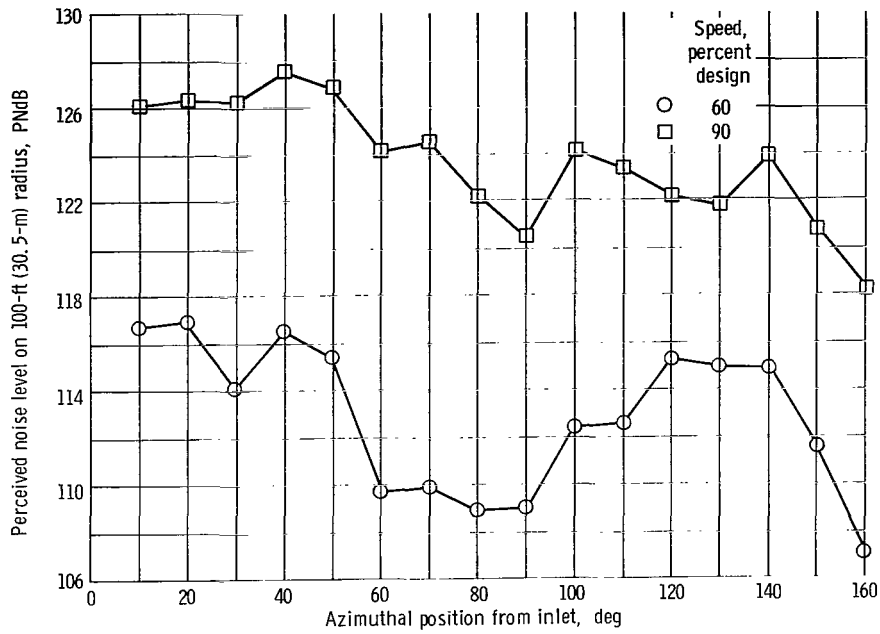

Figure 14. - Azimuthal distribution of perceived noise level at 100-foot (30.5-m) radius from fan rotor plane. Inlet cowl length, 86 inches (2.18 m); nozzle side, 97 percent of design area.

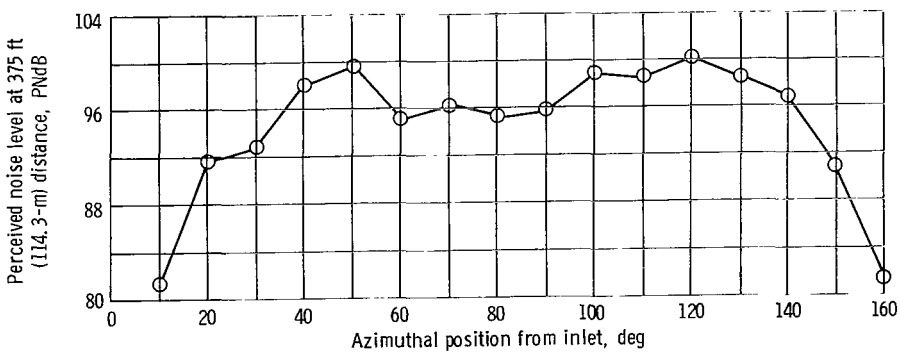

Figure 15. - Azimuthal distribution of perceived noise level on parallel line 375 feet (114.3 m) from fan axis. Inlet cowl length, 86 inches (3.18 m); nozzle size, 97 percent of design area; fan speed; 60 percent of design.

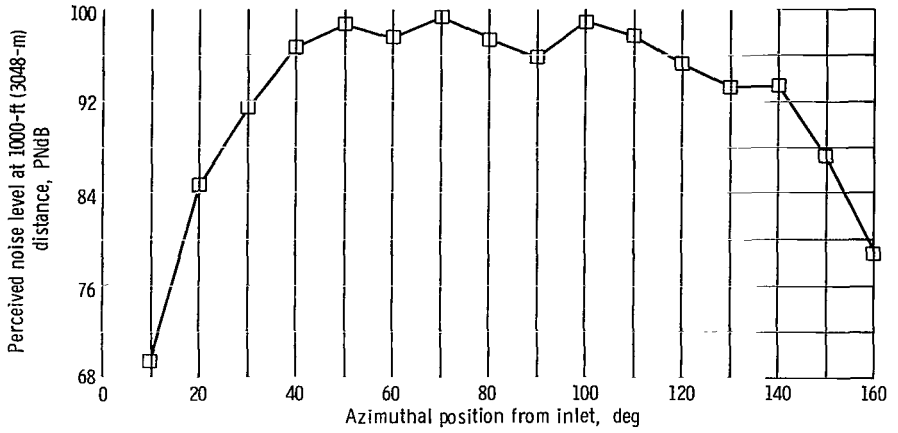

Figure 16. - Azimuthal distribution of perceived noise level on parallel line 1000 feet (304.8 m) from fan.

of the relatively low level of aft radiated noise. The noise of the fan jet is included in the rear quadrant broad-band noise (fig. 12) and contributes substantially to this total. Broad-band power levels varied with speed with an exponent of from 4.5 to 5.7. One may assume from this that the correlation value of 6.0 used by Smith and House (ref. 5) and by Sharland (ref. 15) for turbulent streams and 5.4 by Sharland for smooth flows (vortex shedding) are adequate to correlate the present data. Comparison of the curves of figure 13 shows a definite higher exponent for the blade passing tone as compared with the broad-band noise; this disagrees with Smith and House, who use the exponent 6.0 for both noise components.

Perceived noise level. - Perceived noise levels were calculated according to the SAE standards (ref. 16). Angular distributions are shown for both 60 and 90 percent of design speed operation in figure 14 for a 100-foot (30.5-m) radius, in figure 15 for a 375-foot (114.3-m) parallel line, and in figure 16 for a 1000-foot (304.8-m) parallel line. Figure 16 indicates that, at the take-off rating point of 1000 feet (304.8 m) altitude, a four-engined airplane using fans such as the QF-1 would produce a maximum fan noise of about 105 PNdB (adding 6 dB to the maximum value of 99 in fig. 16 to account for four fans). At the approach condition rating point (375-ft (114.3-m) altitude and 60 percent of design speed), the data displayed in figure 15 indicate that the same four-engine airplane would produce a maximum fan noise of about 106 PNdB (again adding 6 dB to account for the four engines). This is a substantial improvement over DC-8 (ref. 17) values of 117 PNdB for take-off at 1000 feet (304.8 m).

It should be noted here than the PNdB rating for the airplane is the total noise from the four current engines, while the 105- and 106-PNdB figures represent only the four-fan component noise from the tests reported herein. However, the addition of the core engine jet and turbine noises would be expected to add no more than a decibel to these

numbers inasmuch as the fan noise in a high-bypass ratio turbofan engine is the dominant component. The overall engine PNdB values could be lowered considerably by appropriate noise suppression treatment on the internal flow surfaces of the fan cowling because of the low level of the noise from other engine components.

SUMMARY OF RESULTS

The overall aerodynamic and acoustic characteristics are presented for a full-scale fan designed for propulsion of a subsonic transport with minimum noise production. No sound absorbing treatment was included, so that these test results present essentially the noise generated by the fan. Tests are reported in the speed range from 60 to 90 percent of design cruise values.

At 90 percent speed the desired corrected weight flow of 786 pounds per second (356 kg/sec) was achieved. The maximum pressure ratio at this speed is about 1.36, but inadequate design procedures produced a low estimated efficiency of 77 percent.

Spectrograms showed broad-band noise, with superimposed blade-passing tones and harmonics, and multiple pure tones. The multiple pure tones first appeared at 80 percent speed (when the maximum gas Mach number relative to the blade surface was 1.16), and, as the speed increased, became very prominent as a cluster of pure tones in the frequency region about one-half the blade-passing tone frequency, with a frequency spacing equal to the shaft speed. The multiple pure tones did not appear noticeably when the blades were highly loaded, but when the loading was medium, they appeared with a concomitant reduction in blade-passing tone level. Almost the entire multiple pure-tone energy appeared in front of the fan, implying that its origin is at the rotor.

Broad-band noise varied about 5 to 8 decibels with angular location. Total front and rear broad-band noise varied with the rotor speed to the exponent 4.5 to 5.7. The exponent did not vary with blade loading. The level of this noise is also independent of the blade loading.

The blade-passing tone varied only slightly with blade loading at low speeds, but at 80 and, more markedly, at 90 percent speed, medium loading resulted in minimum blade-passing tone and maximum multiple pure tone. In all cases, the blade-passing tone increased at a slower rate with speed in the region from 80 to 90 percent speed than it did in the lower speed range. At low speeds with the smallest nozzle, the blade-passing tone increased with the eighth or ninth power of the rotor speed; whereas with the two larger nozzles the increase was with the 6.5 to 7 power, approximately.

The method of Smith and House (ref. 5) for estimating the blade passing tone noise level was satisfactory for the rear quadrant, but, because of possible interference from the inflow distortion, a good check was not possible in the front quadrant. Broad-band

noise estimates for 60 percent of design speed were about 10 decibels too high in the rear and about 4 decibels too high in the front.

The peak perceived noise level of a single fan at an approach speed of 60 percent and a cruise altitude of 375 feet (114.3 m) was 100 PNdB peak. At a take-off speed of 90 percent cruise and an altitude of 1000 feet (304.8 m), the peak value was 99 PNdB per fan.

Lewis Research Center,
National Aeronautics and Space Administration,
Cleveland, Ohio, July 13, 1970,
737-52.

REFERENCES

1. McBride, Joseph F.: Quiet Engine Program-Preliminary Engine Design and Aircraft Integration. Progress of NASA Research Relating to Noise Alleviation of Large Subsonic Jet Aircraft. NASA SP-189, 1968, pp. 263-272.

2. Kramer, James J.: Quiet Engine Program - Detailed Engine Designs. Progress of NASA Research Relating to Noise Alleviation of Large Subsonic Jet Aircraft. NASA SP-189, 1968, pp. 273-285.

3. Marsh, Alan H.; and McPike, A. L.: Noise Levels of Turbojet- and Turbofan-Powered Aircraft. Sound, vol. 2, no. 5, Sept.-Oct. 1963, pp. 8-13.

4. Leonard, B. R.; Schmiedlin, R. F.; Stakolich, E. G.; and Newmann, H. E.: Acoustic and Aerodynamic Performance of 6-Foot Diameter Fans for Turbofan Engines. Part I. Design of Facility and QF-1 Fan. NASA TN D-5877, 1970.

5. Smith, M. T. J.; and House, M. E.: Internally Generated Noise from Gas Turbine Engines. Measurement and Prediction. Paper 66-GT/N-43, ASME, Mar. 1966.

6. Tyler, J. M.; and Sofrin, T. G.: Axial Flow Compressor Noise Studies. SAE Trans., vol. 70, 1962, pp. 309-332.

7. Morfey, C. L.: Rotating Pressure Patterns in Ducts: Their Generation and Transmission. J. Sound Vib., vol. 1, 1964, pp. 60-87.

8. Lowson, Martin V.: Compressor Noise Analysis. Progress of NASA Research Relating to Noise Alleviation of Large Subsonic Jet Aircraft. NASA SP-189, 1968, pp. 287-306.

9. Harley, K. G.; and Burdsall, E. A.: High-Loading Low-Speed Fan Study. II. Data and Performance Unslotted Blades and Vanes. Rep. PWA-3653, Pratt & Whitney Aircraft (NASA CR-72667), 1970.

10. Anon.: Standard Values of Atmospheric Absorption as a Function of Temperature and Humidity for Use in Evaluating Aircraft Flyover Noise. Aerospace Recommended Practice 886, SAE, Aug. 31, 1964.

11. Anon.: Jet Noise Prediction. Aerospace Information Report 876, SAE, July 10, 1965.

12. Ehrich, F. F.: Acoustic Resonance and Multiple Pure Tone Noise in Turbomachinery Inlets. Paper 69-GT-2, ASME, Mar. 1969.

13. Kester, J. D.; and Slaiby, T. G.: Designing the JT9D Engine to Meet Low Noise Requirements for Future Transports. Paper 670331, SAE, 1967.

14. Chestnutt, David; and Crigler, John L.: Potential of Inlet-Guide-Vane Configuration for Inlet Noise Reduction. Progress of NASA Research Relating to Noise Alleviation of Large Subsonic Jet Aircraft. NASA SP-189, 1968, pp. 307-317.

15. Sharland, I. J.: Sources of Noise in Axial Flow Fans. J. Sound Vib., vol. 1, no. 3, 1964, pp. 302-322.

16. Anon.: Definitions and Procedures for Computing Perceived Noise Levels of Aircraft Noise. Aerospace Recommended Practice 865, SAE, Oct. 15, 1964.

17. Pendley, Robert E.; and Marsh, Alan H.: Noise Predictions and Economic Effects of Nacelle Modifications to McDonnell-Douglas DC-8 Airplanes. Progress of NASA Research Relating to Noise Alleviation of Large Subsonic Jet Aircraft. NASA SP-189, 1968, pp. 173-195.

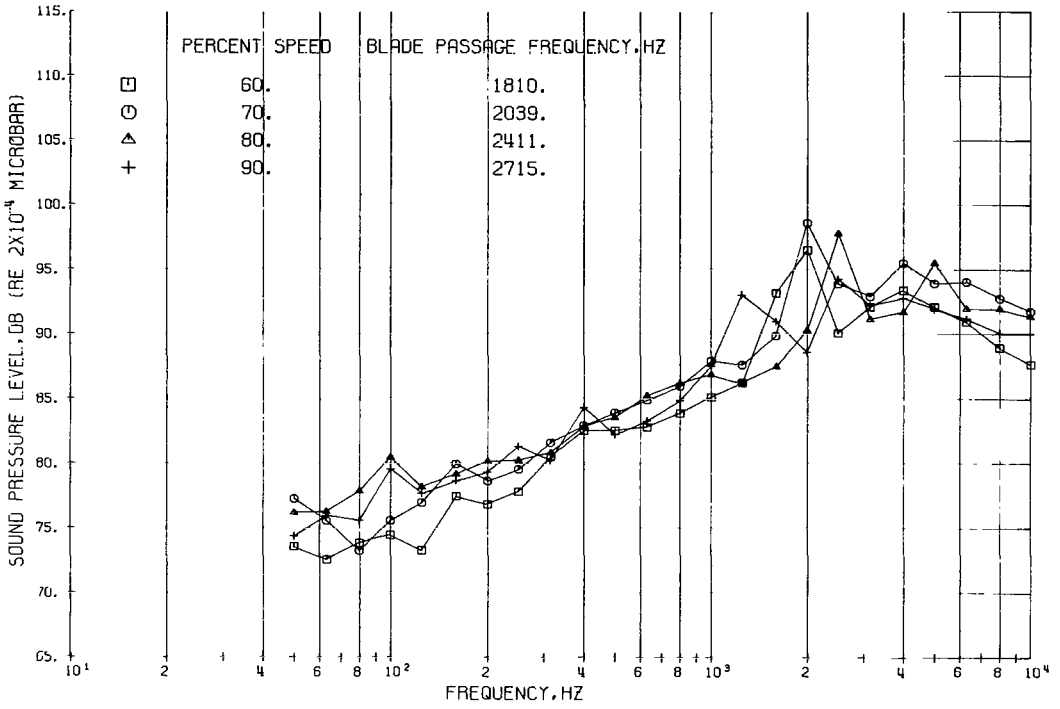

(a) Microphone location, 10°.

Figure 17. - Sound pressure levels on 100-foot (30.5-m) radius as function of frequency. Configuration 1: inlet cowl length, 86 inches (2.18 m); nozzle size, 110 percent of design area. (Microphone locations are given in degrees from shaft centerline.)

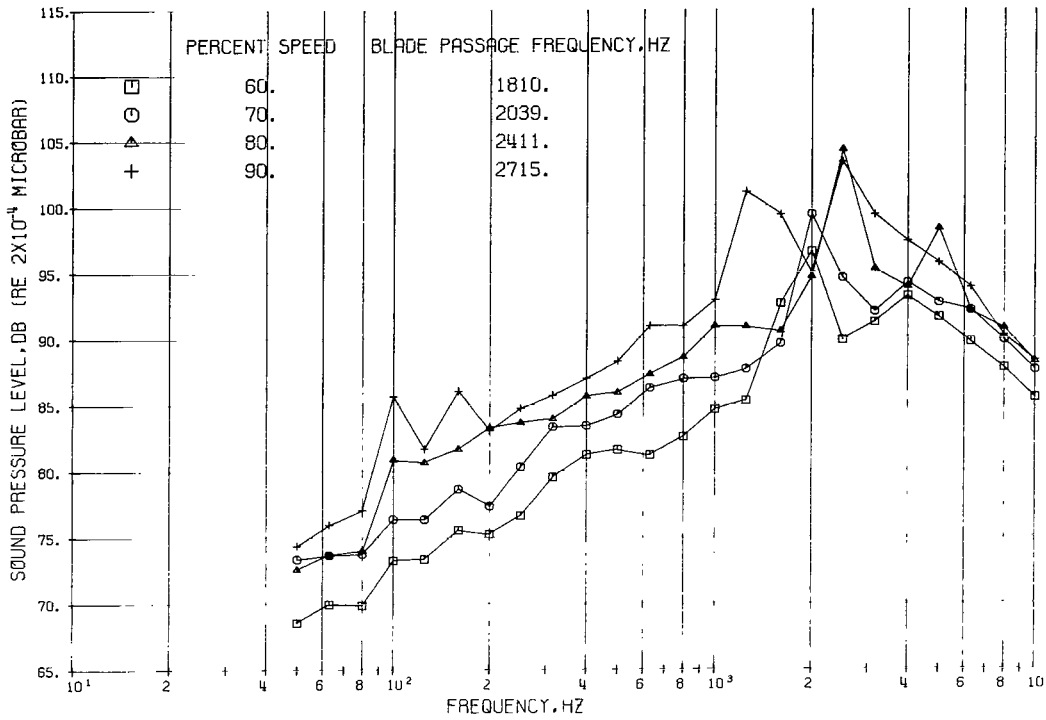

(b) Microphone location, 20°.

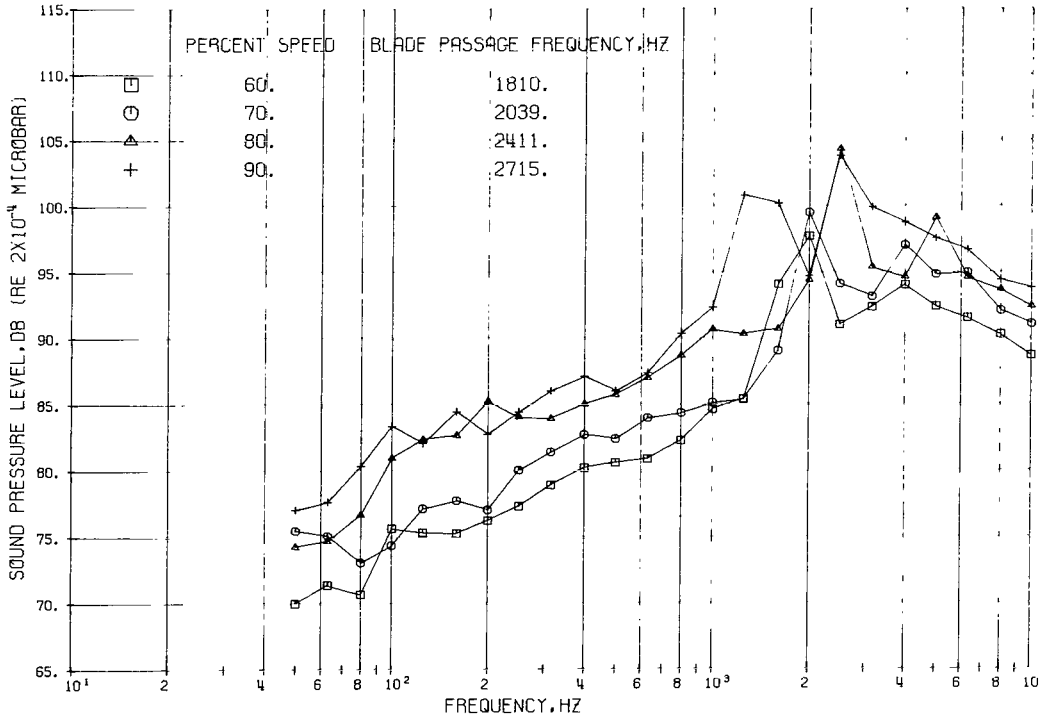

(c) Microphone location, 30°.

Figure 17. - Continued.

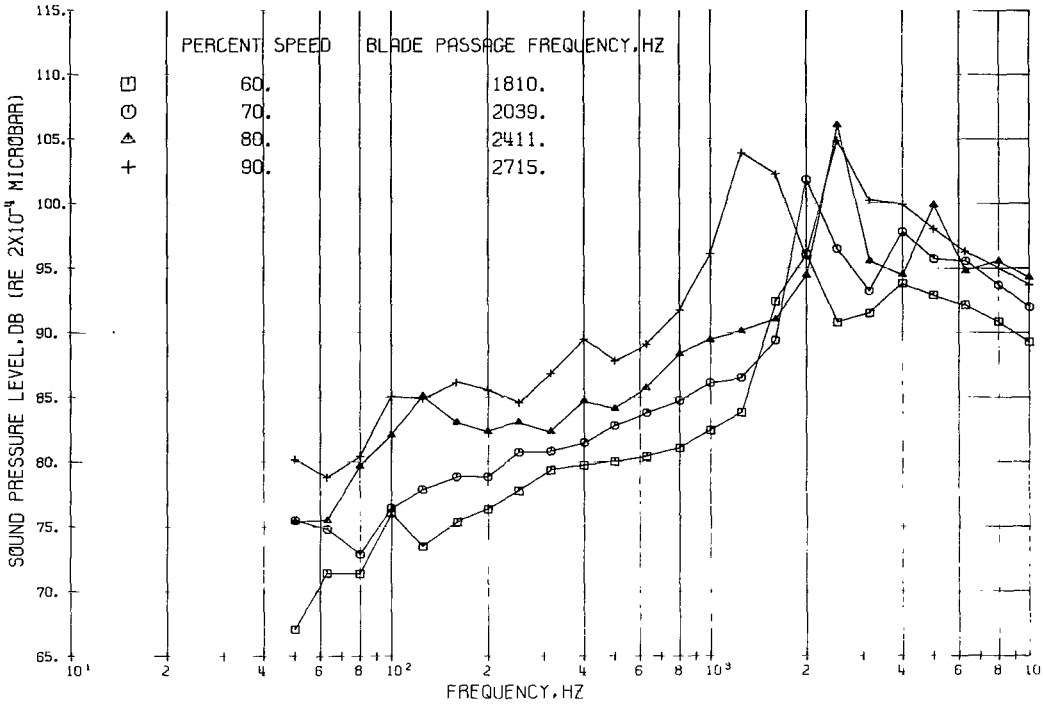

(d) Microphone location, 40°.

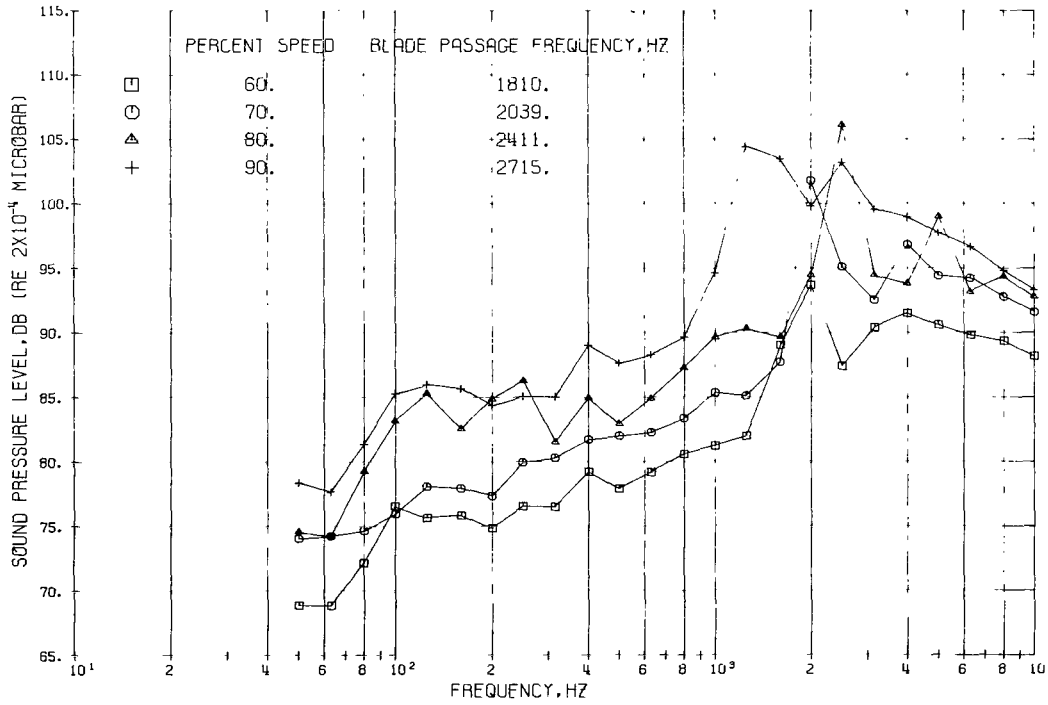

(e) Microphone location, 50°.

Figure 17. - Continued.

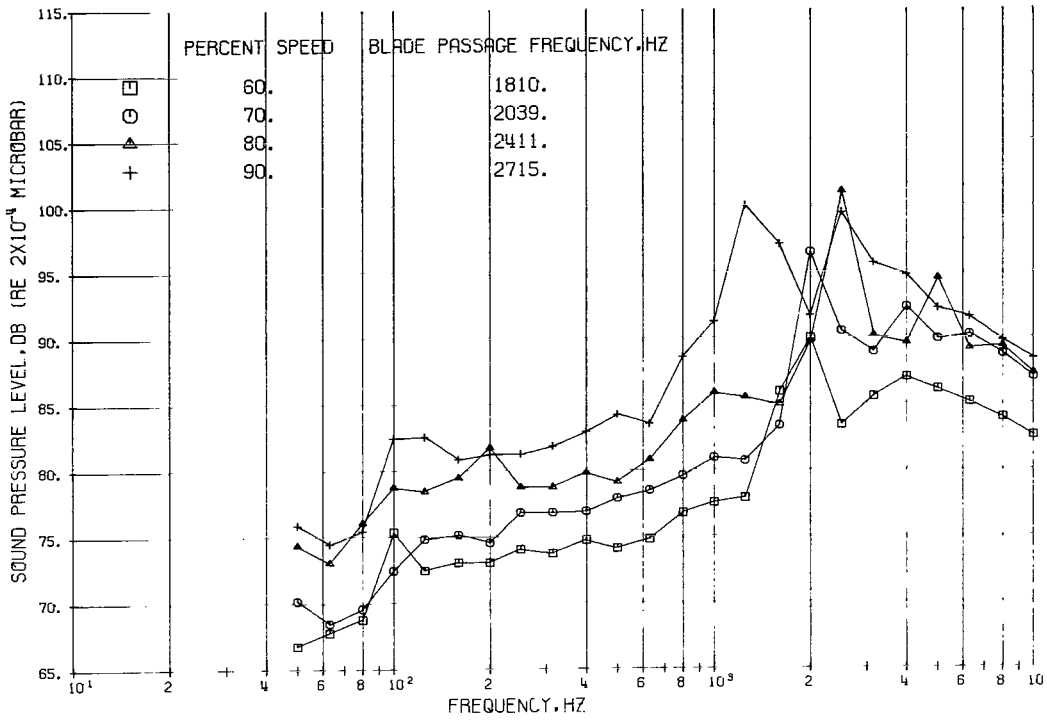

(f) Microphone location, 60°.

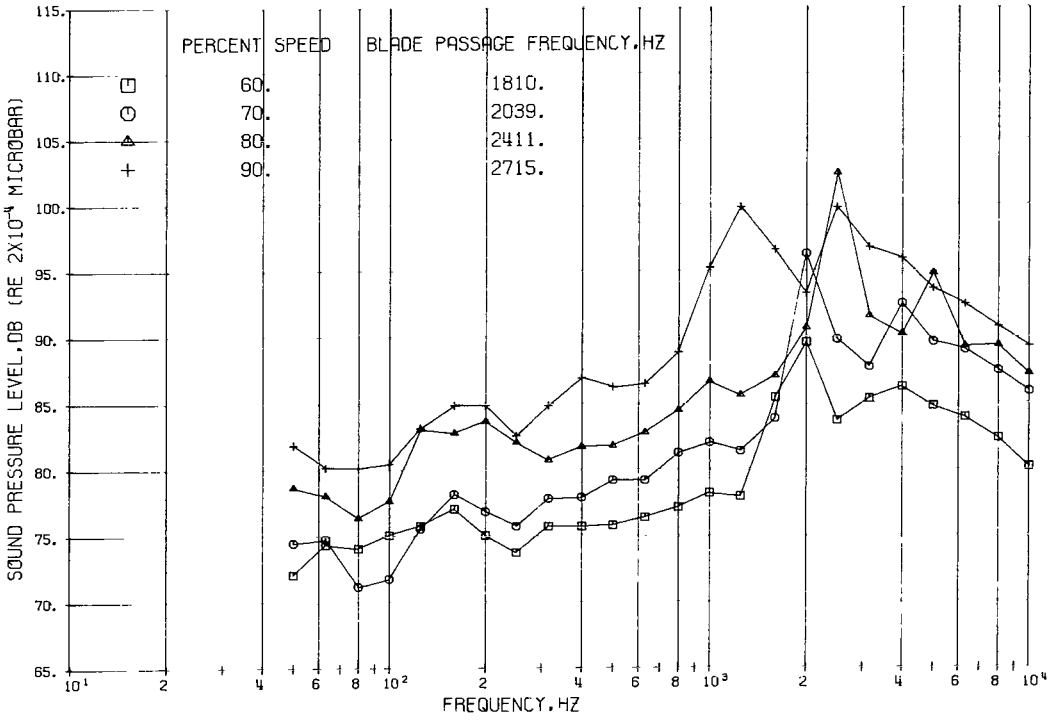

(g) Microphone location, 70°.

Figure 17. - Continued.

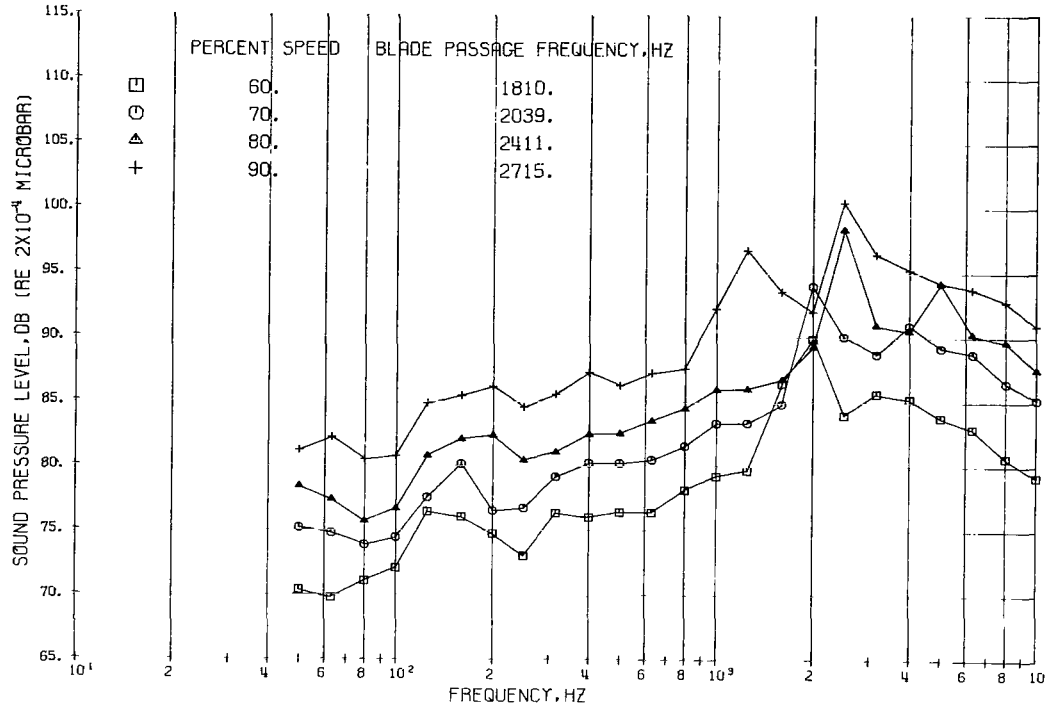

(h) Microphone location, 80°.

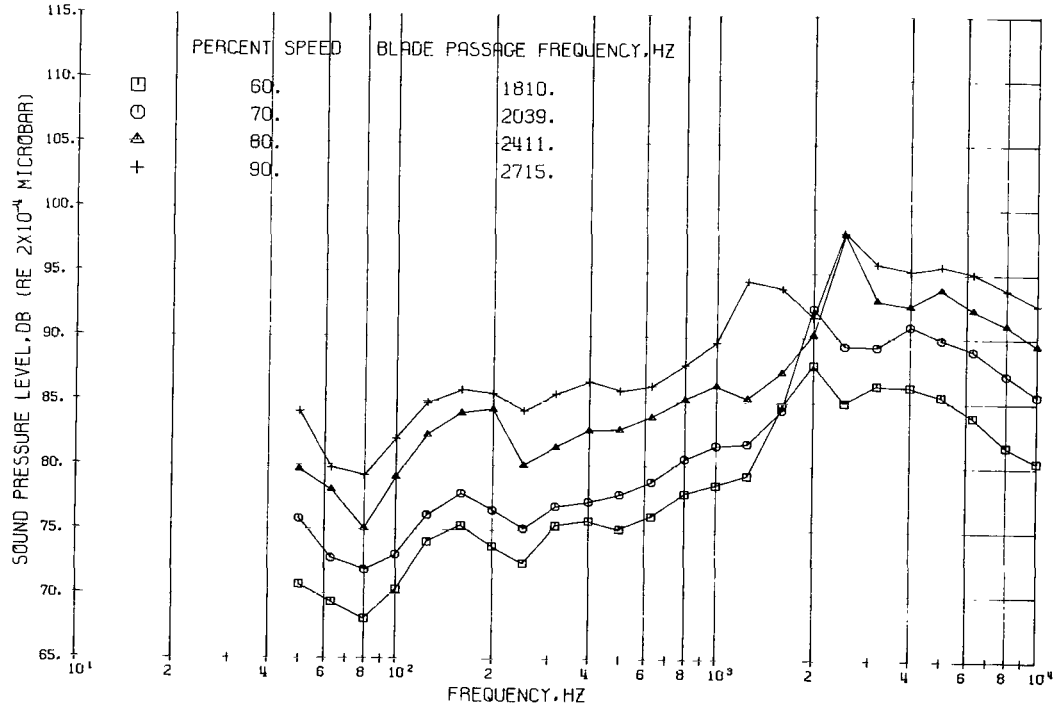

(i) Microphone location, 90°.

Figure 17. - Continued.

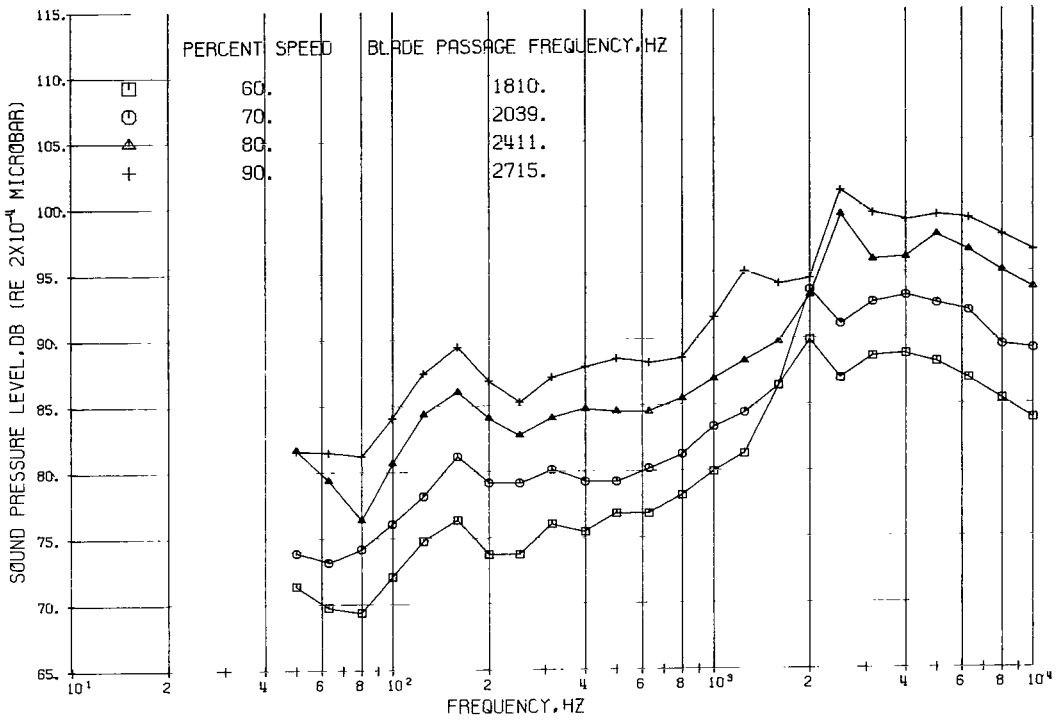

(j) Microphone location, 100°.

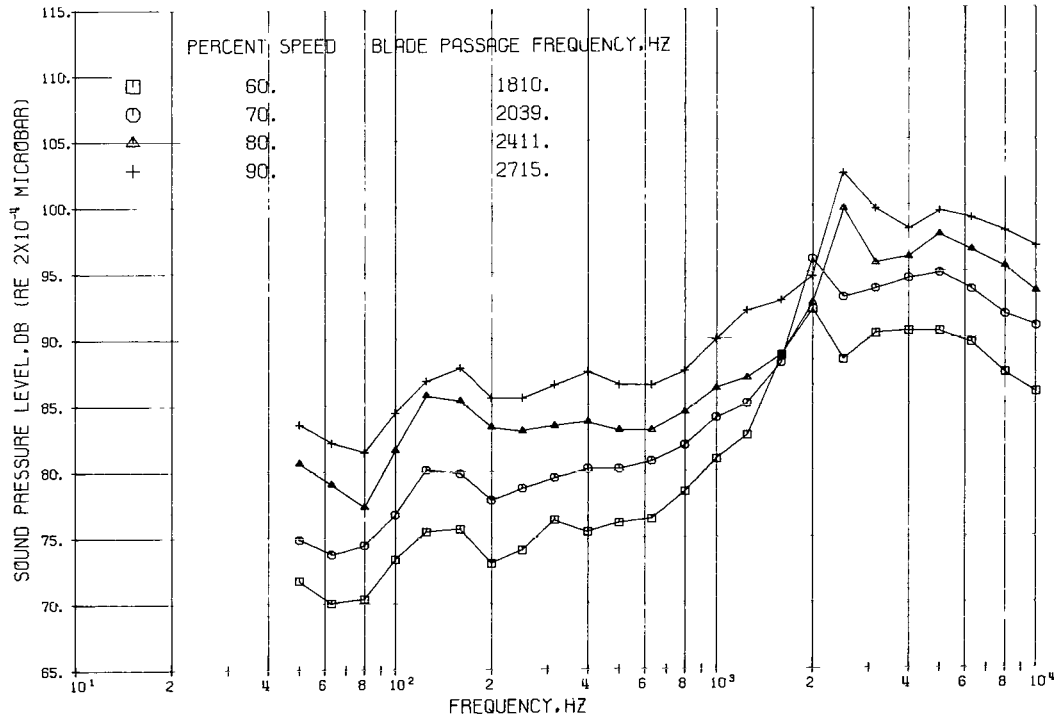

(k) Microphone location, 110°.

Figure 17. - Continued.

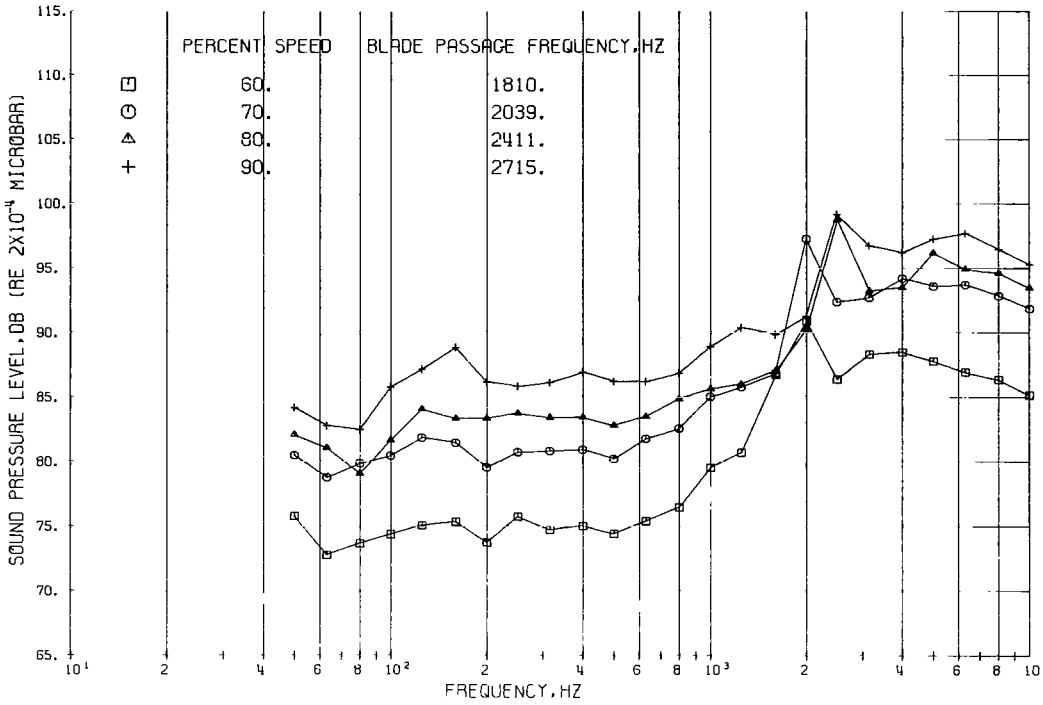

(l) Microphone location, 120°.

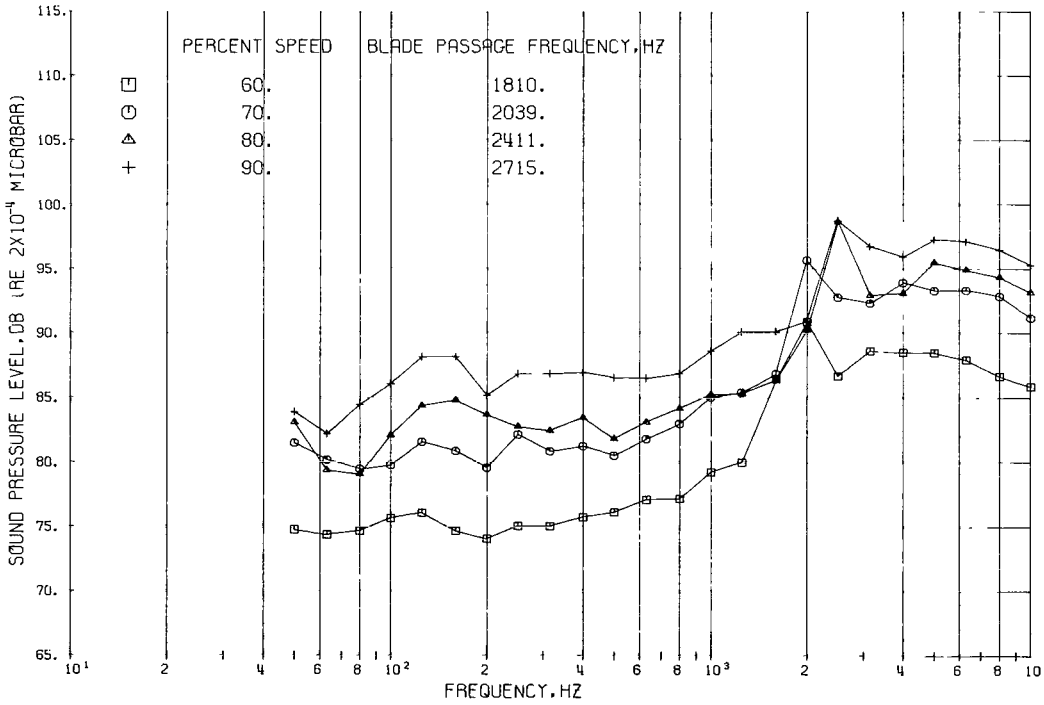

(m) Microphone location, 130°.

Figure 17. - Continued.

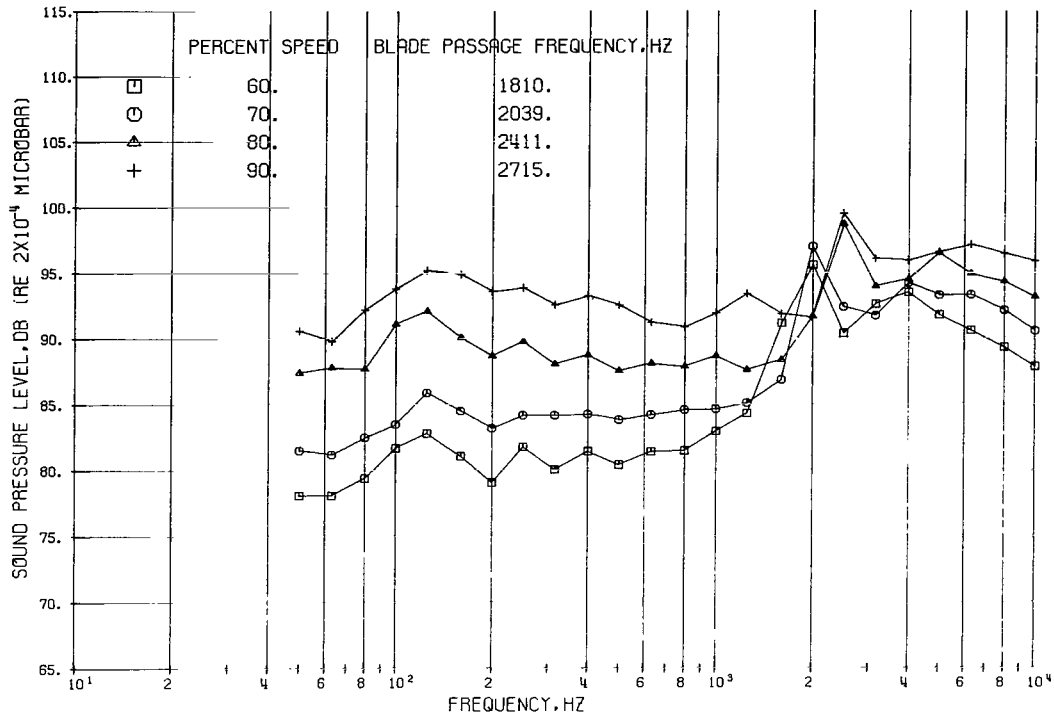

(n) Microphone location, 140°.

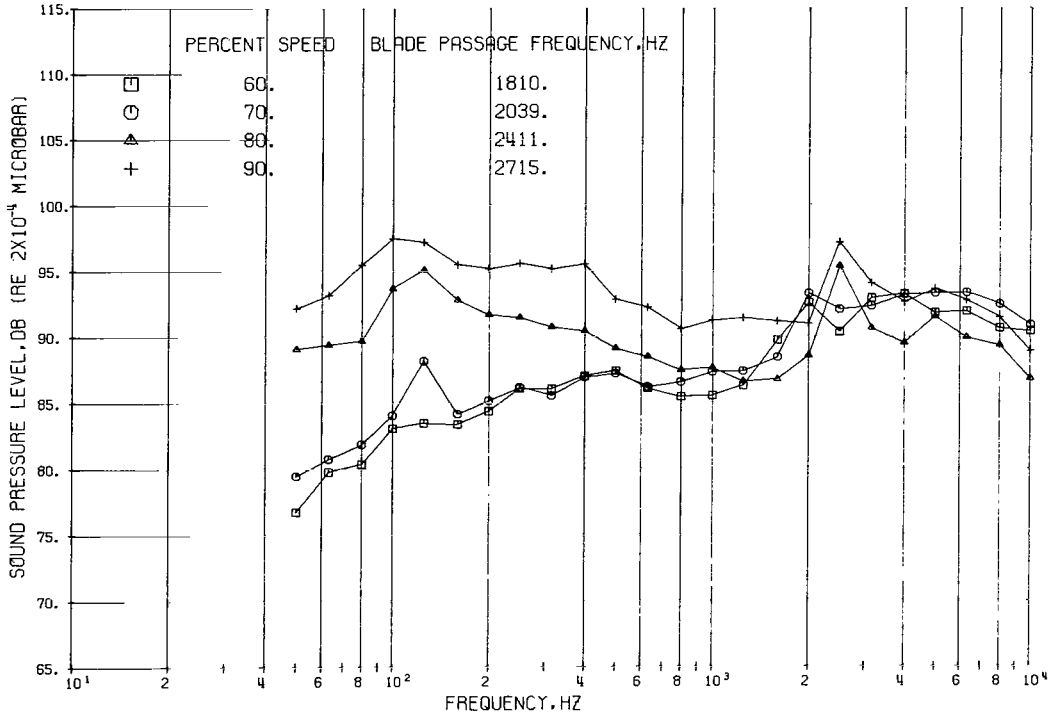

(o) Microphone location, 150°.

Figure 17. - Continued.

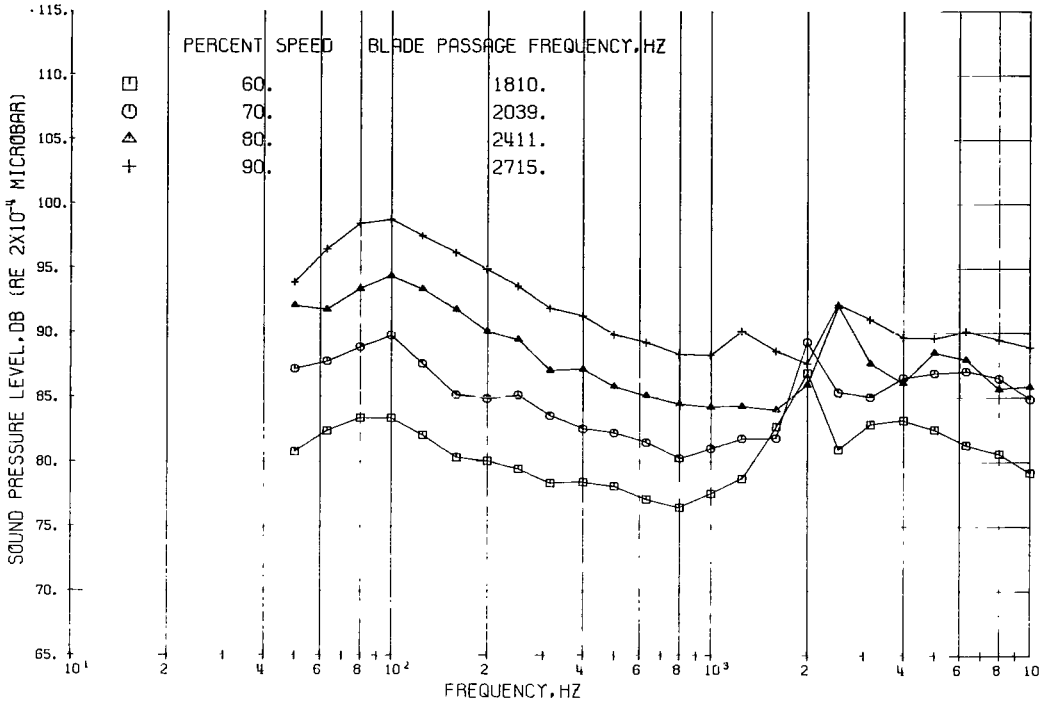

(p) Microphone location, 160°.

Figure 17. - Concluded.

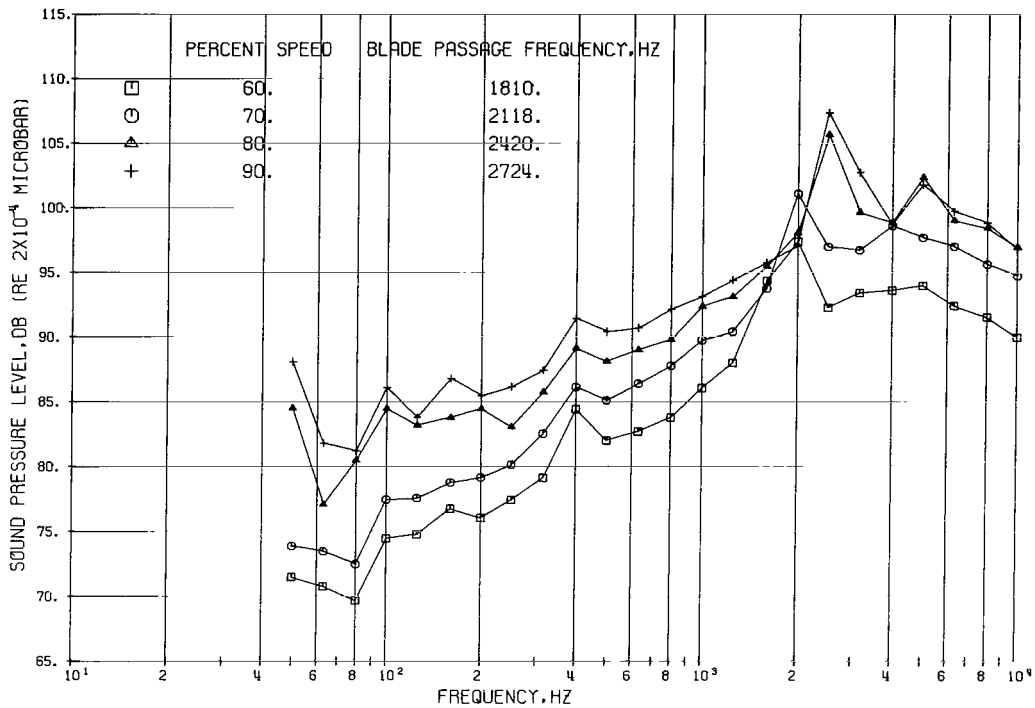

(a) Microphone location, 10°.

Figure 18. - Sound pressure levels on 100-foot (30.5-m) radius as function of frequency. Configuration 2: inlet cowl length, 86 inches (2.18 m); nozzle size, 97 percent of design area. (Microphone locations are given in degrees from shaft centerline.)

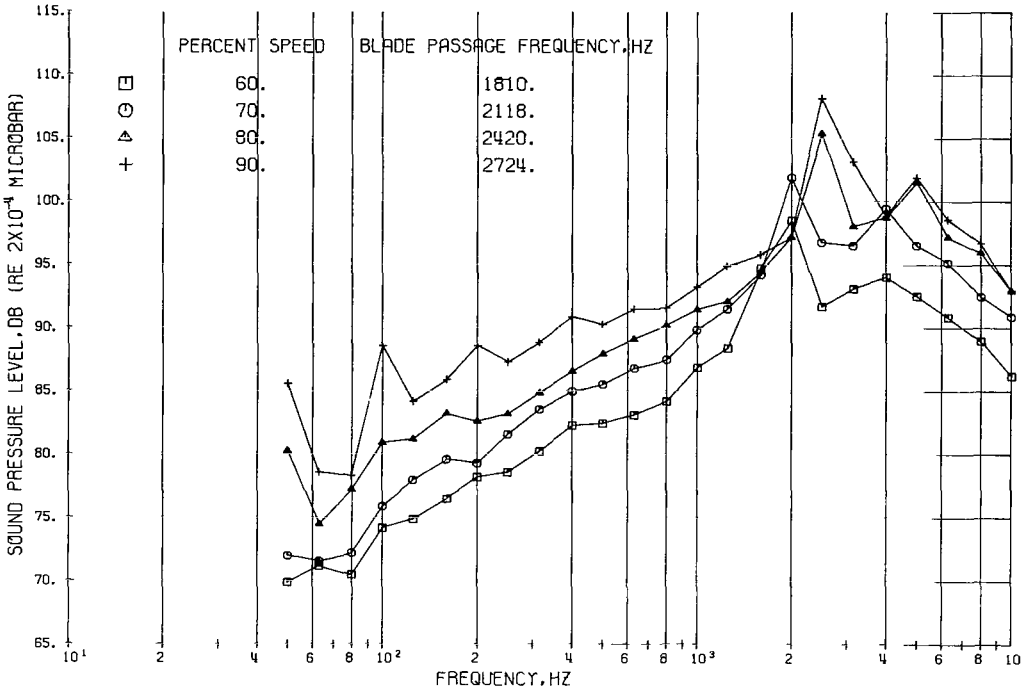

(b) Microphone location, 20°.

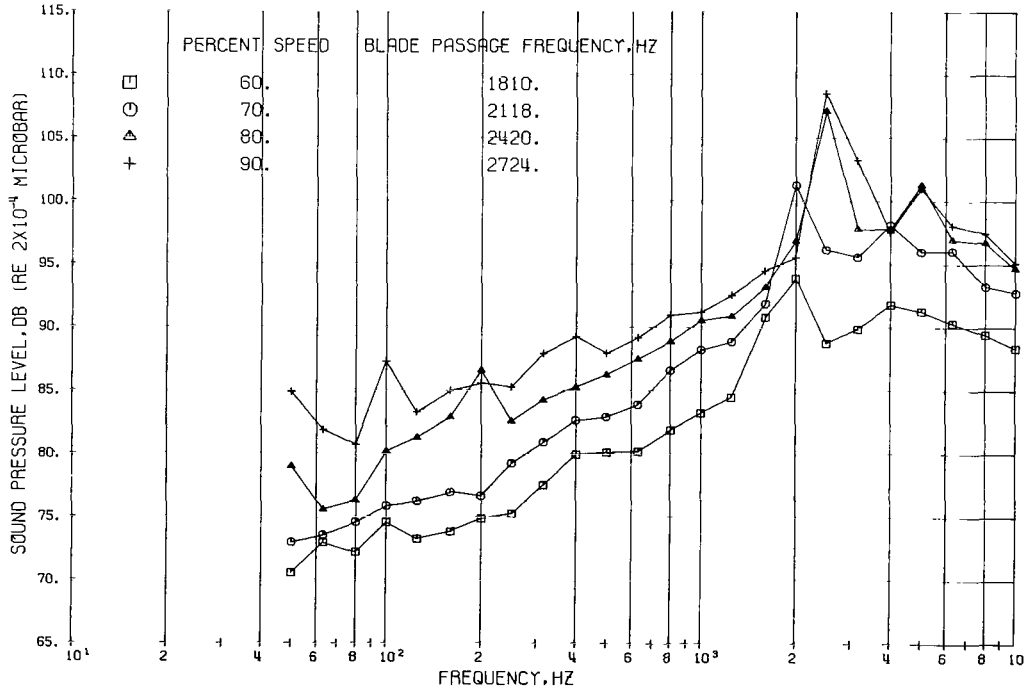

(c) Microphone location, 30°.

Figure 18. - Continued.

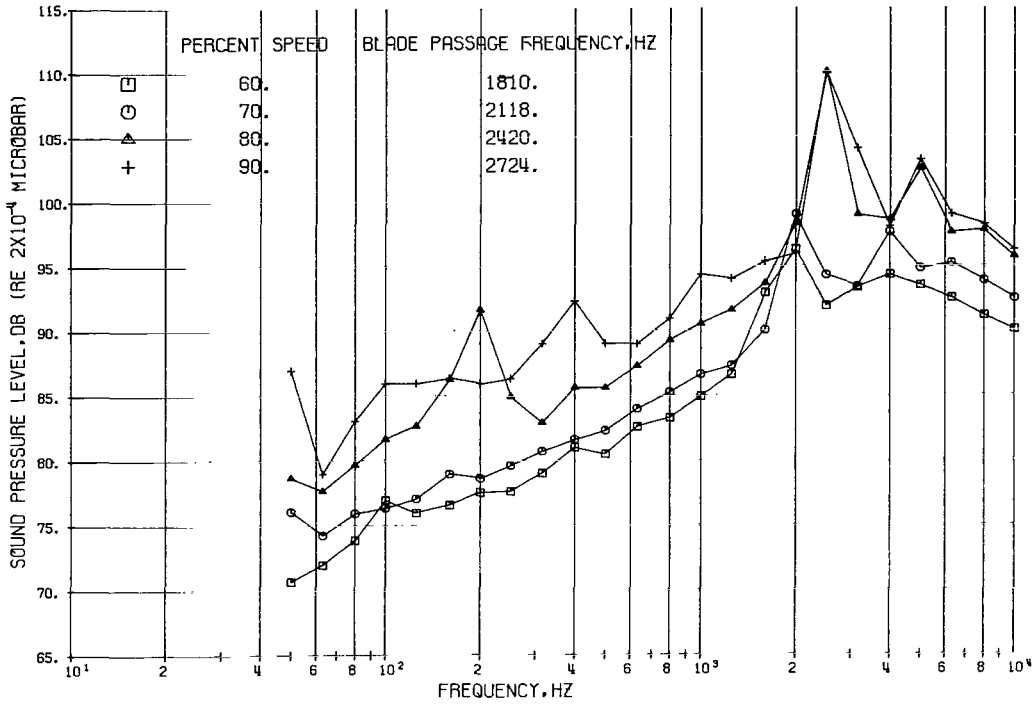

(d) Microphone location, 40°.

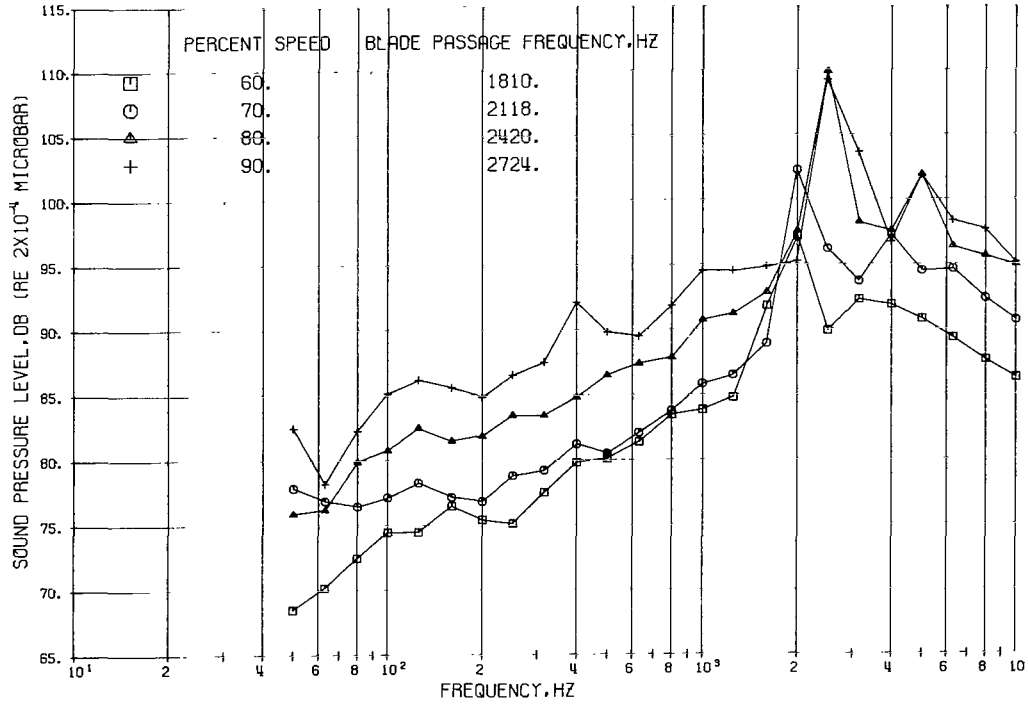

(e) Microphone location, 50°.

Figure 18. - Continued.

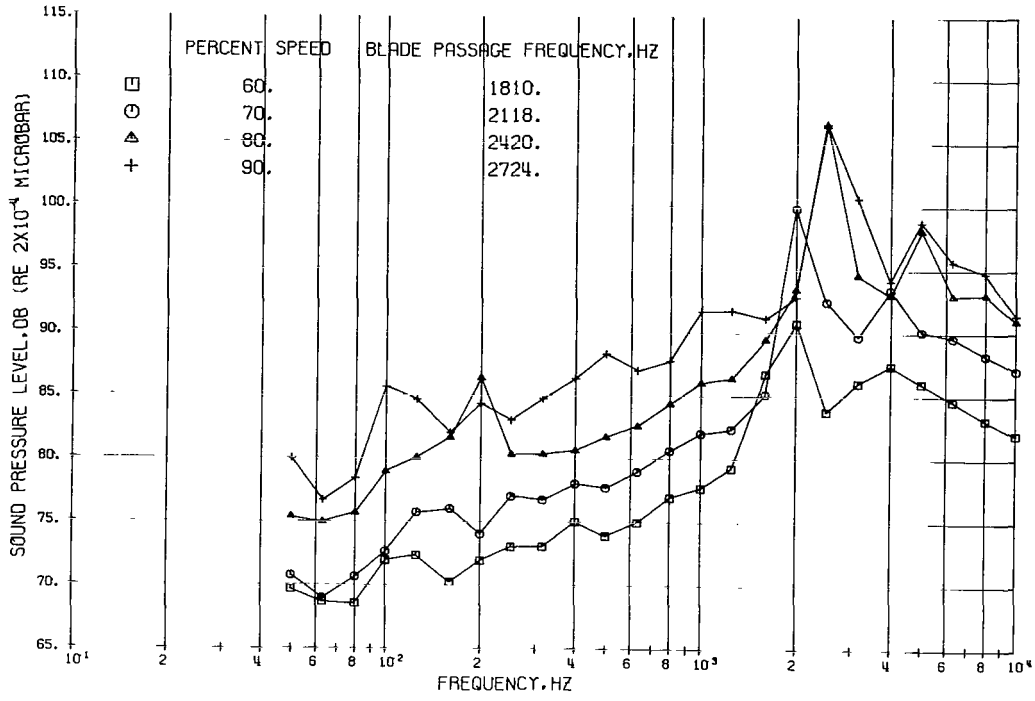

(f) Microphone location, 60°.

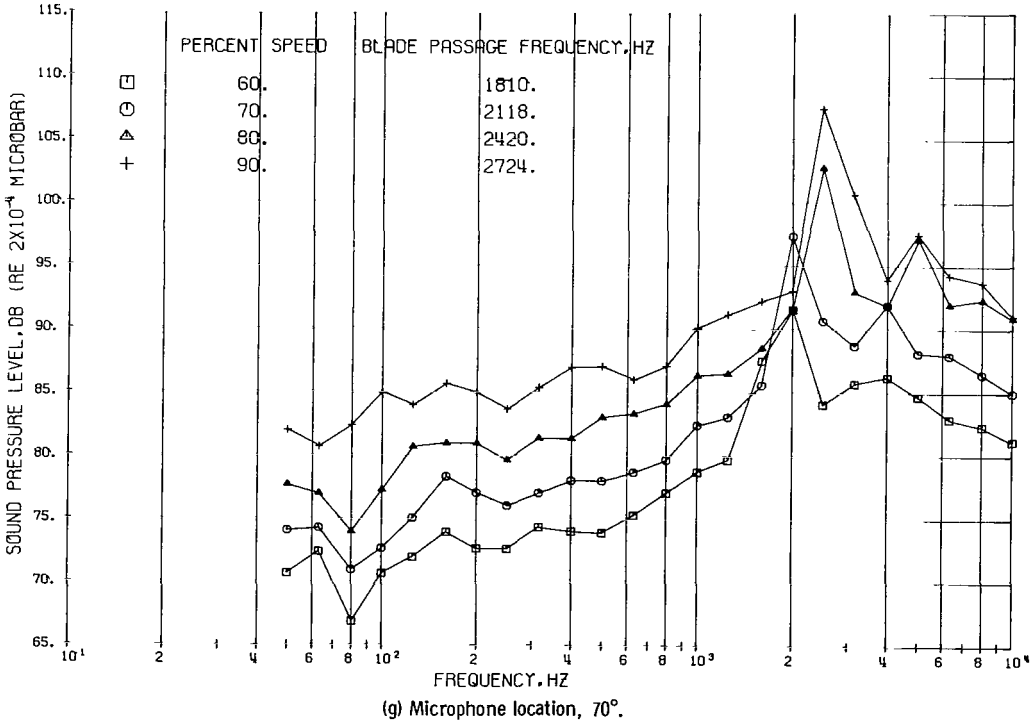

(g) Microphone location, 70°.

Figure 18. - Continued.

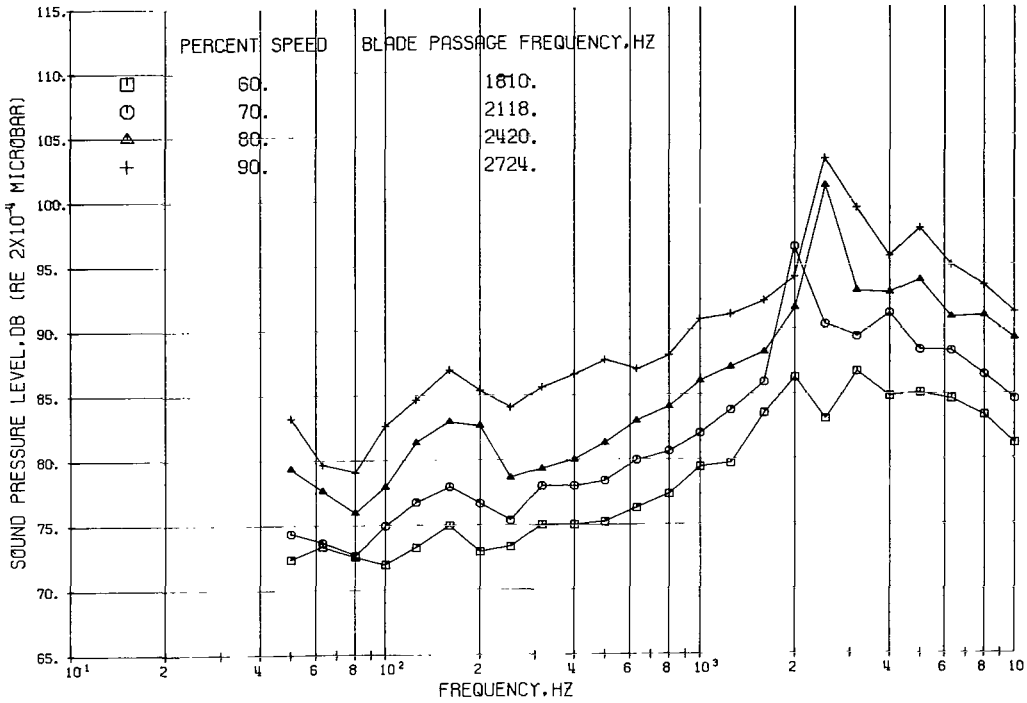

(h) Microphone location, 80°.

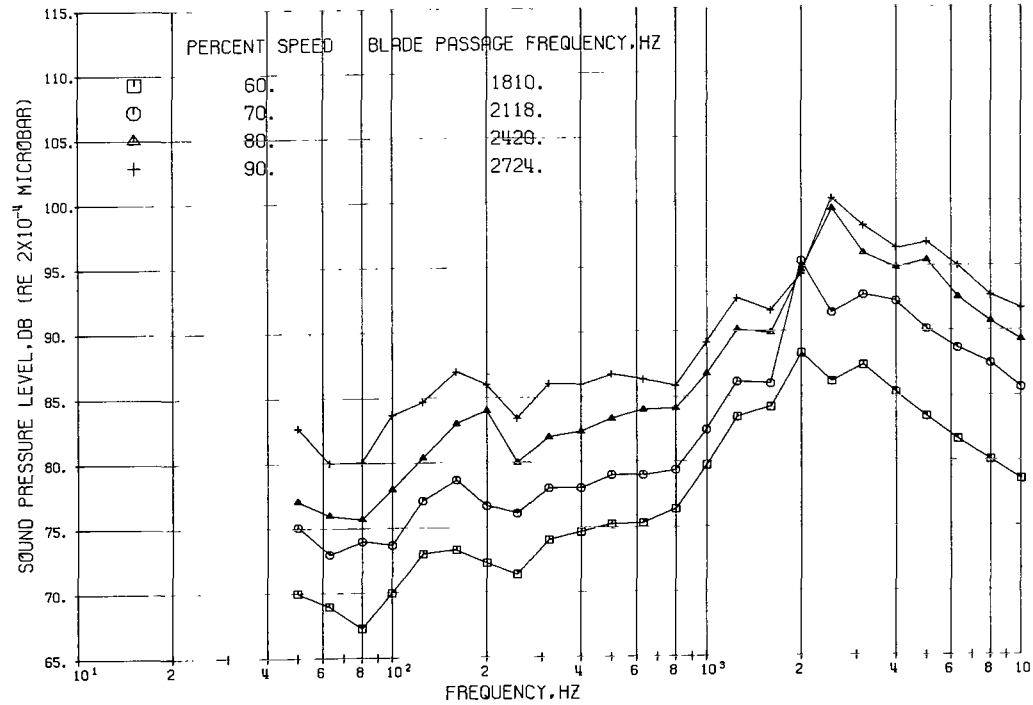

(i) Microphone location, 90°.

Figure 18. - Continued.

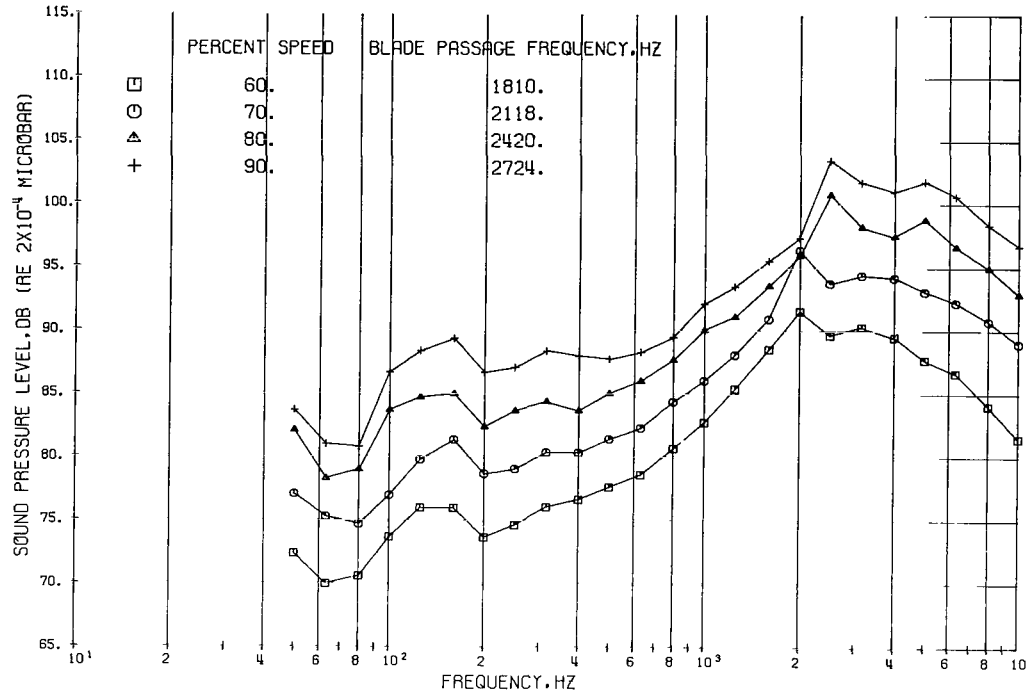

(j) Microphone location, 100°.

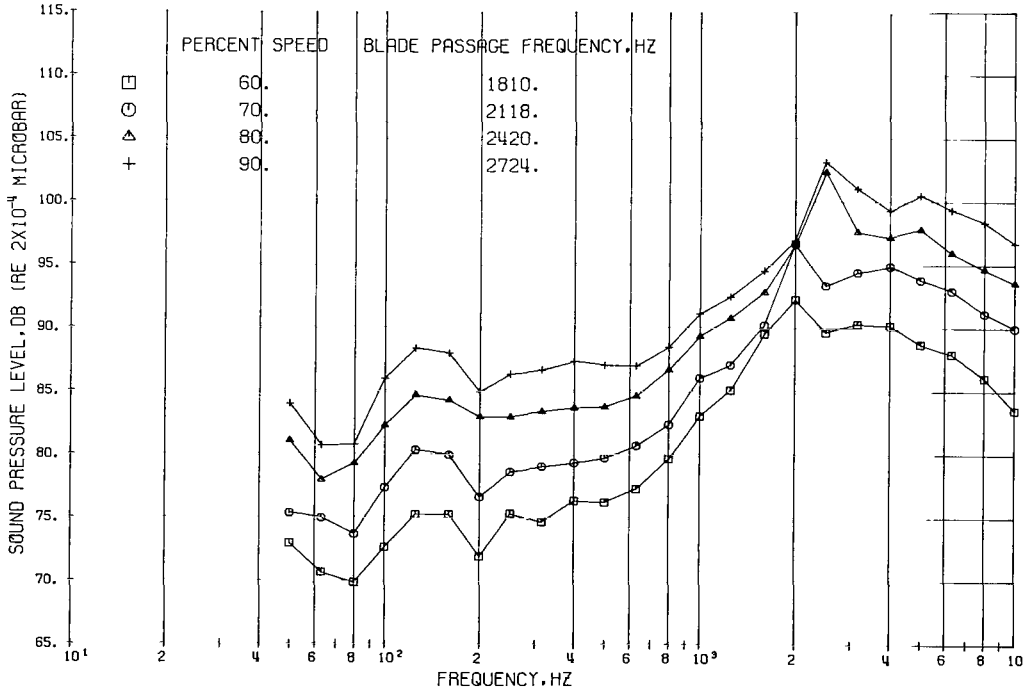

(k) Microphone location, 110°.

Figure 18. - Continued.

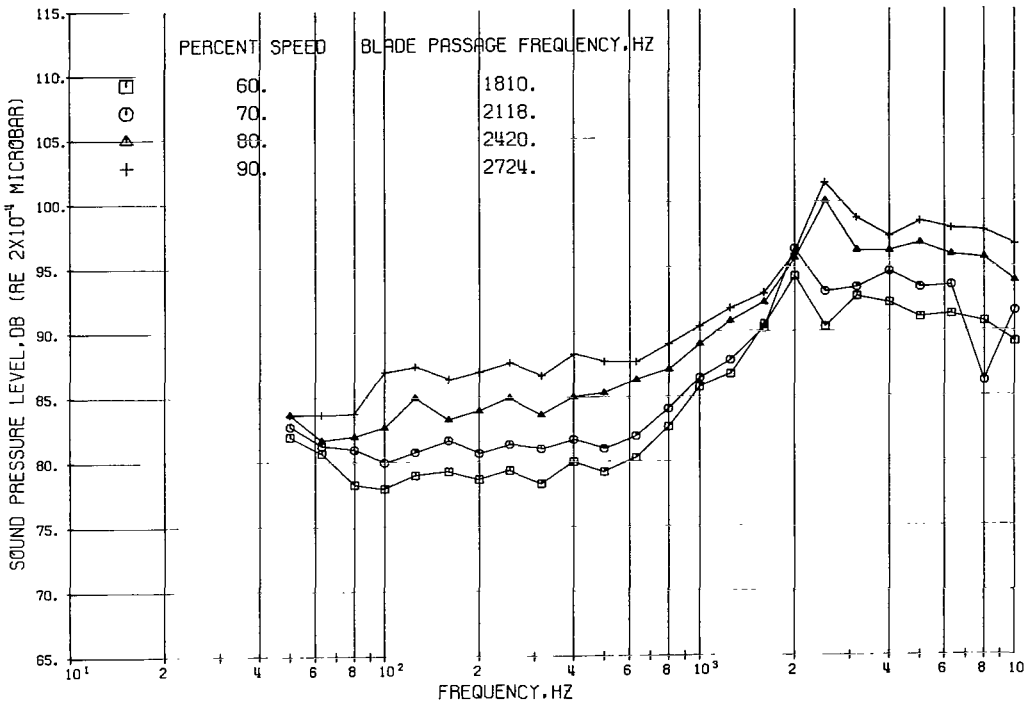

(l) Microphone location, 120°.

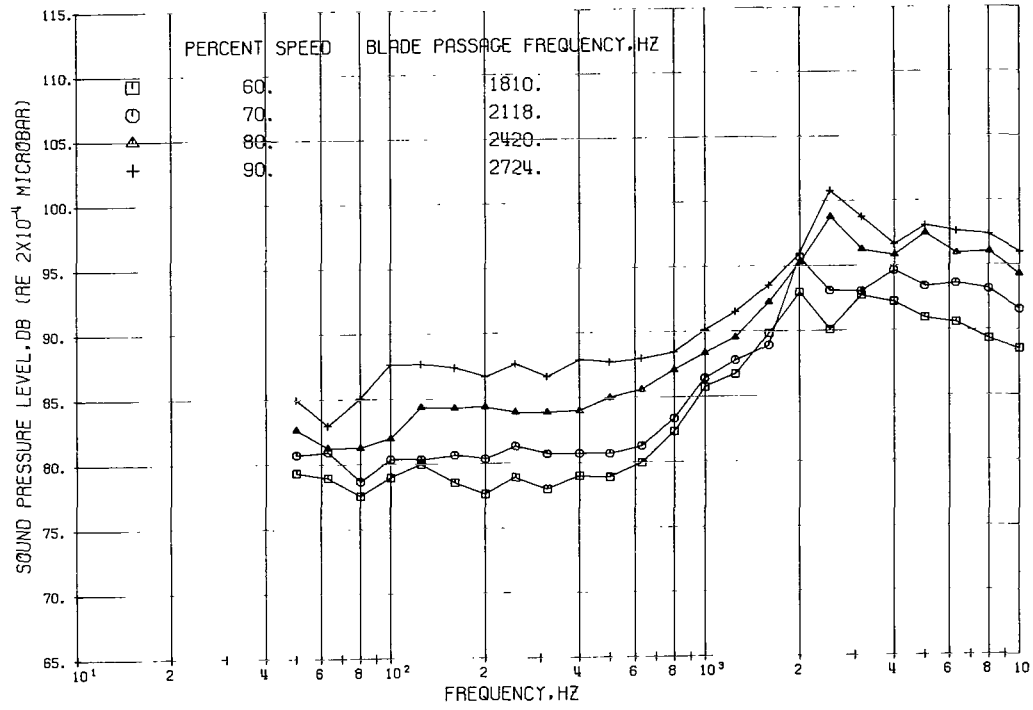

(m) Microphone location, 130°.

Figure 18. - Continued.

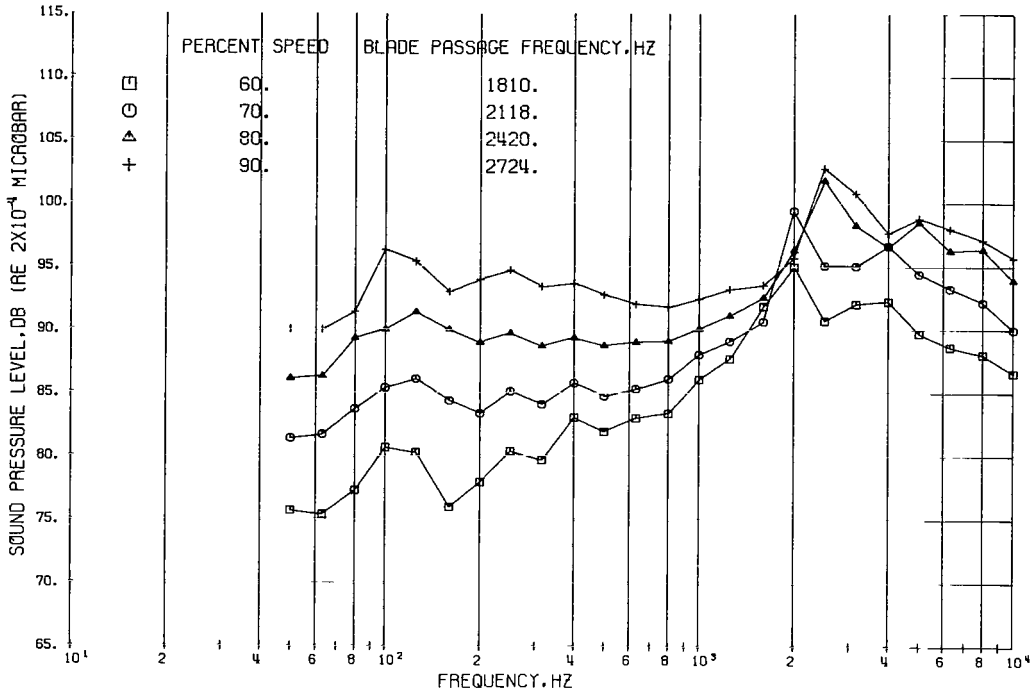

(n) Microphone location, 140°.

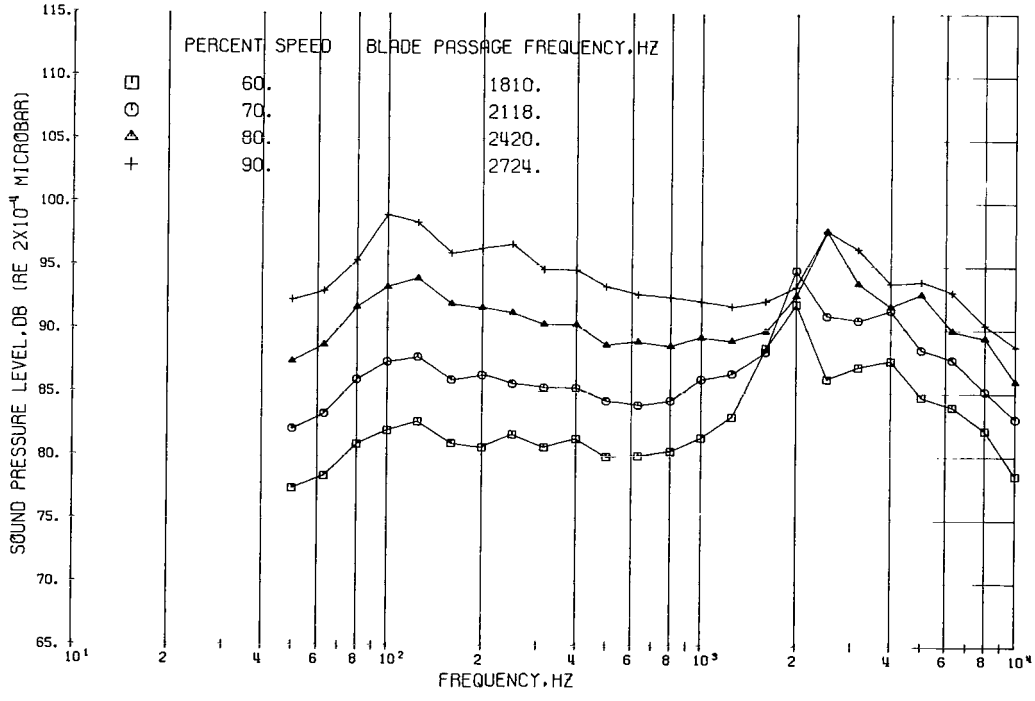

(o) Microphone location, 150°.

Figure 18. - Continued.

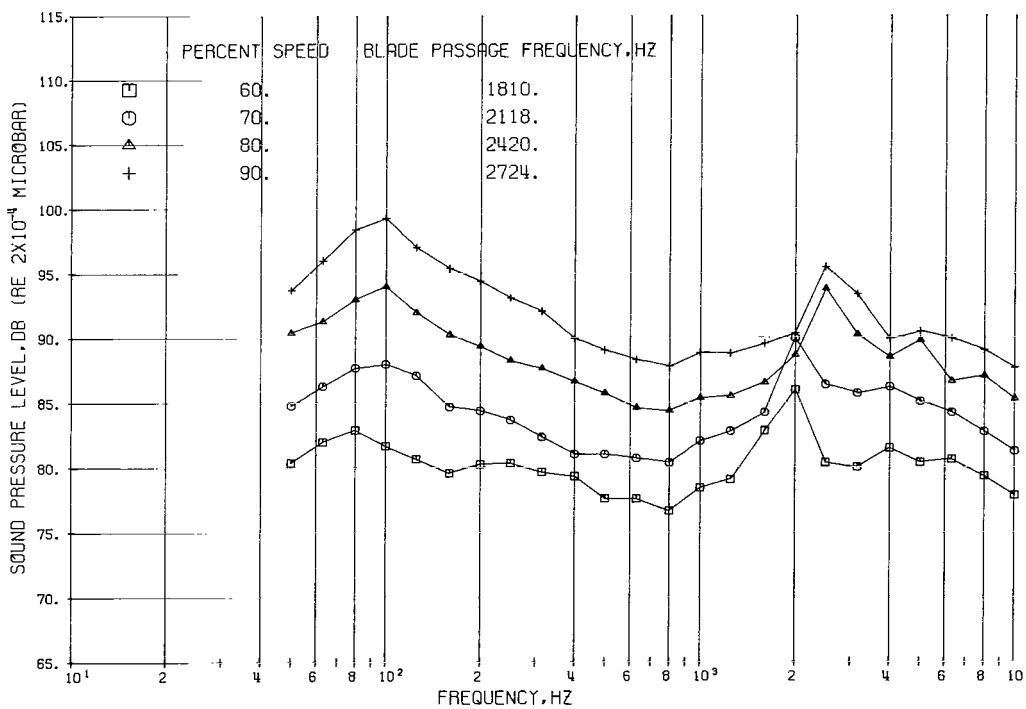

(p) Microphone location, 160°.

Figure 18. - Concluded.

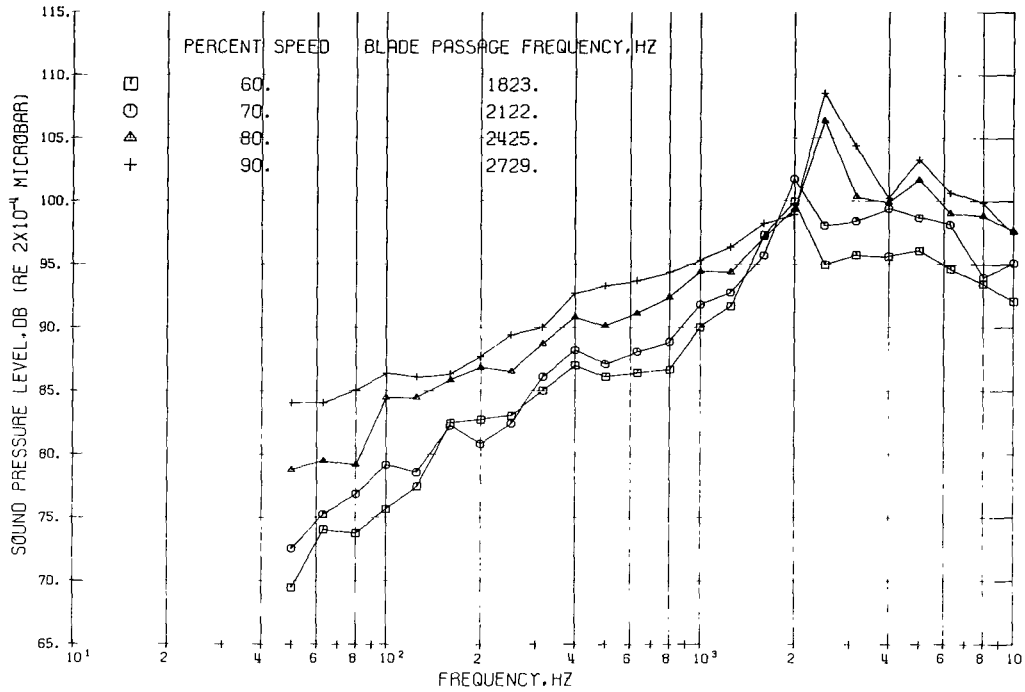

(a) Microphone location, 10°.

Figure 19. - Sound pressure levels on 100-foot (30.5-m) radius as function of frequency. Configuration 3; inlet cowl length, 127 inches (3.23 m); nozzle size, 97 percent of design area. (Microphone locations are given in degrees from shaft centerline.)

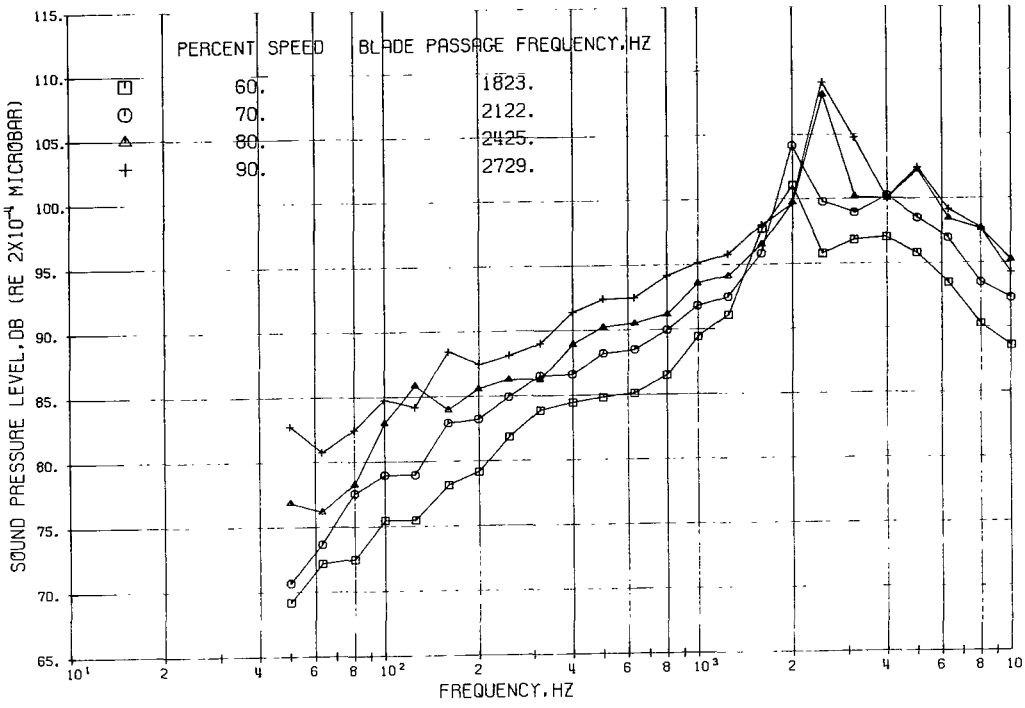

(b) Microphone location, 20°.

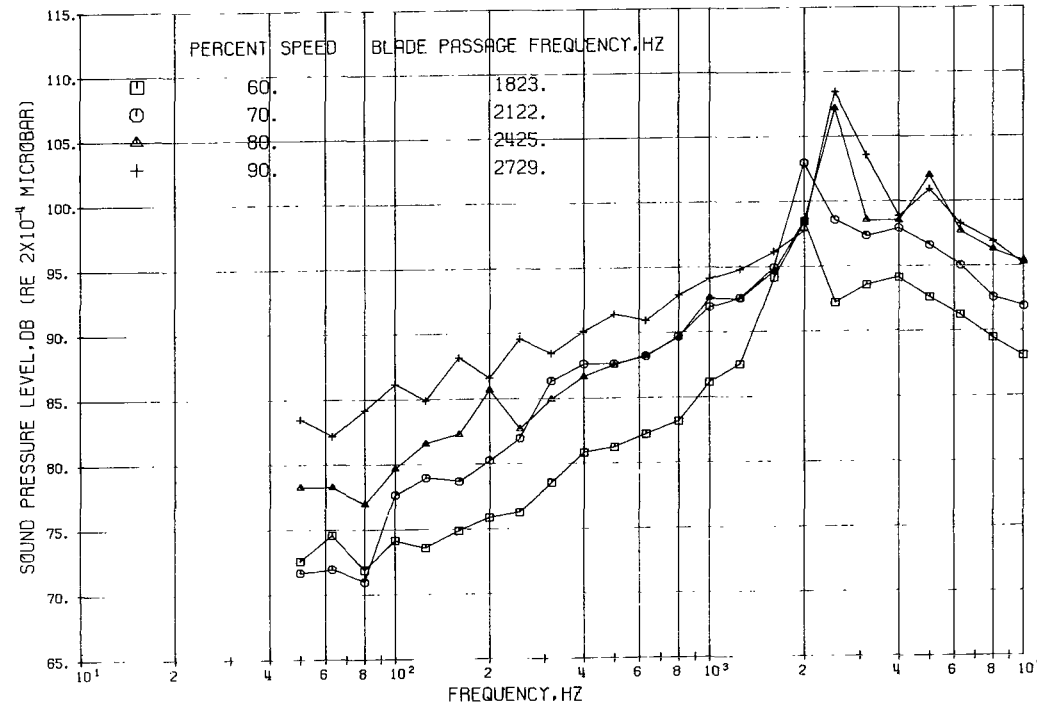

(c) Microphone location, 30°.

Figure 19. - Continued.

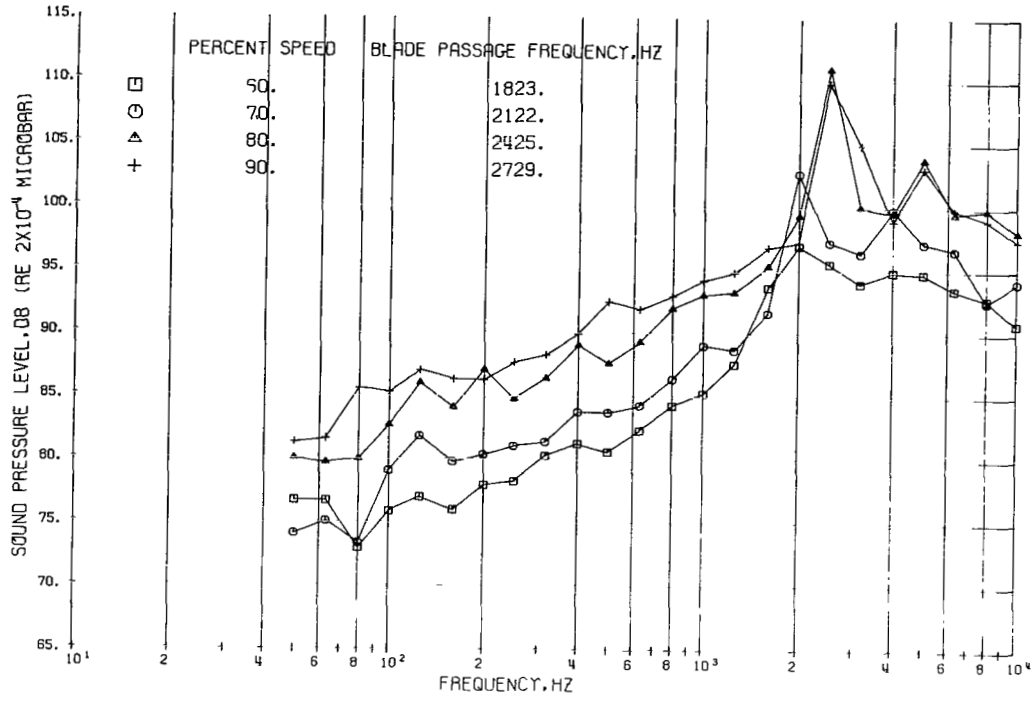

(d) Microphone location, 40°.

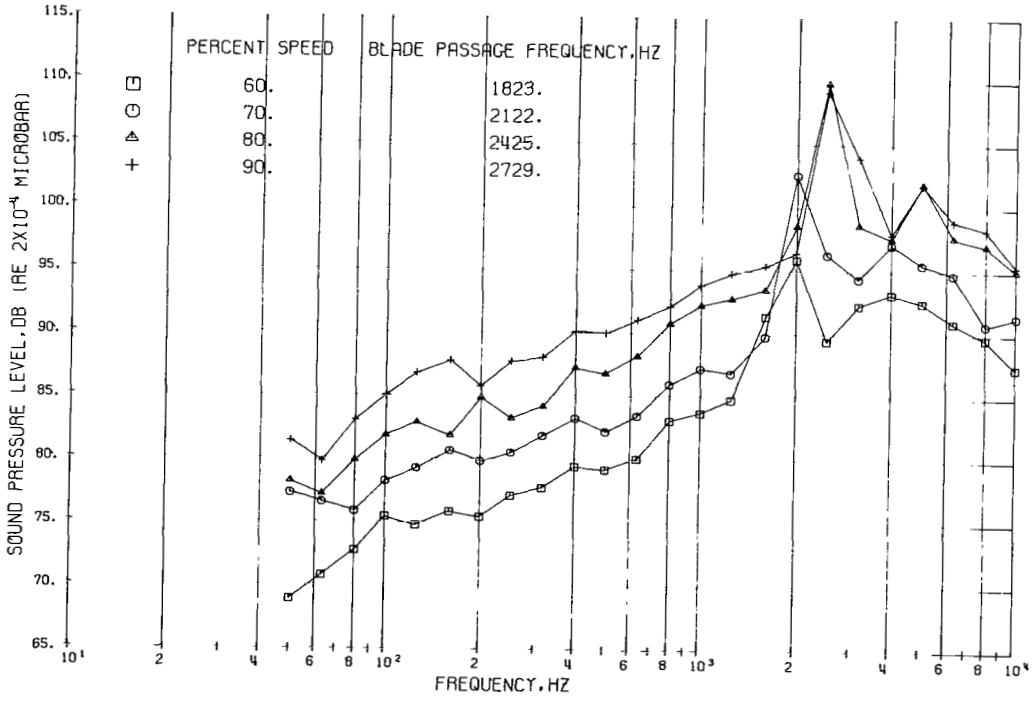

(e) Microphone location, 50°.

Figure 19. - Continued.

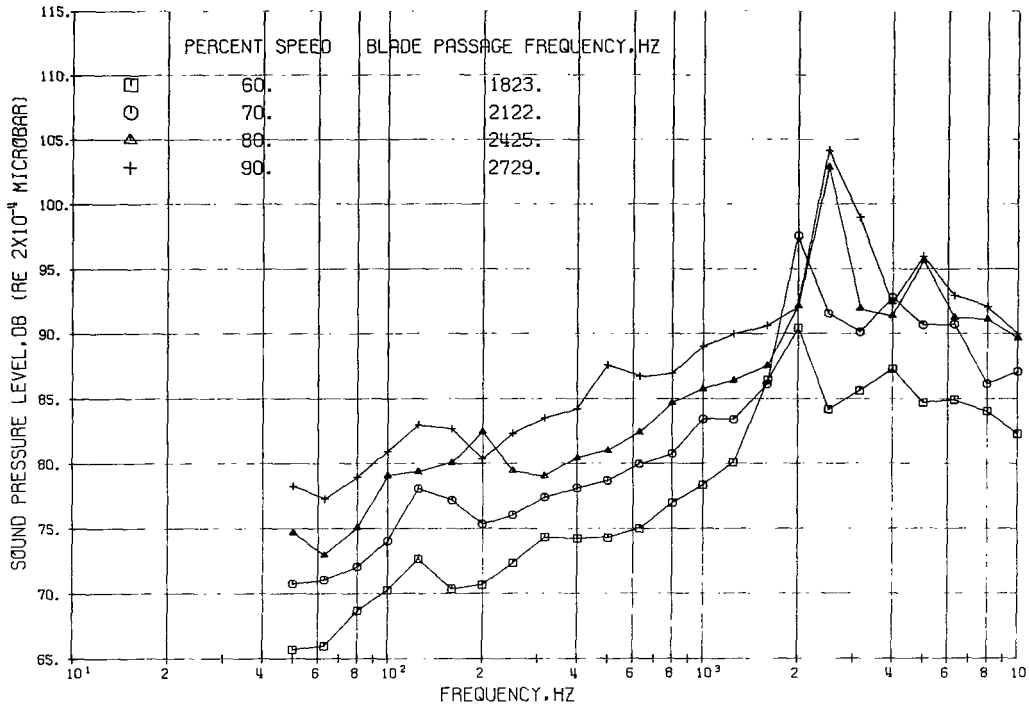

(f) Microphone location, 60°.

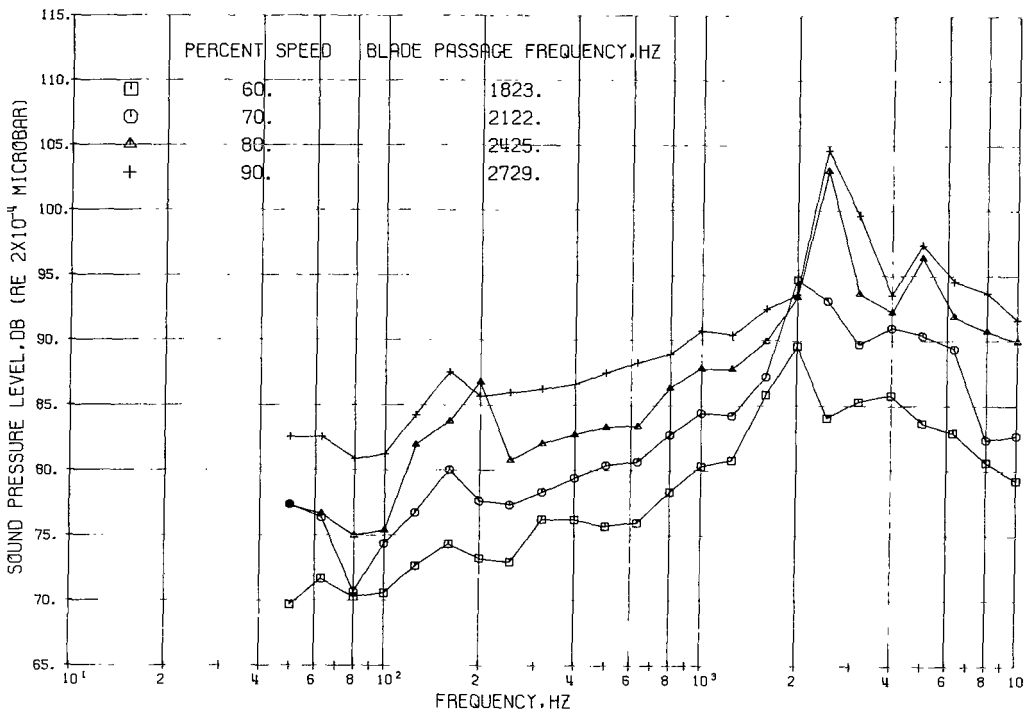

(g) Microphone location, 70°.

Figure 19. - Continued.

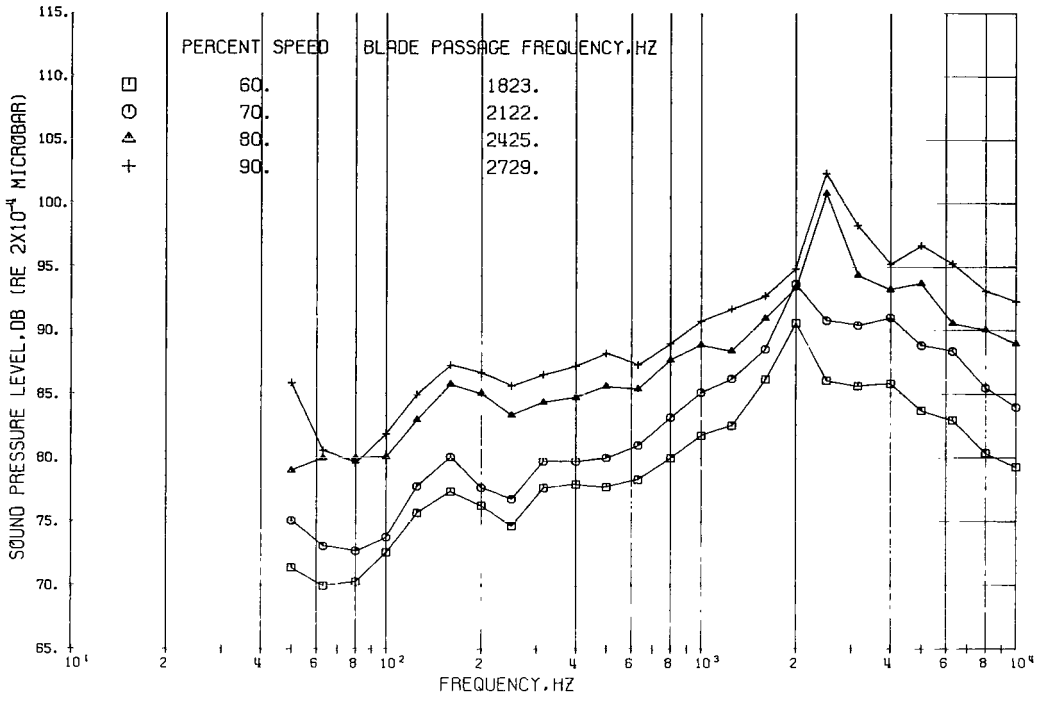

(h) Microphone location, 80°.

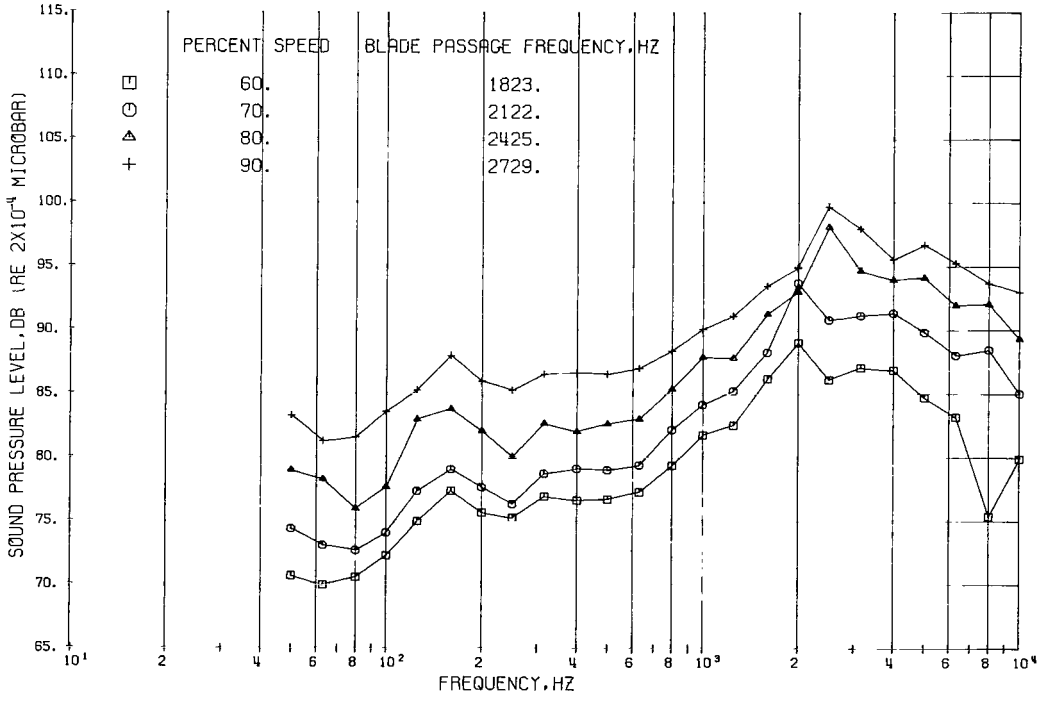

(i) Microphone location, 90°.

Figure 19. - Continued.

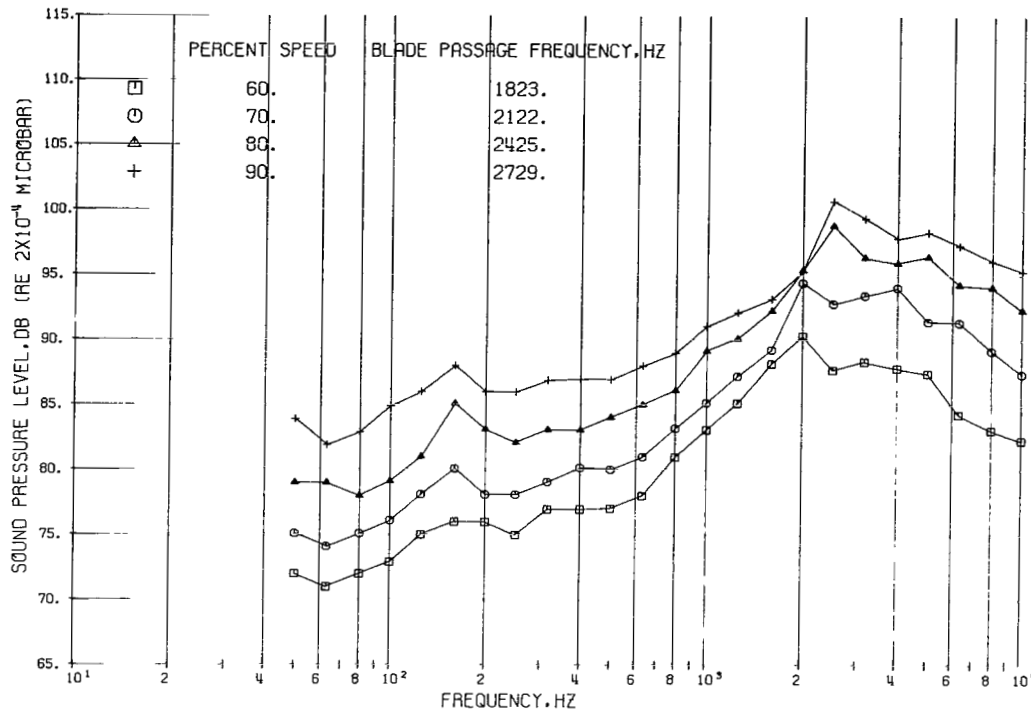

(j) Microphone location, 100°.

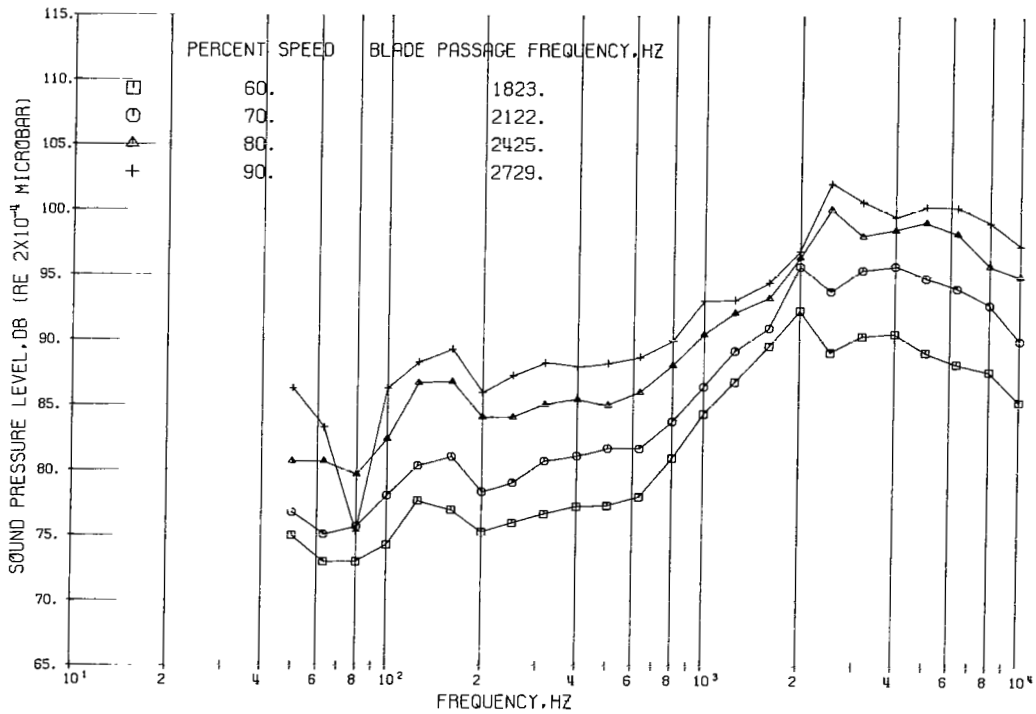

(k) Microphone location, 110°.

Figure 19. - Continued.

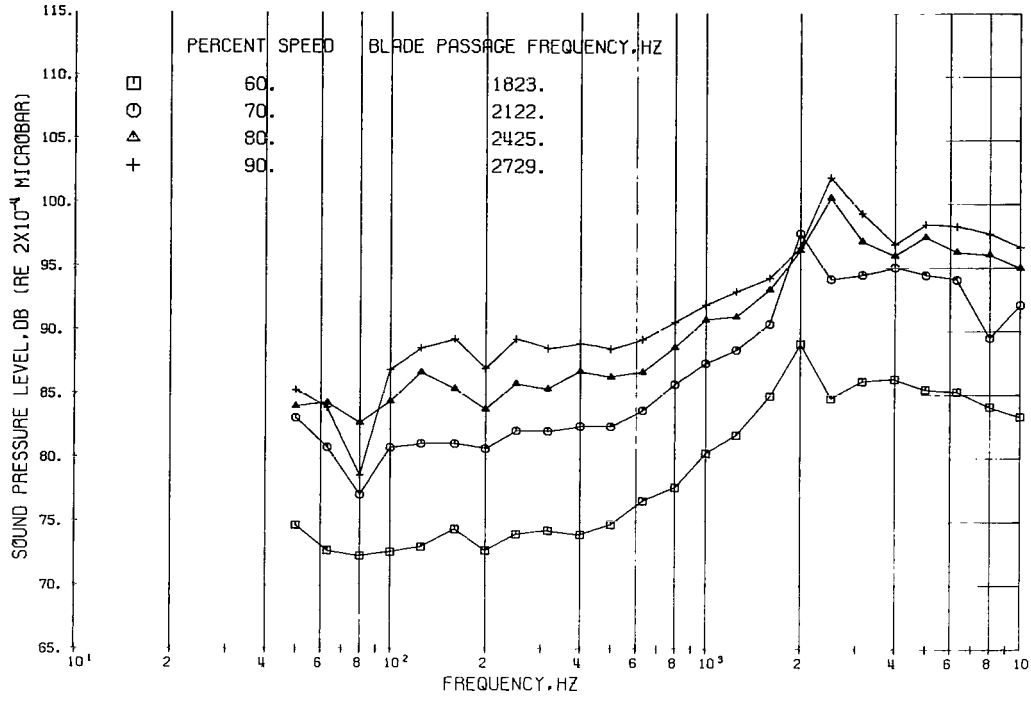

(l) Microphone location, 120°.

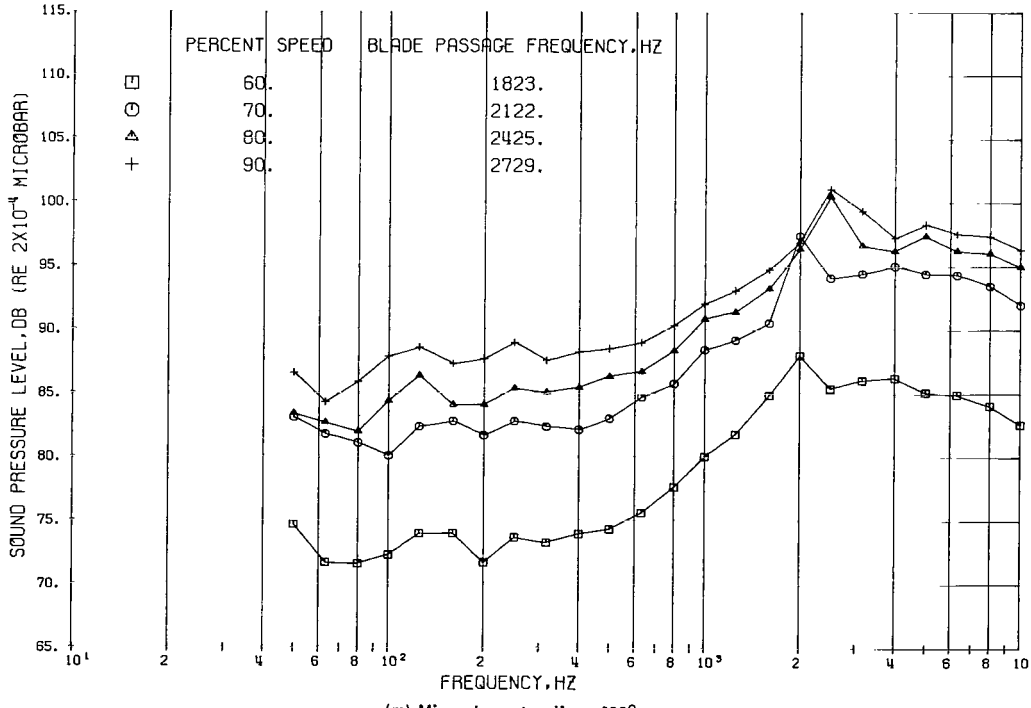

(m) Microphone location, 130°.

Figure 19. - Continued.

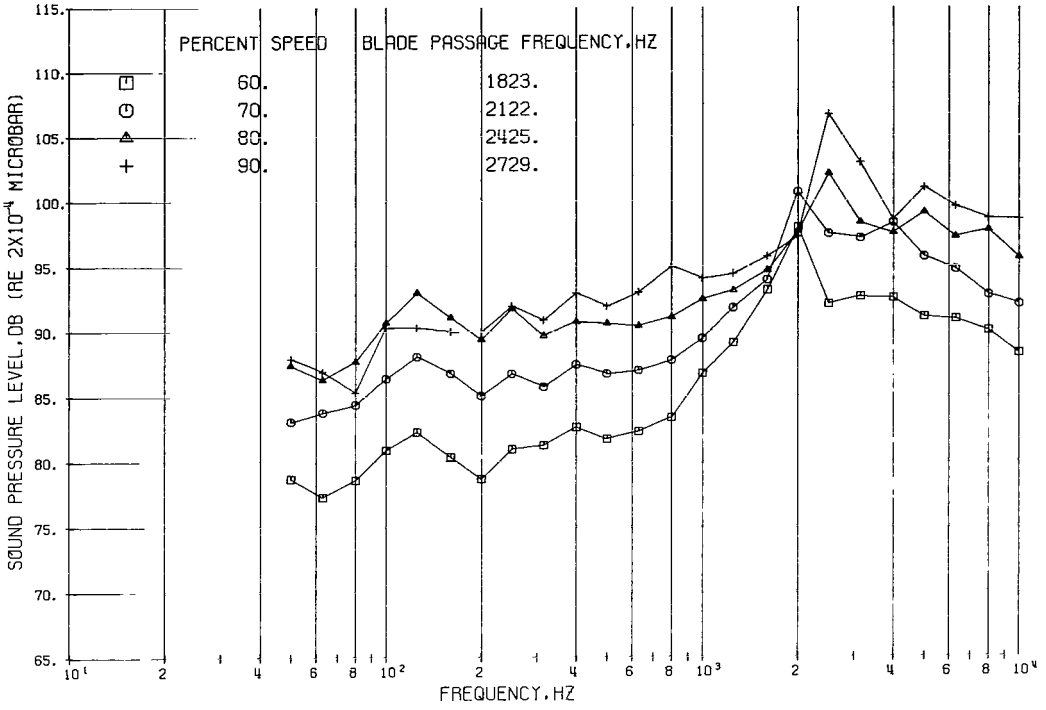

(n) Microphone location, 140°.

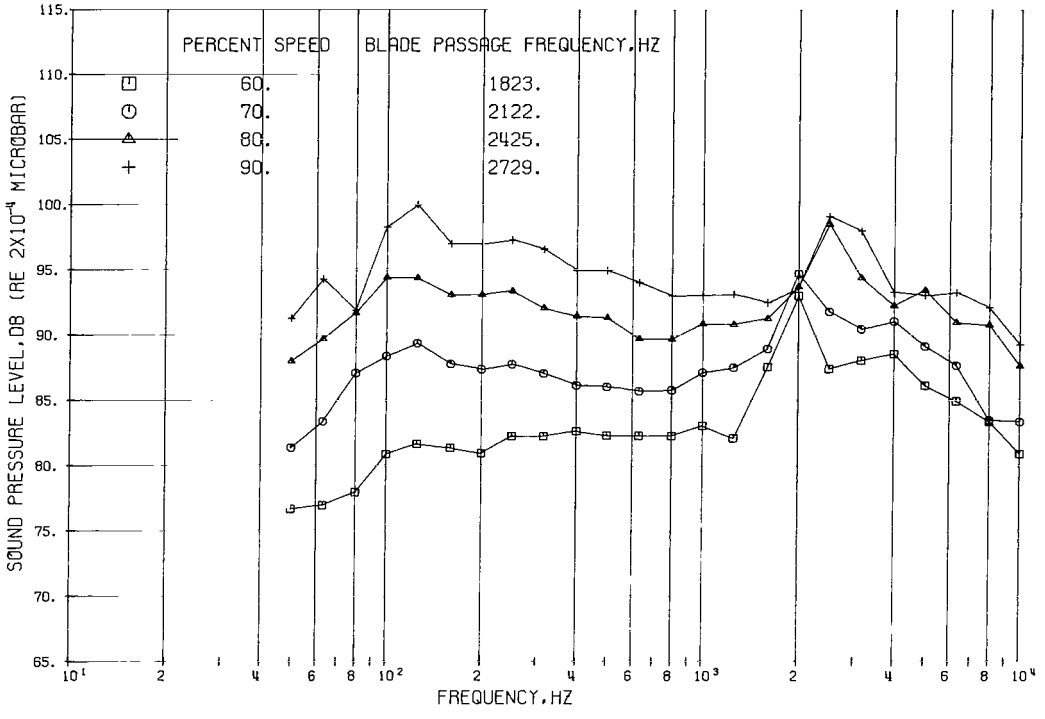

(o) Microphone location, 150°.

Figure 19. - Continued.

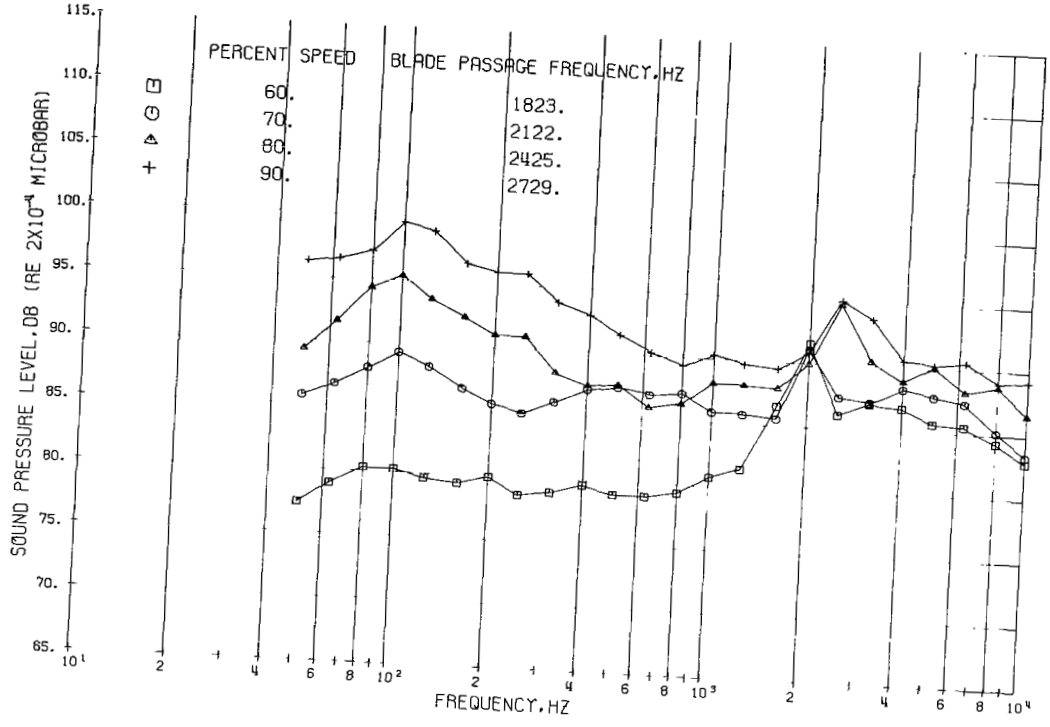

(p) Microphone location, 160°.

Figure 19. - Concluded.

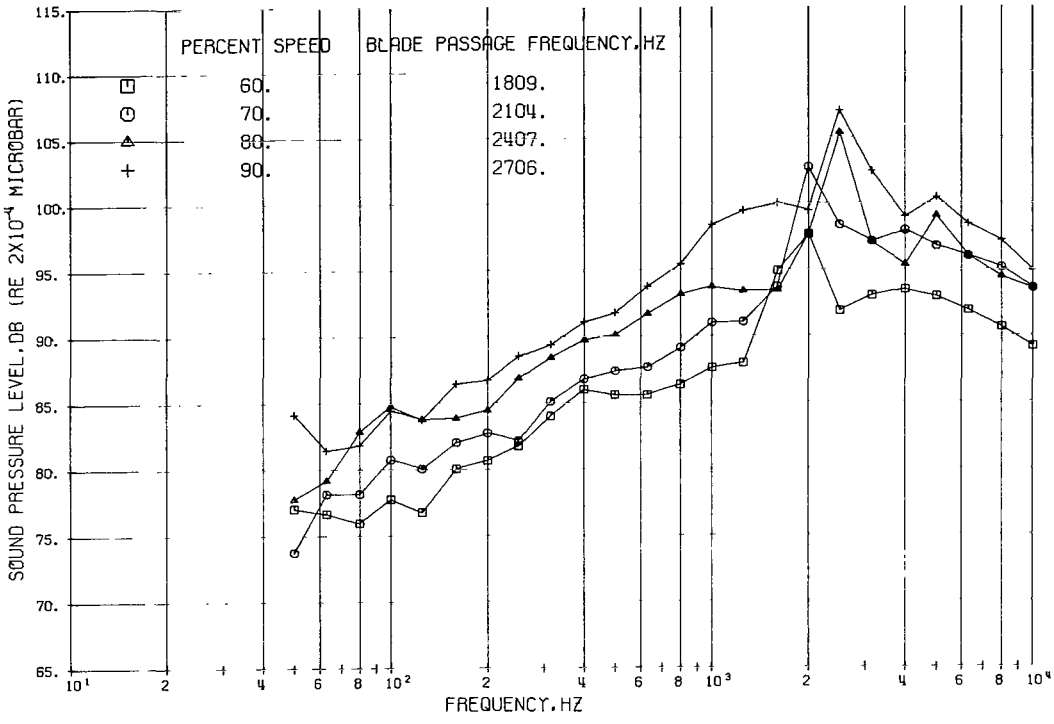

(a) Microphone location, 10°.

Figure 20. - Sound pressure levels on 100-foot (30.5-m) radius as function of frequency. Configuration 4: inlet cowl length, 127 inches (3.23 m); nozzle size, 110 percent of design area. (Microphone locations are given in degrees from shaft centerline.)

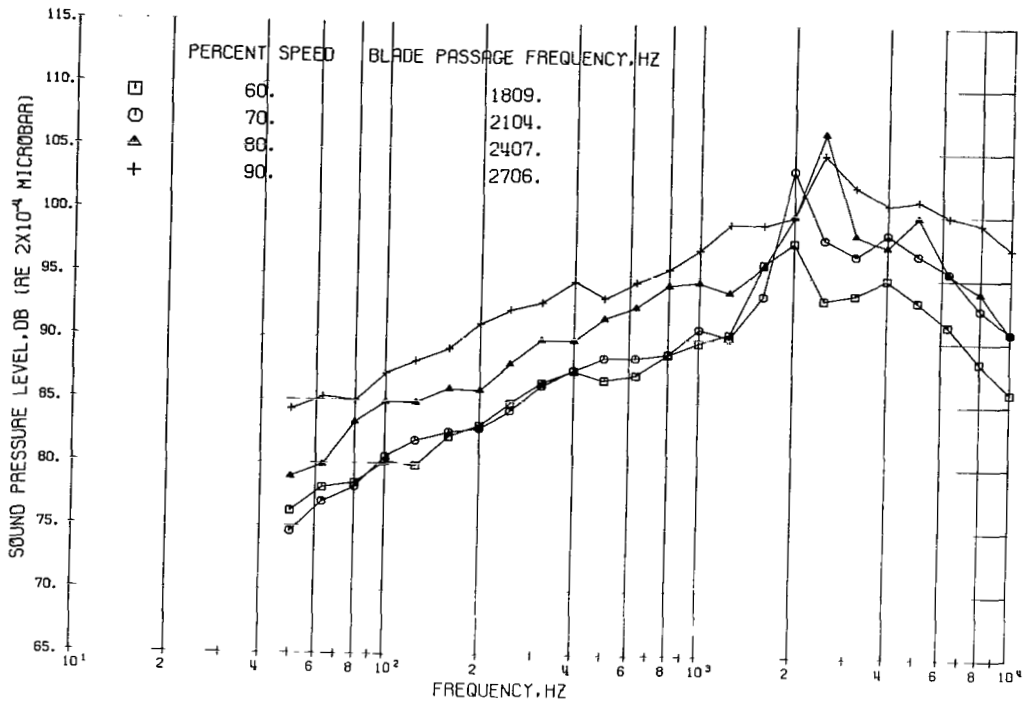

(b) Microphone location, 20°.

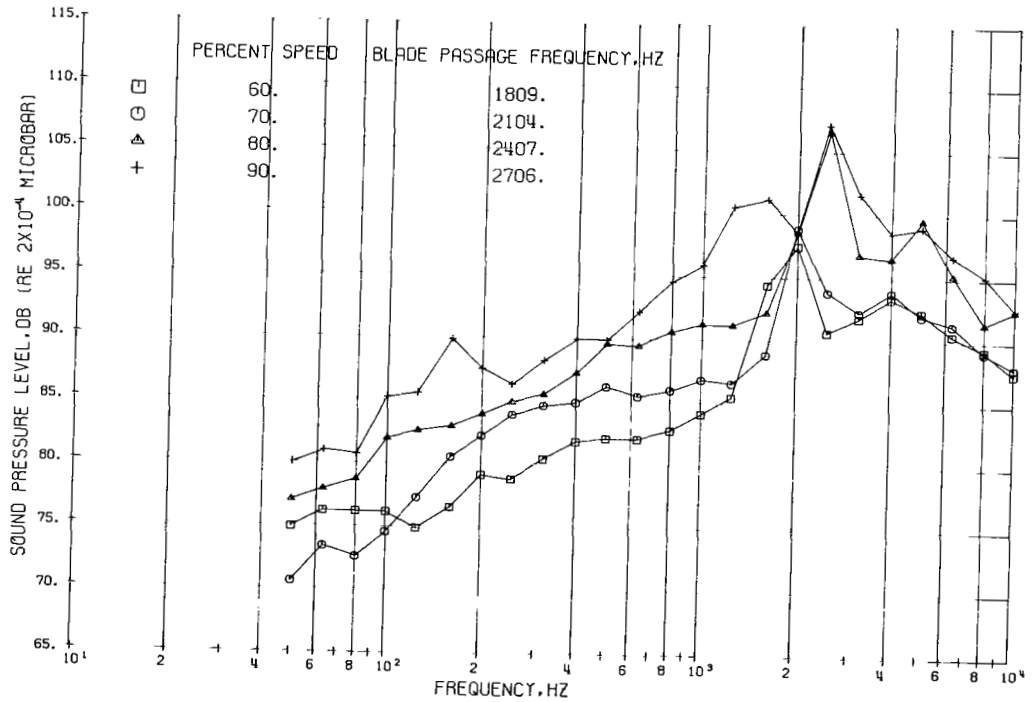

(c) Microphone location, 30°.

Figure 20. - Continued.

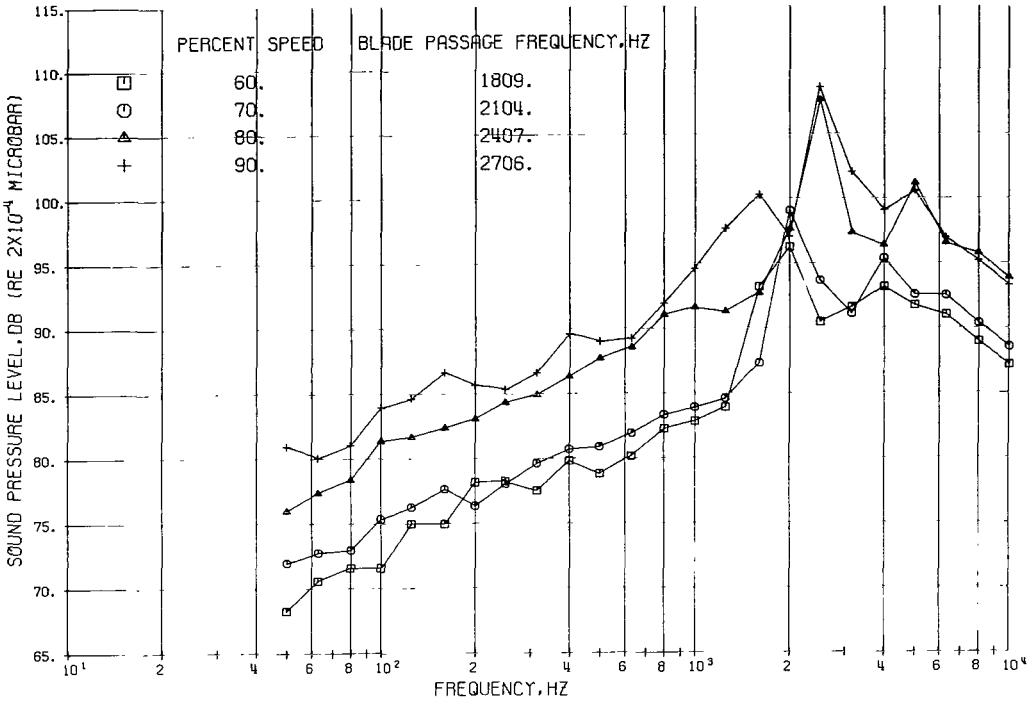

(d) Microphone location, 40°.

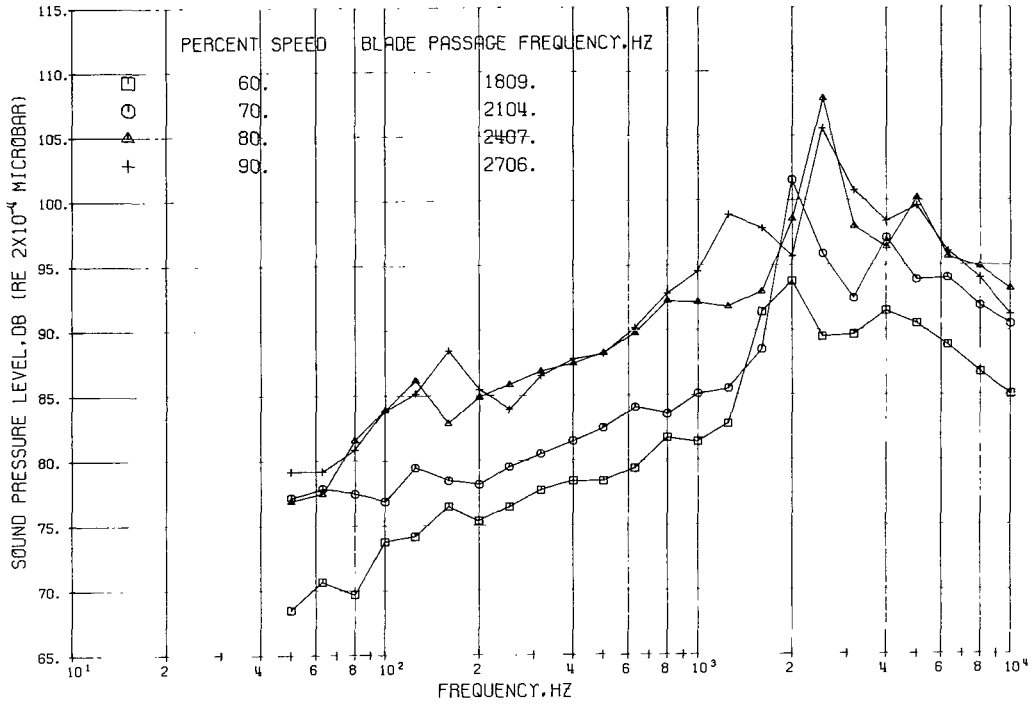

(e) Microphone location, 50°.

Figure 20. - Continued.

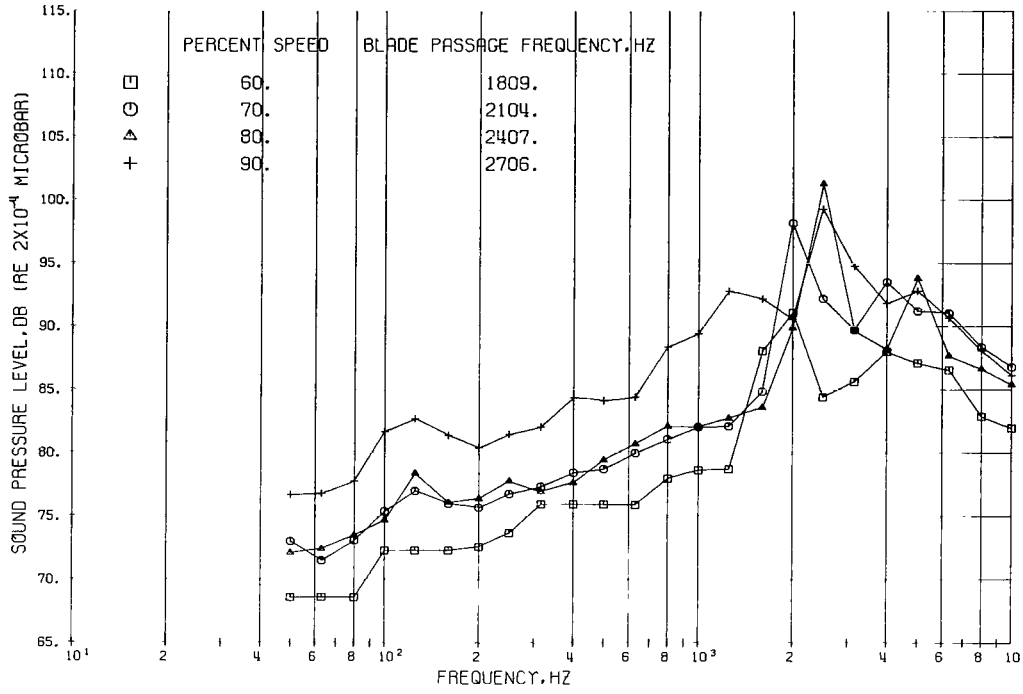

(f) Microphone location, 60°.

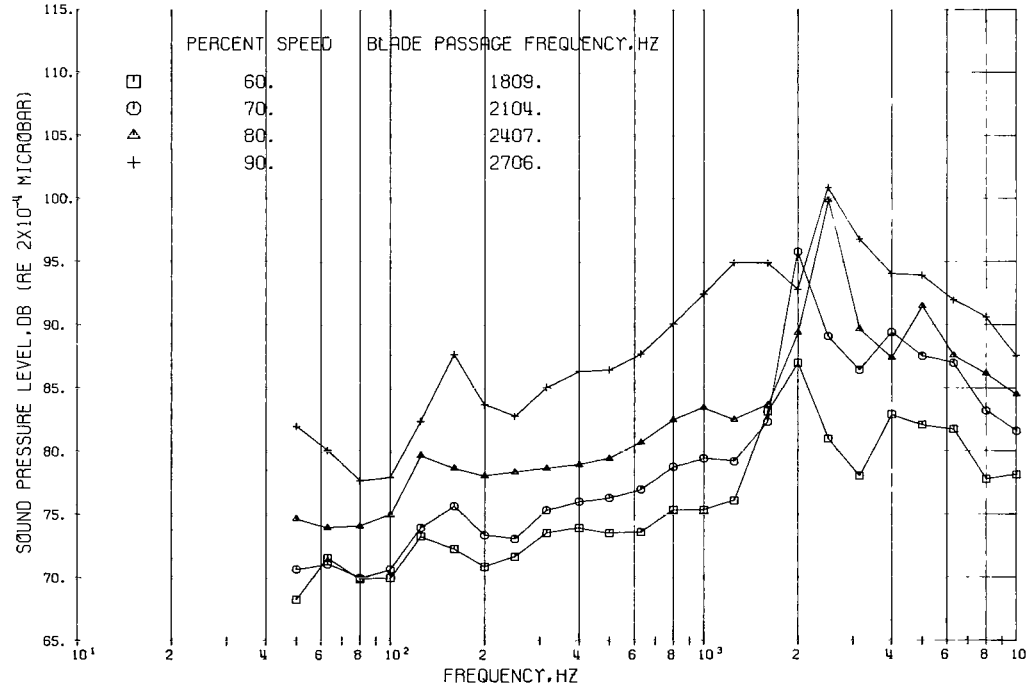

(g) Microphone location, 70°.

Figure 20. - Continued.

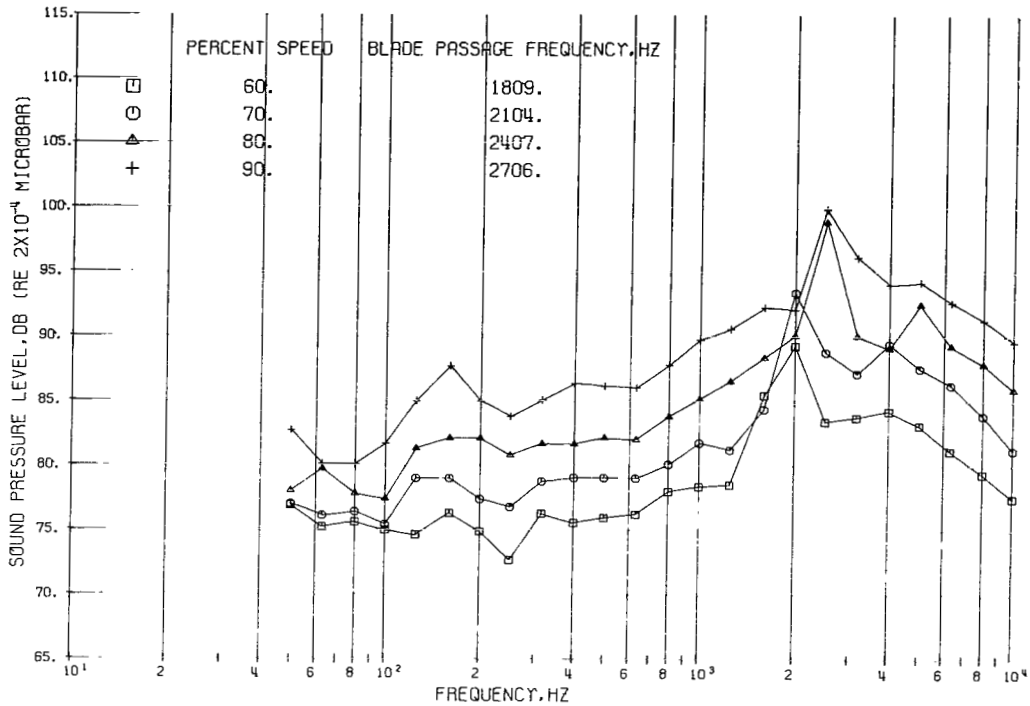

(h) Microphone location, 80°.

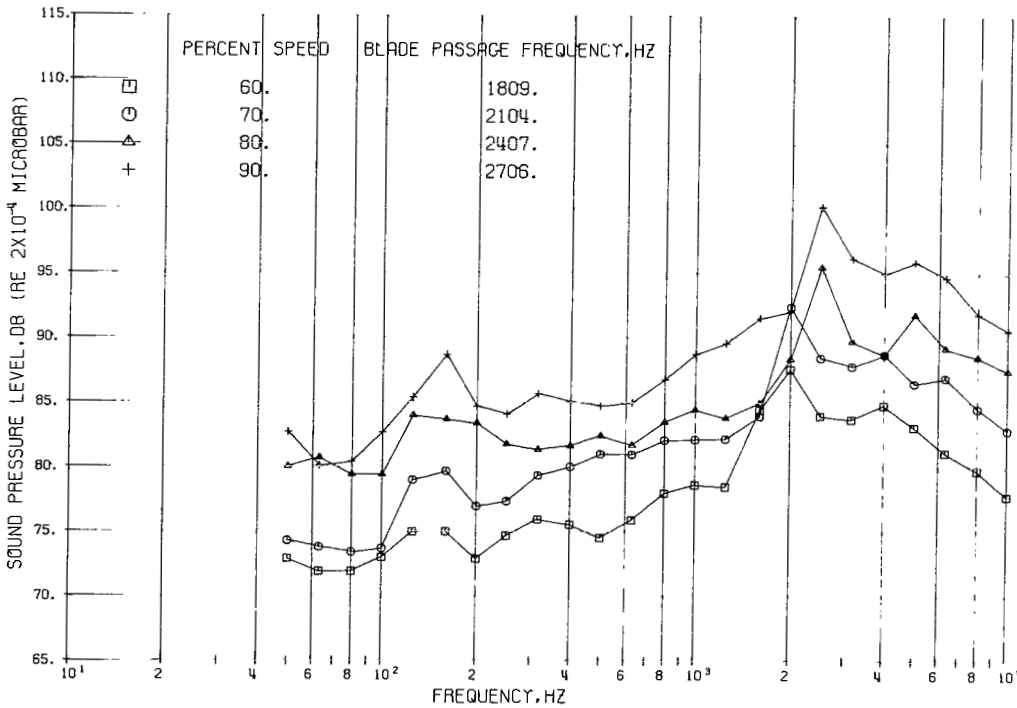

(i) Microphone location, 90°.

Figure 20. - Continued.

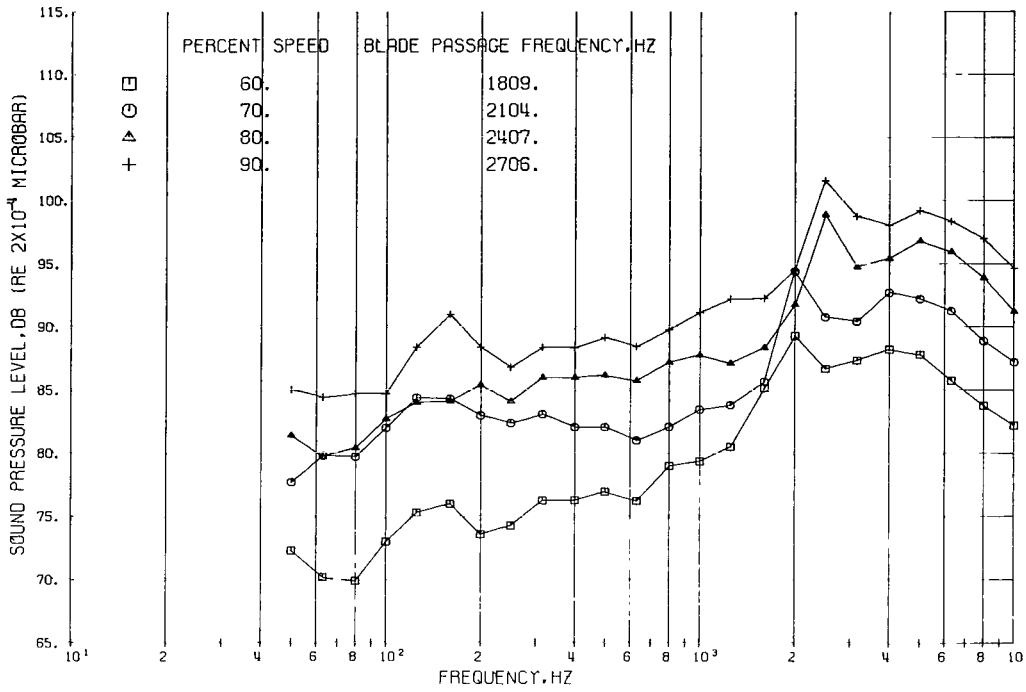

(j) Microphone location, 100°.

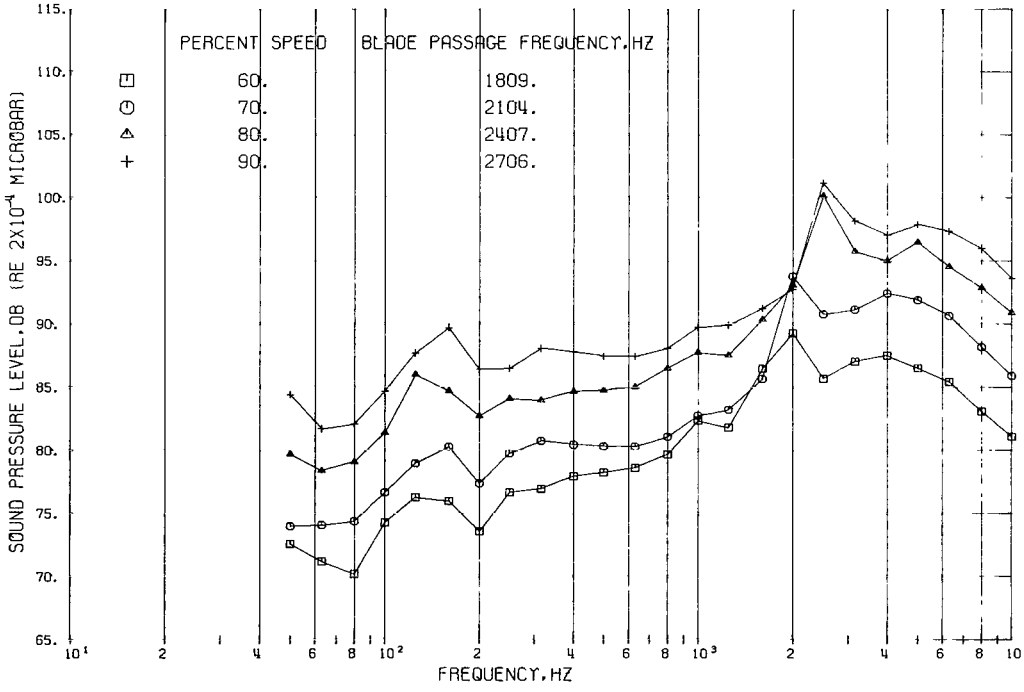

(k) Microphone location, 110°.

Figure 20. - Continued.

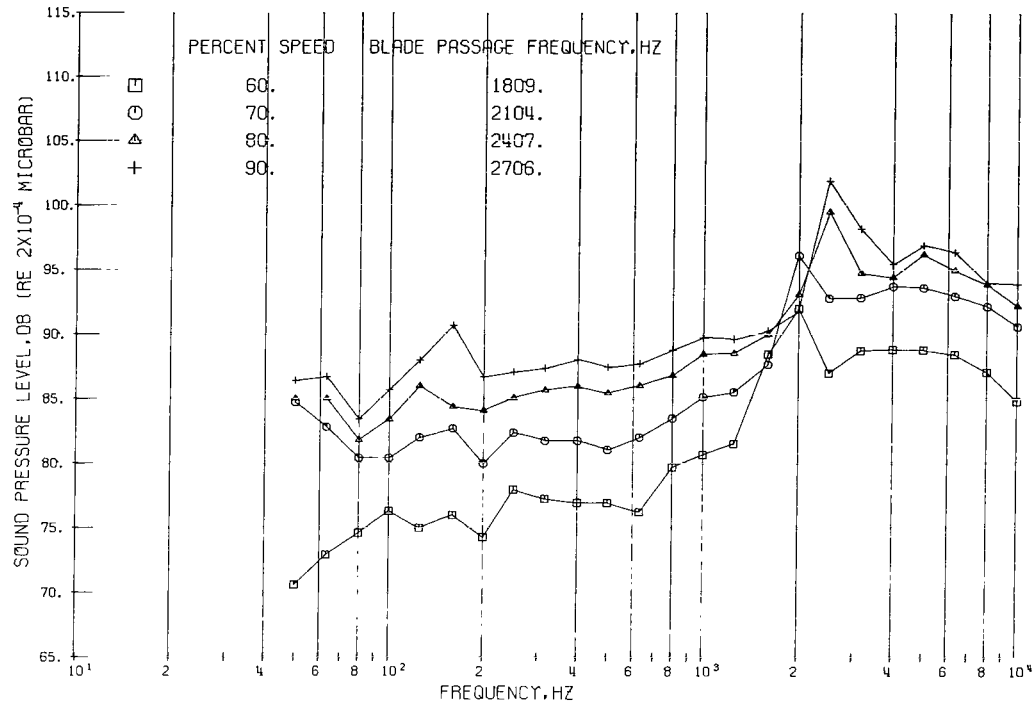

(l) Microphone location, 120°.

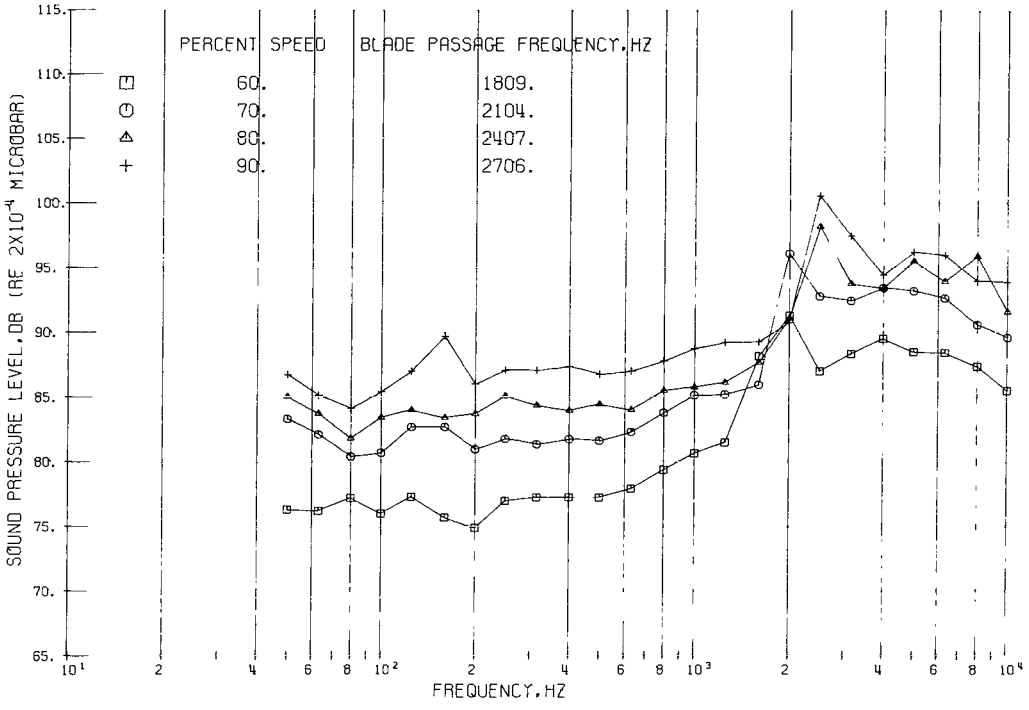

(m) Microphone location, 130°.

Figure 20. - Continued.

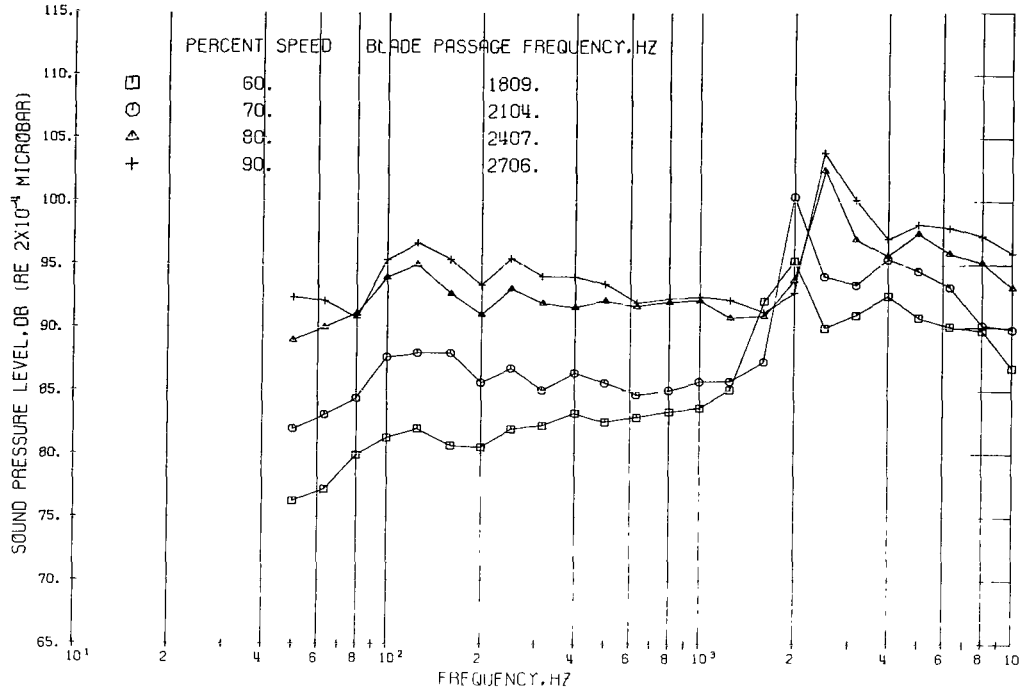

(n) Microphone location, 140°.

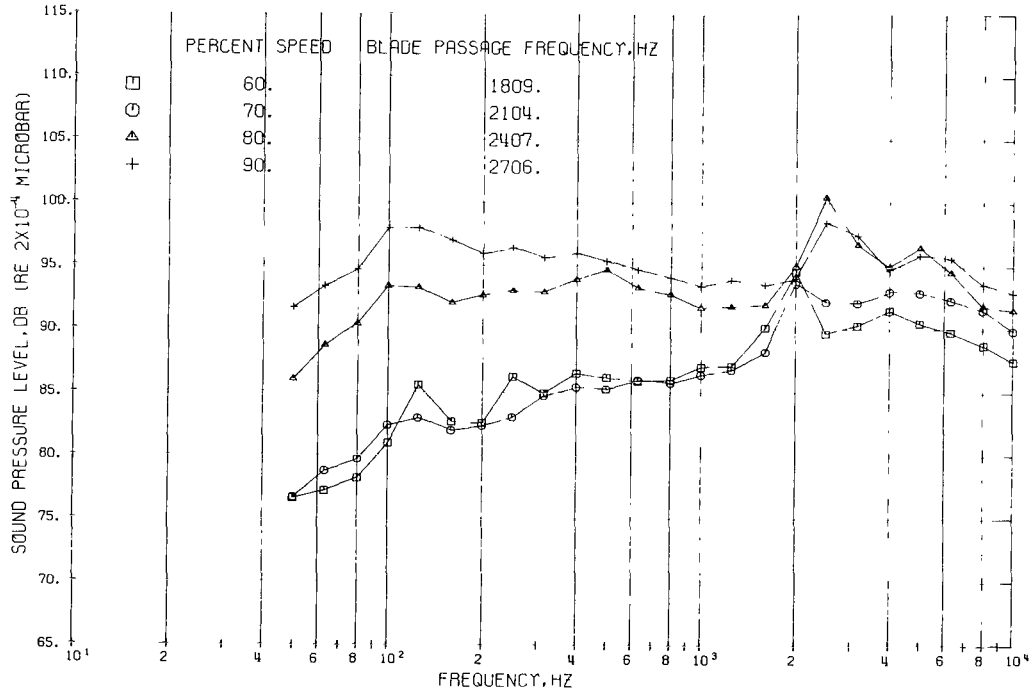

(o) Microphone location, 150°.

Figure 20. - Continued.

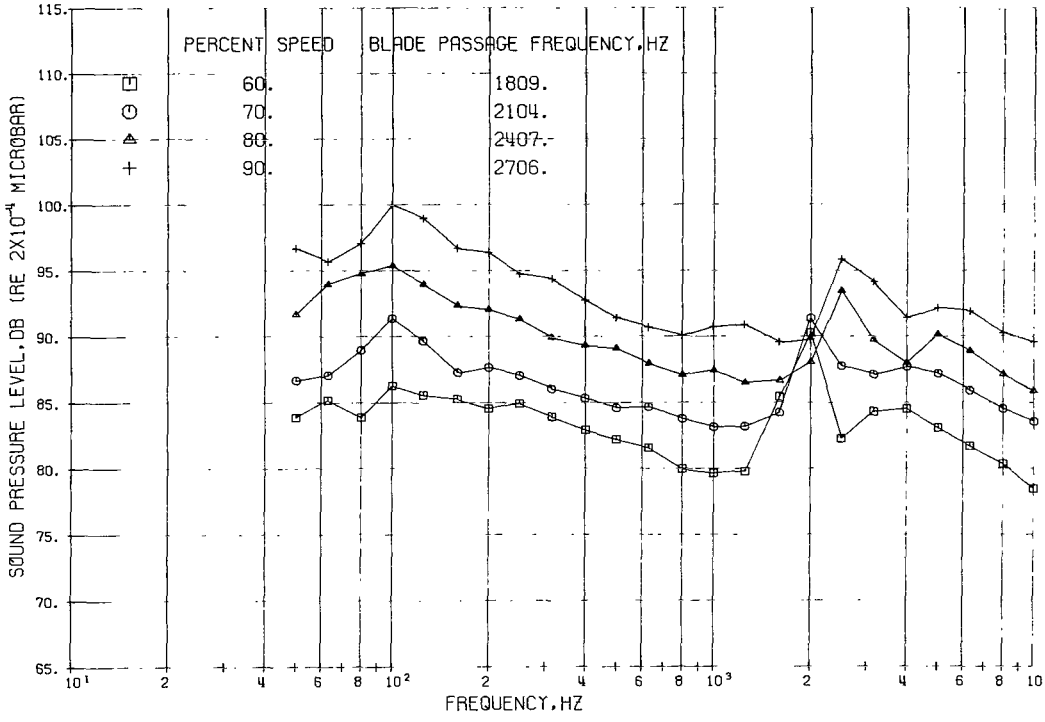

(p) Microphone location, 160°.

Figure 20. - Concluded.

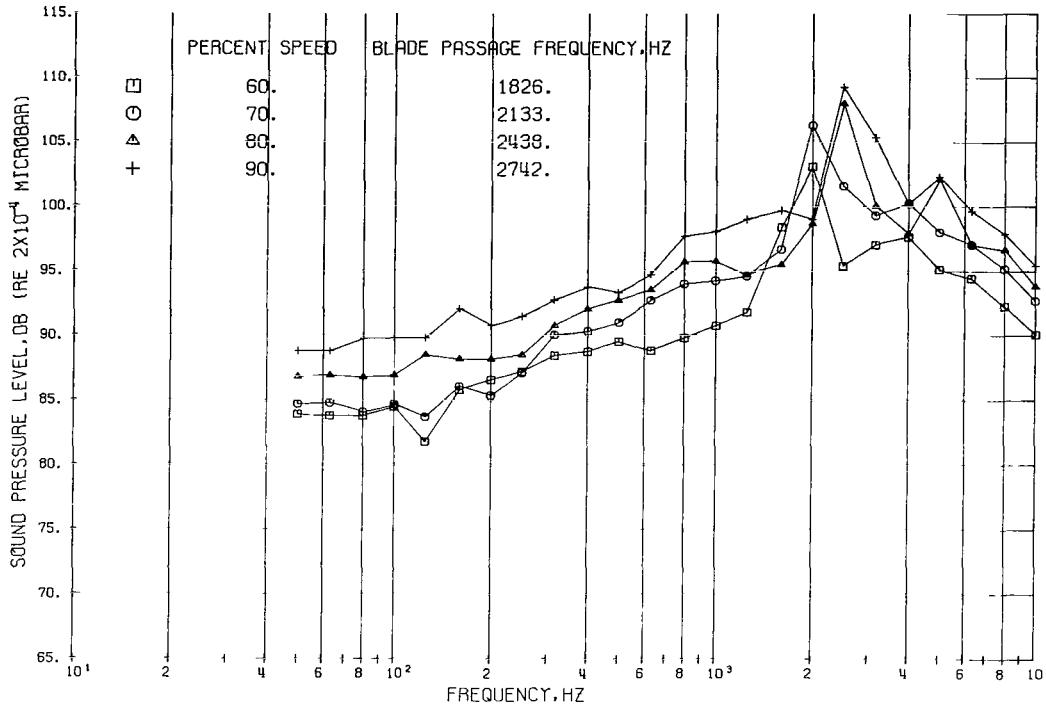

(a) Microphone location, 10°.

Figure 21. - Sound pressure levels on 100-foot (30.5-m) radius as function of frequency. Configuration 5: inlet cowl length, 86 inches (2.18 m); nozzle size, 124 percent of design area. (Microphone locations are given in degrees from shaft centerline.)

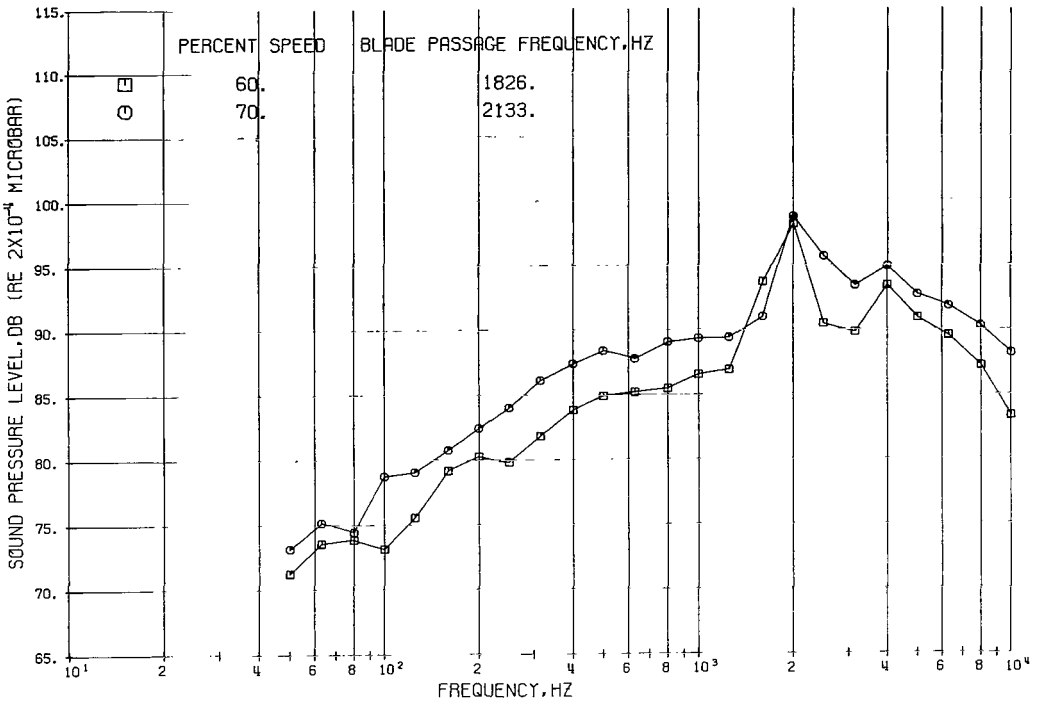

(b) Microphone location, 20°.

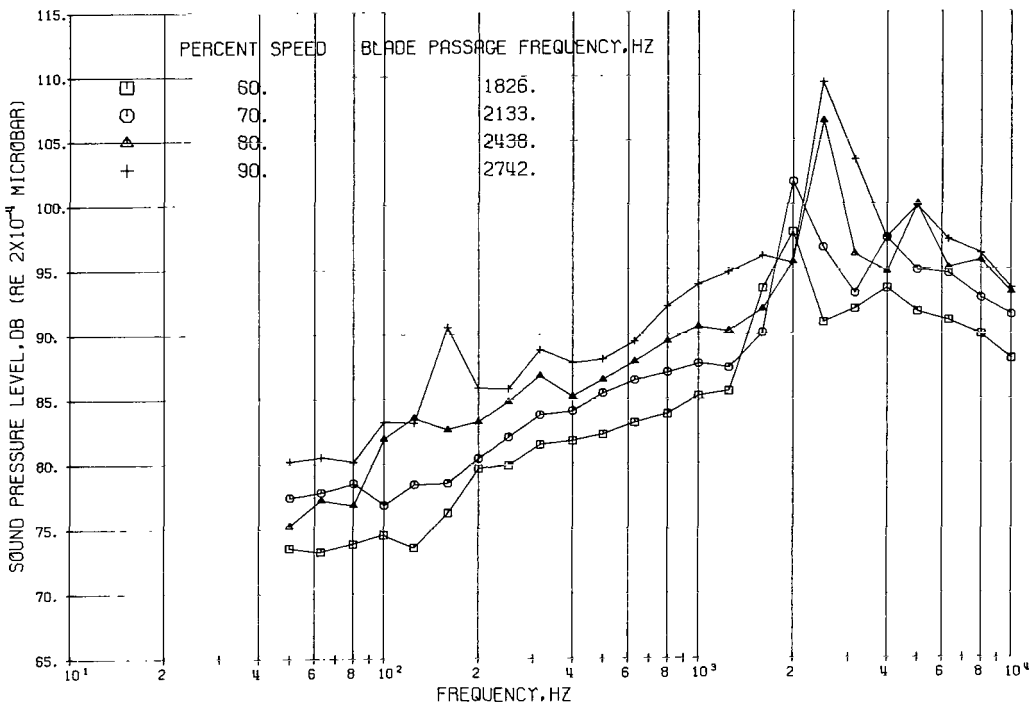

(c) Microphone location, 30°.

Figure 21. - Continued.

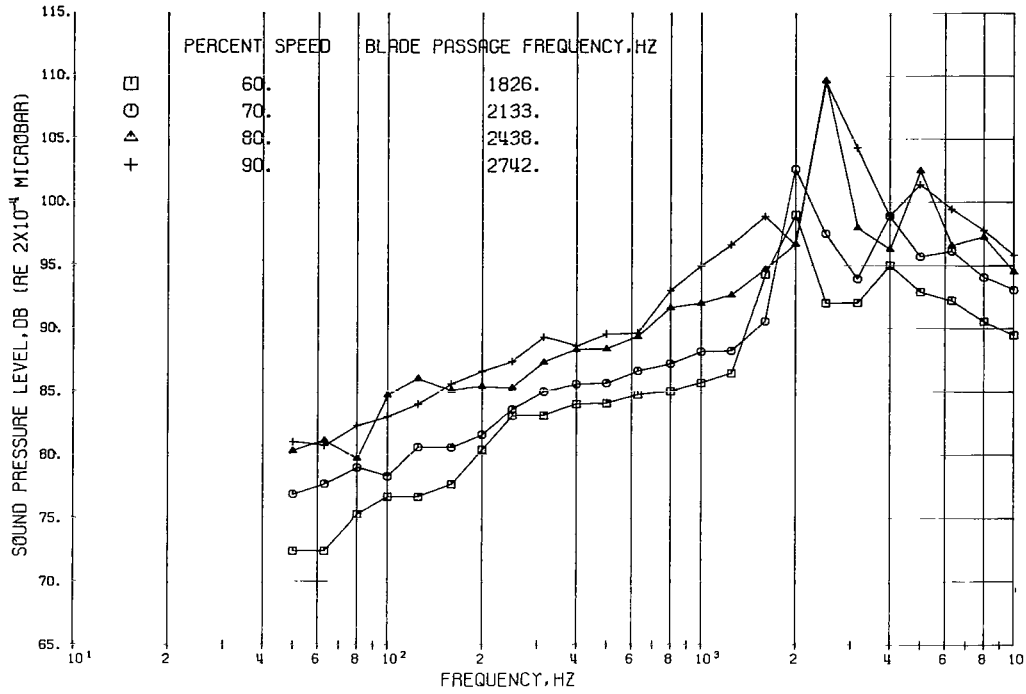

(d) Microphone location, 40°.

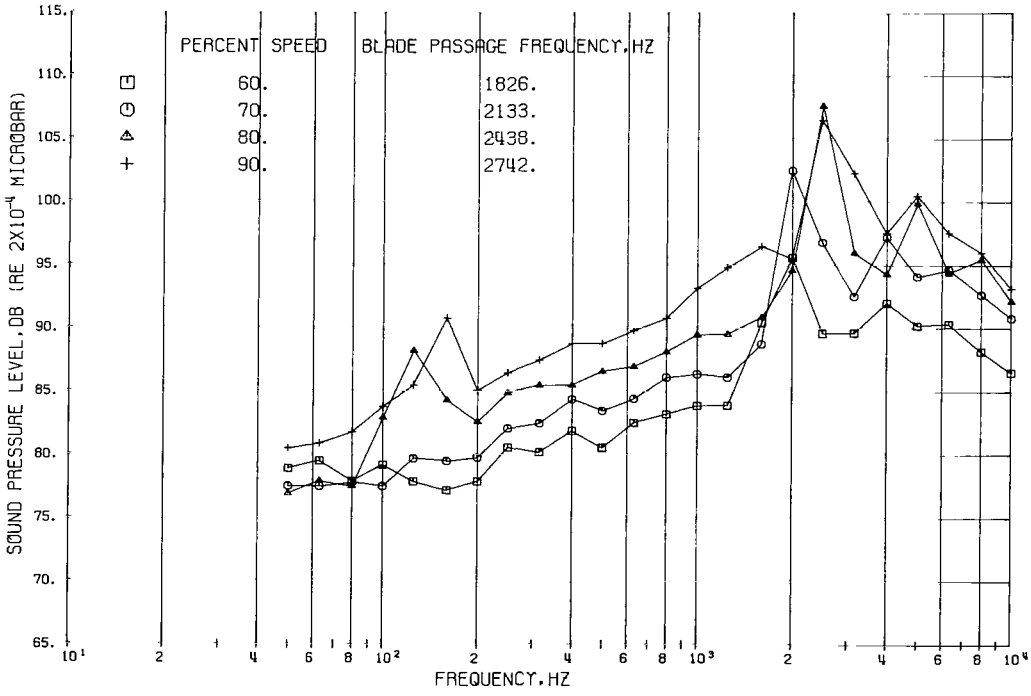

(e) Microphone location, 50°.

Figure 21. - Continued.

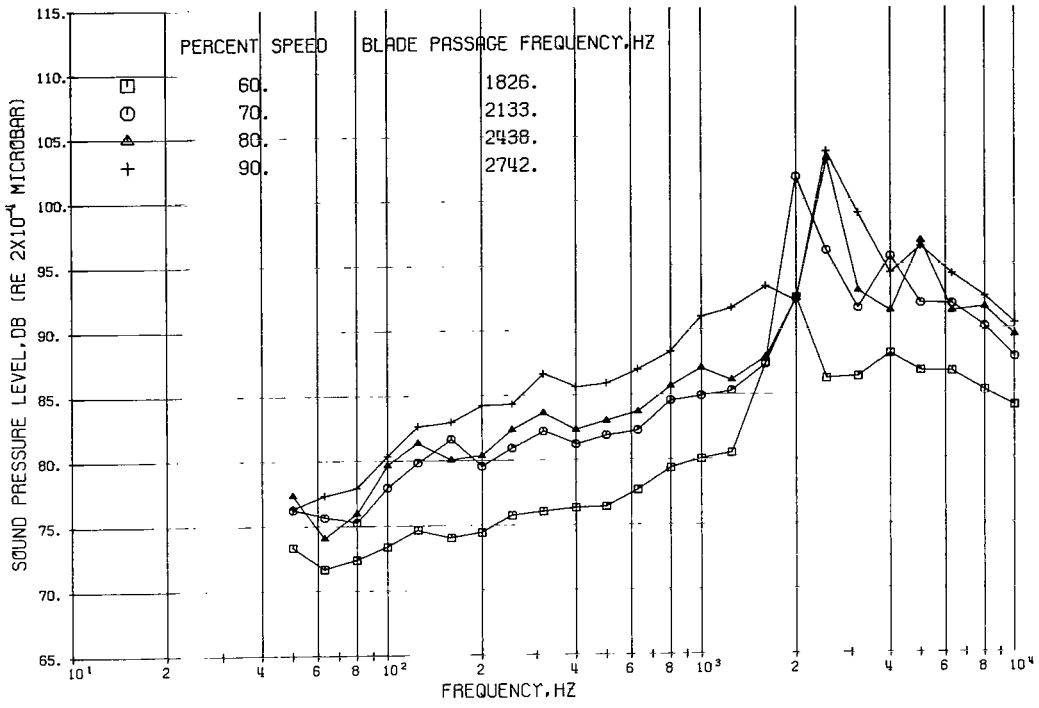

(f) Microphone location, 60°.

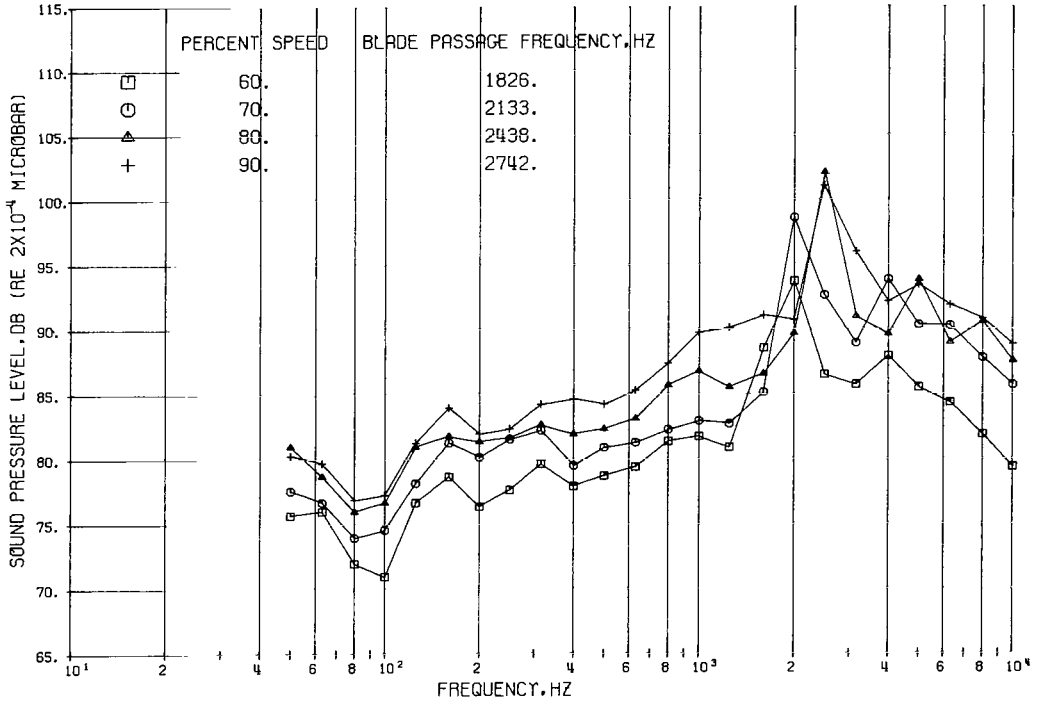

(g) Microphone location, 70°.

Figure 21. - Continued.

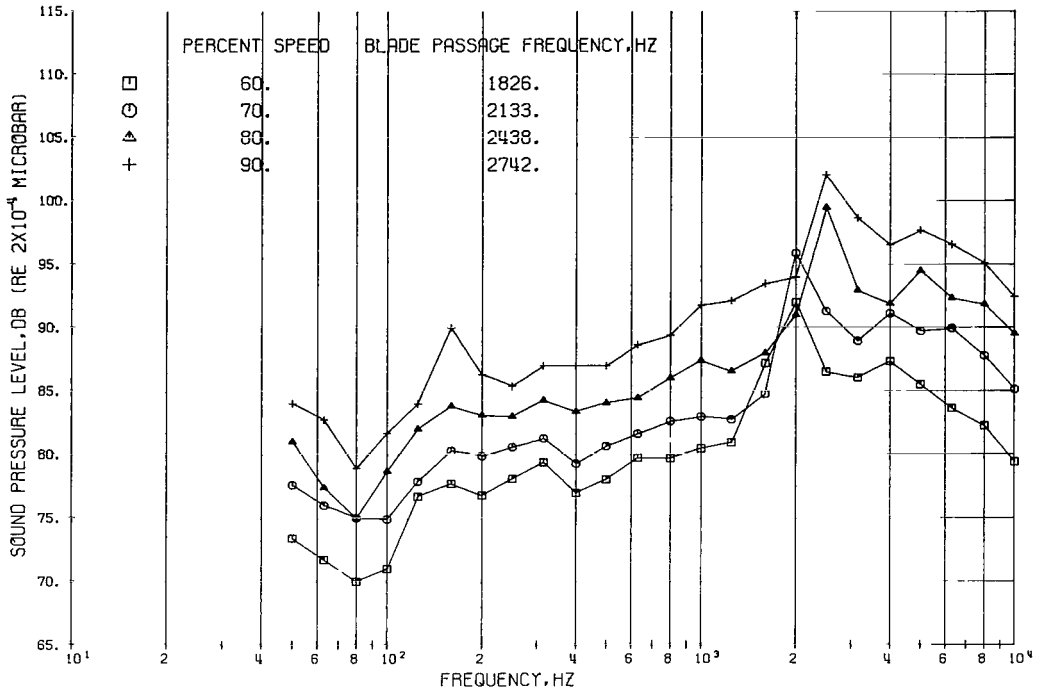

(h) Microphone location, 80°.

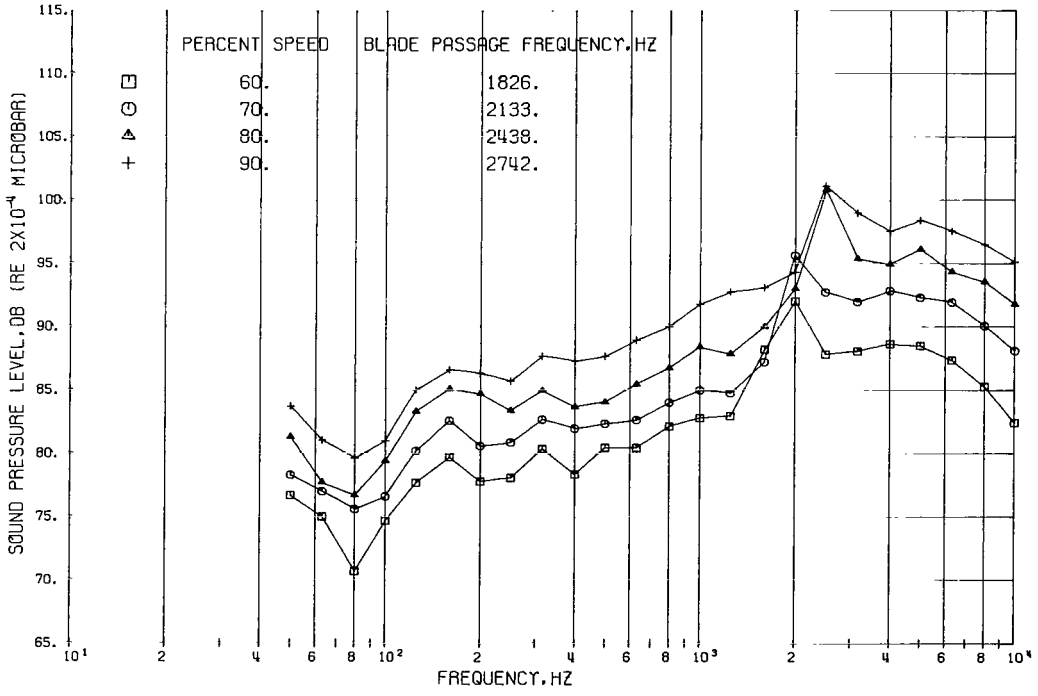

(i) Microphone location, 90°.

Figure 21. - Continued.

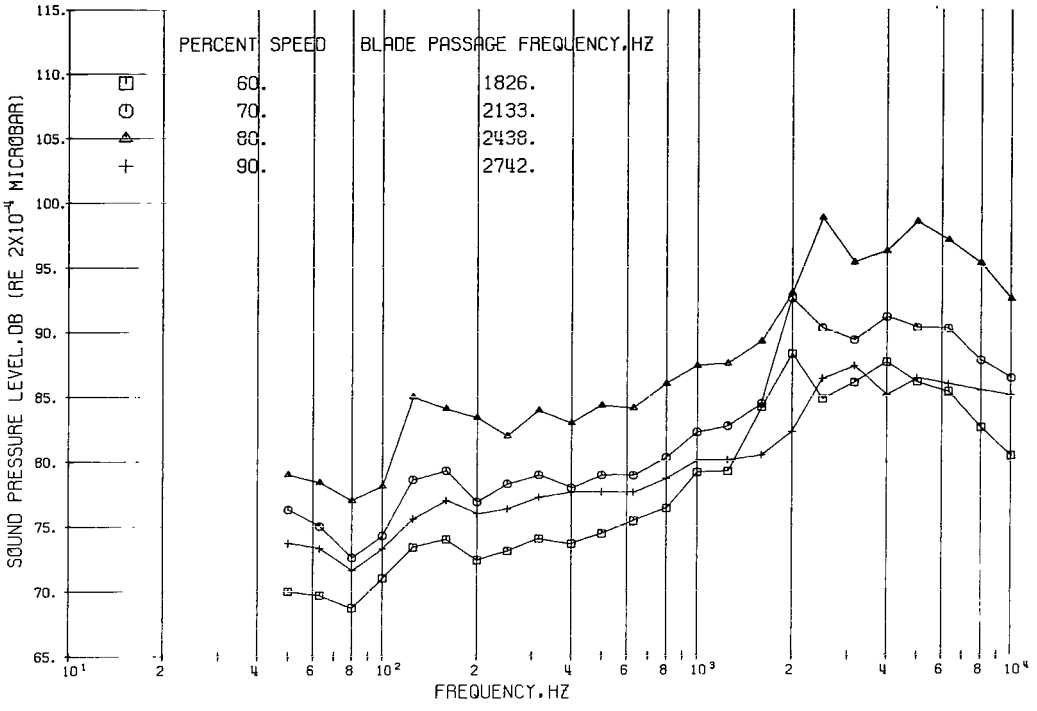

(j) Microphone location, 100°.

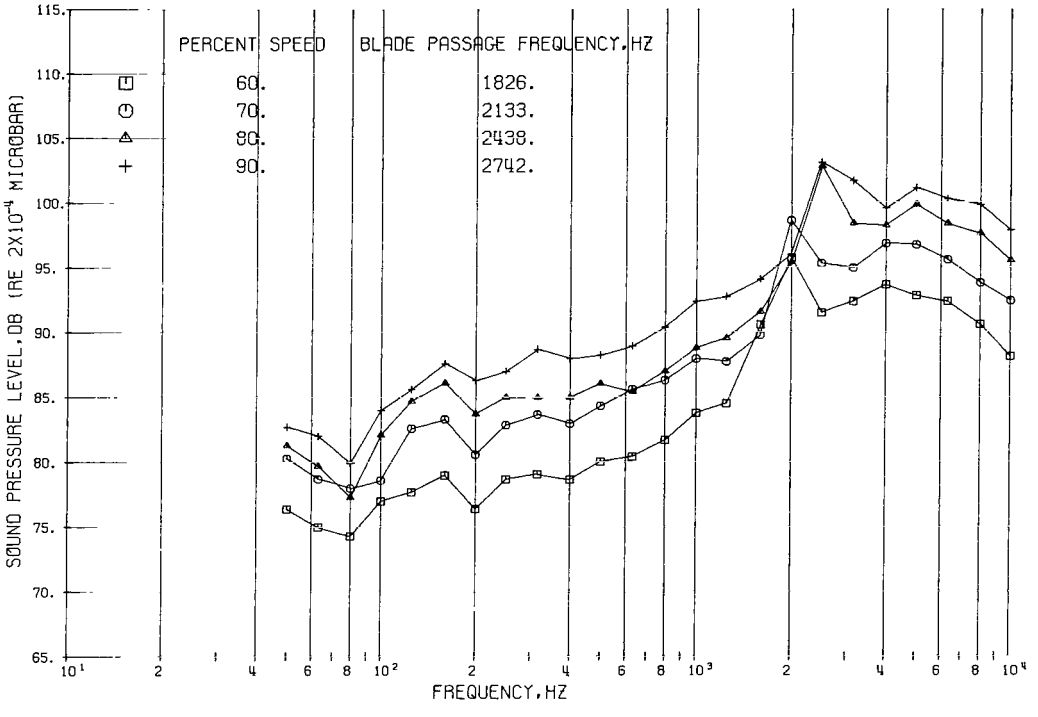

(k) Microphone location, 110°.

Figure 21. - Continued.

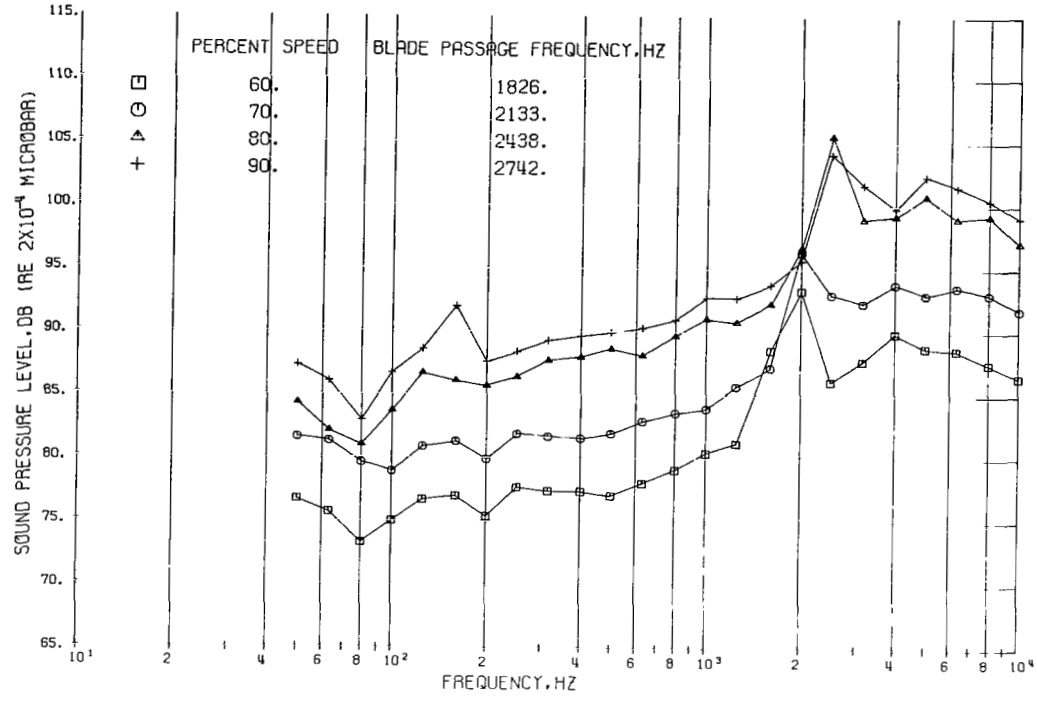

(l) Microphone location, 120°.

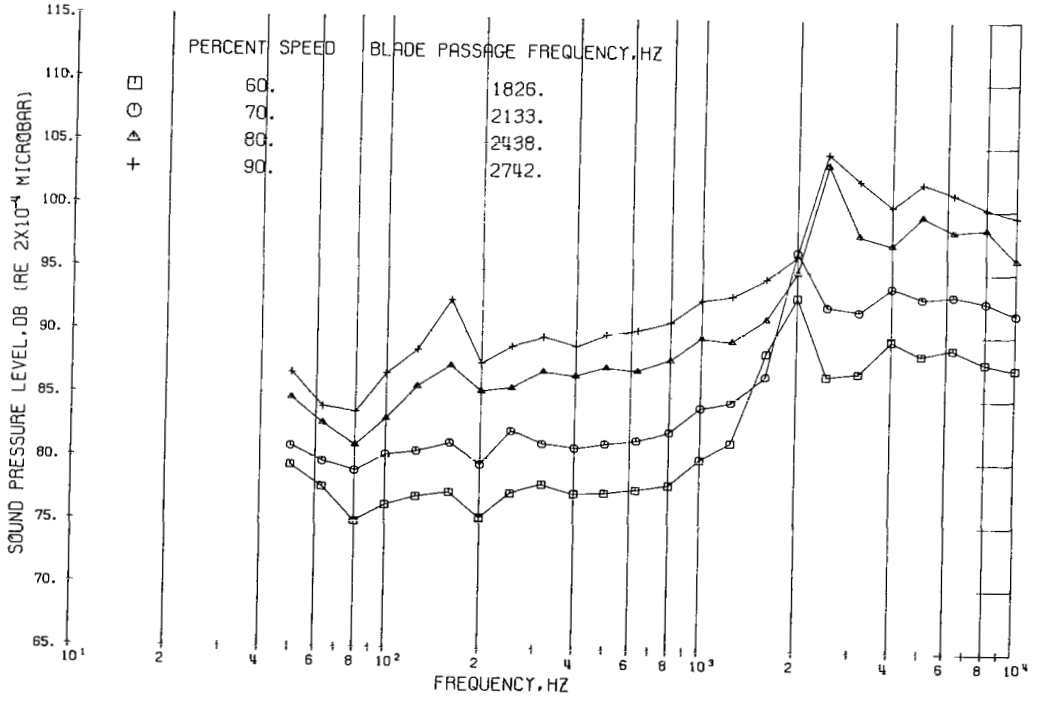

(m) Microphone location, 130°.

Figure 21. - Continued.

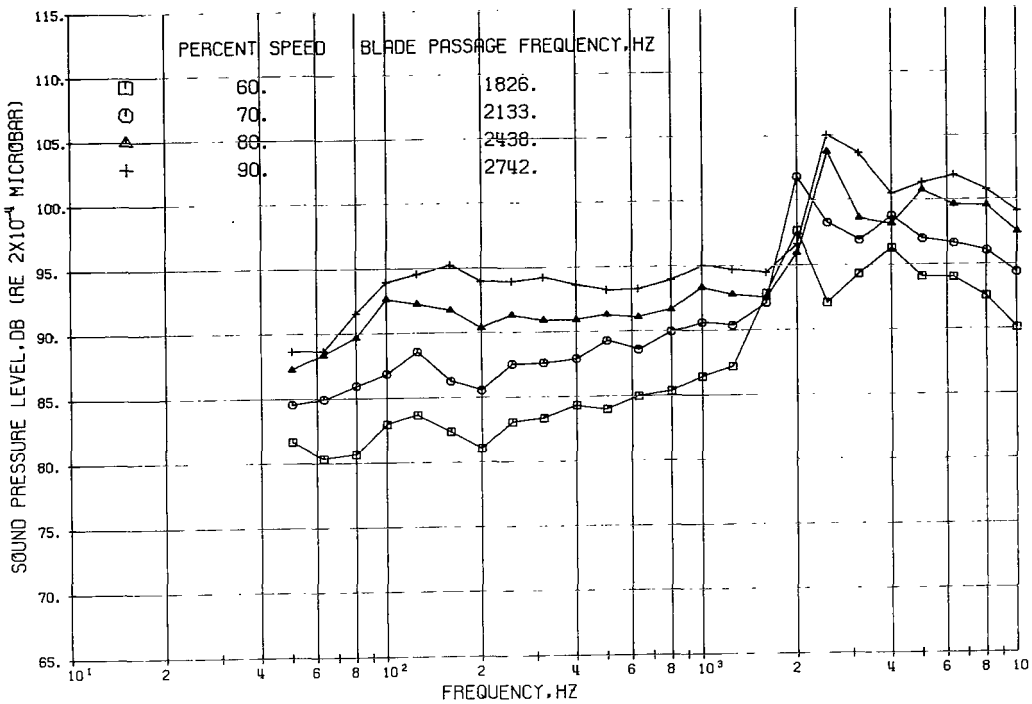

(n) Microphone location, 140°.

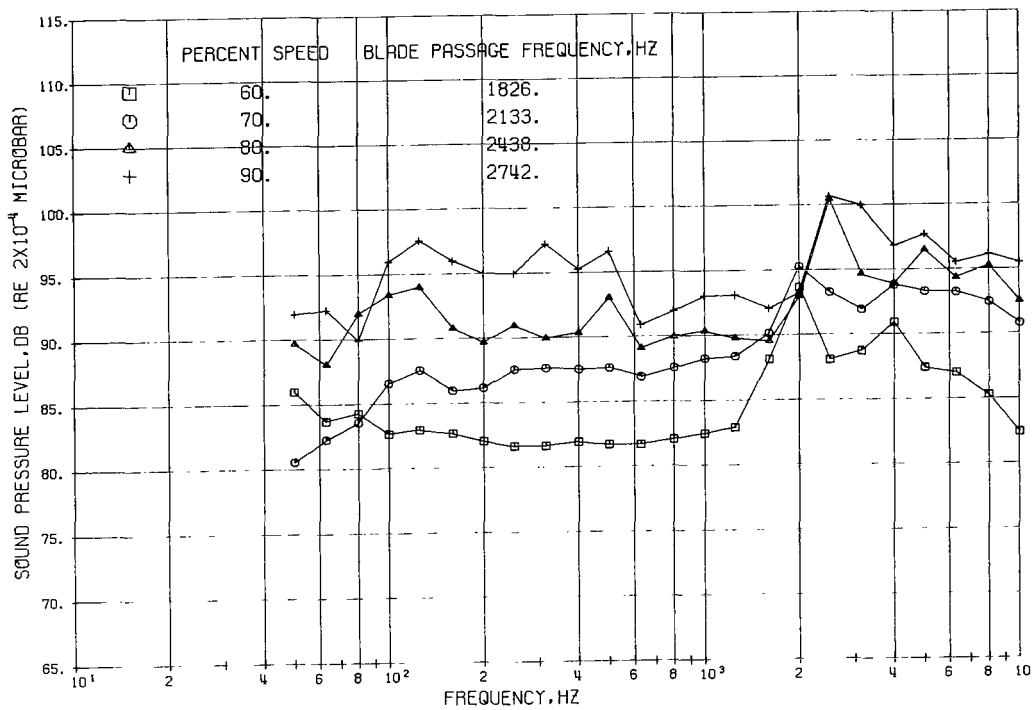

(o) Microphone location, 150°.

Figure 21. - Continued.

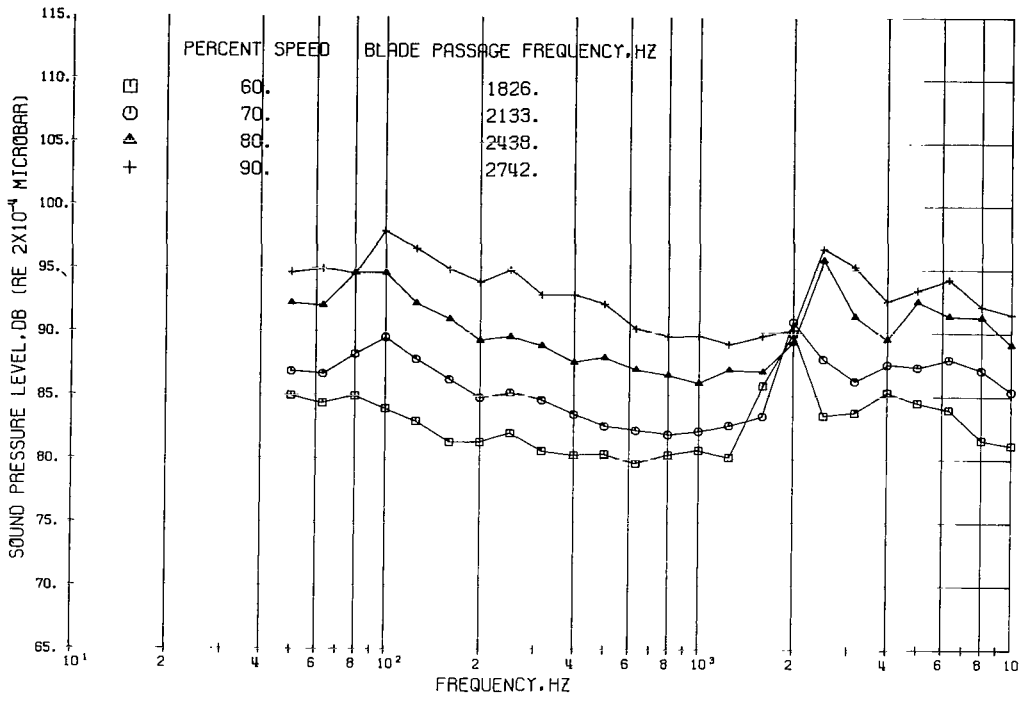

(p) Microphone location, 160°.

Figure 21. - Concluded.

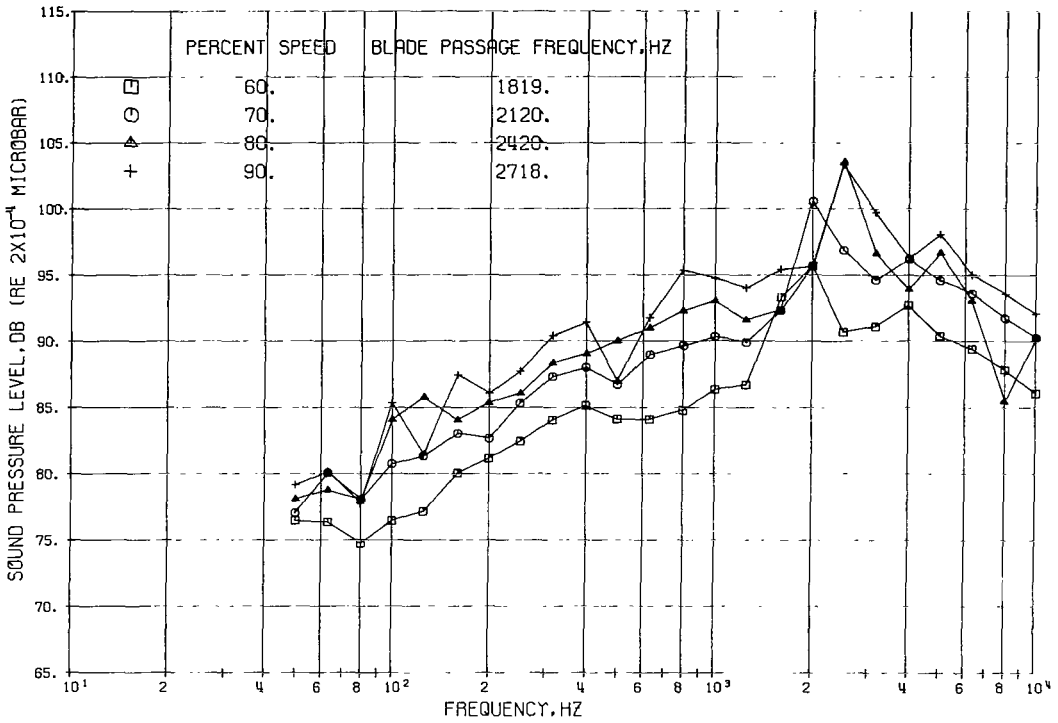

(a) Microphone location, 10°.

Figure 22. - Sound pressure levels on 100-foot (30.5-m) radius as function of frequency. Configuration 6: inlet cowl length, 127 inches (3.23 m); nozzle size, 124 percent of design area. (Microphone locations are given in degrees from shaft centerline.)

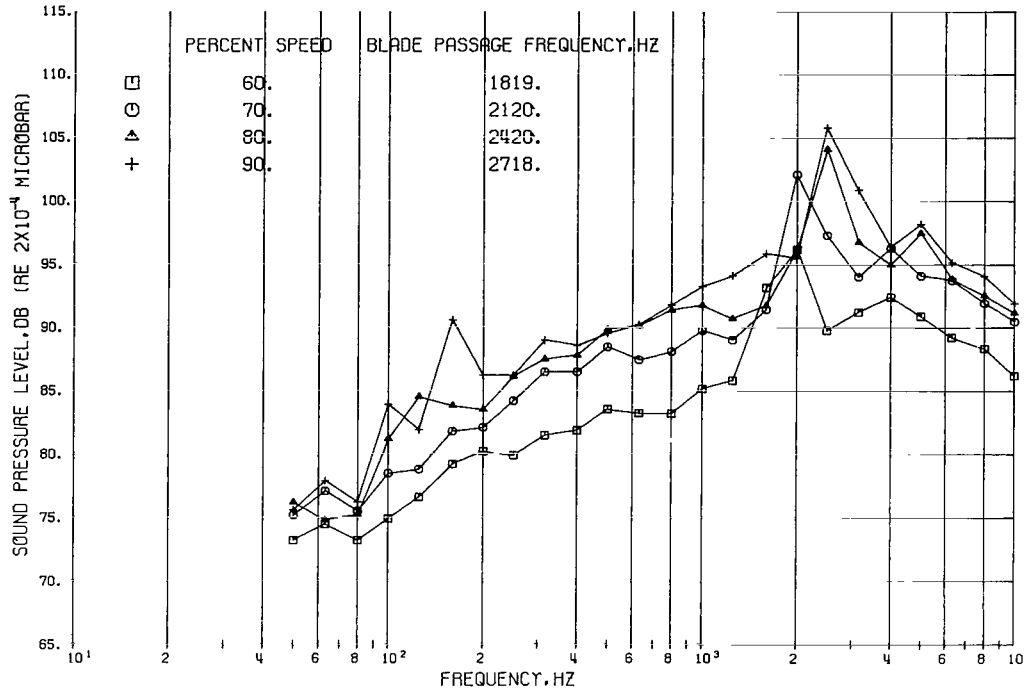

(b) Microphone location, 20°.

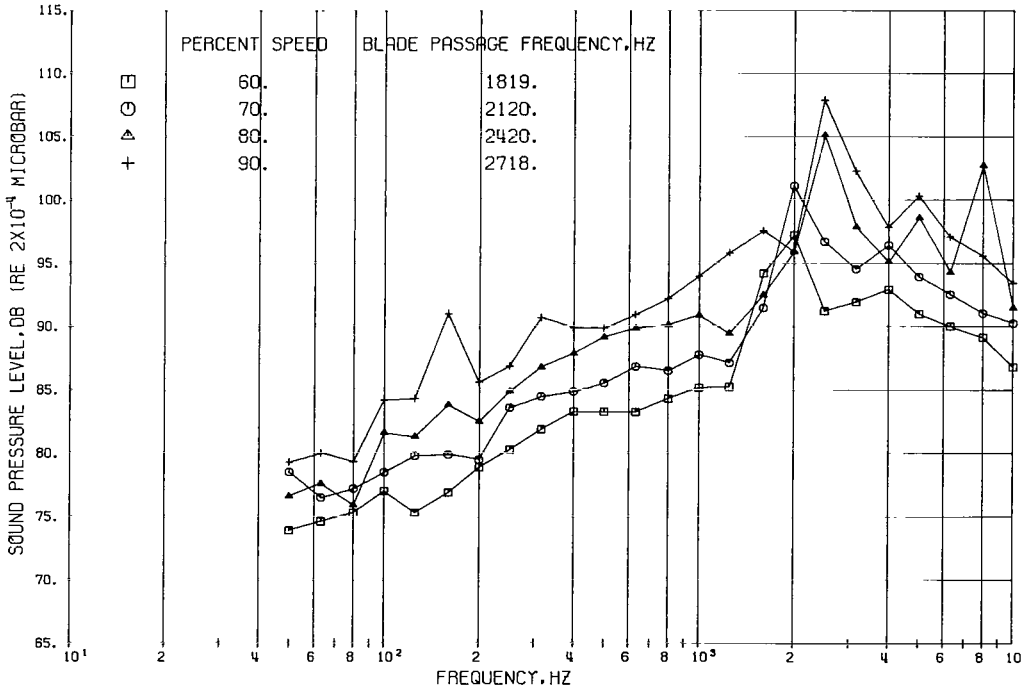

(c) Microphone location, 30°.

Figure 22. - Continued.

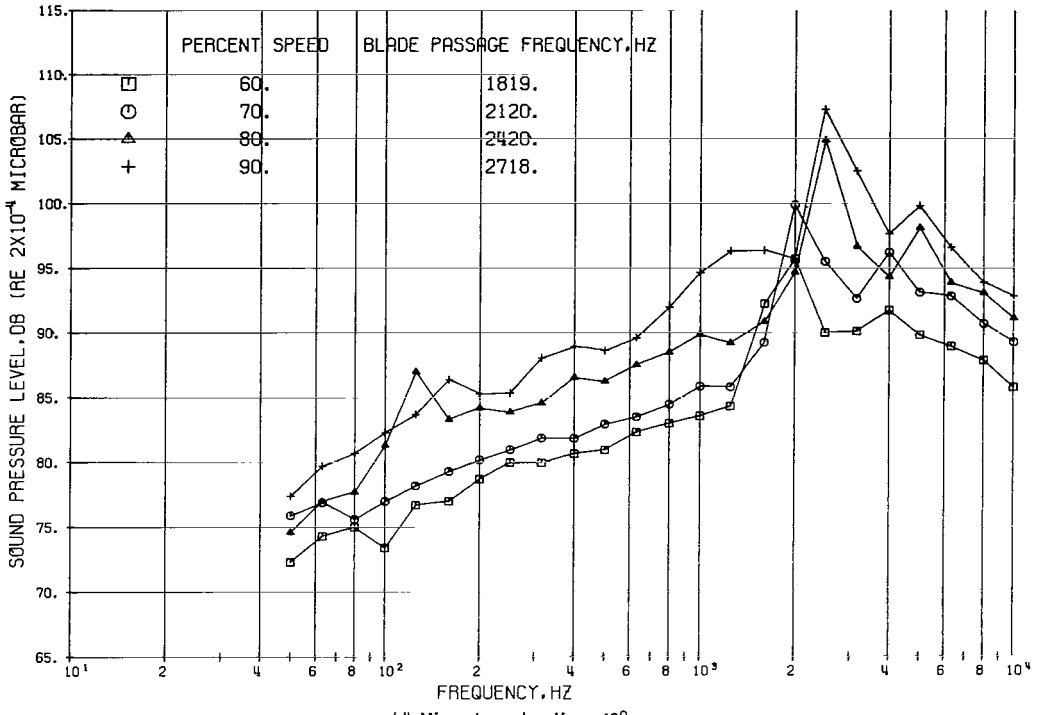

(d) Microphone location, 40°.

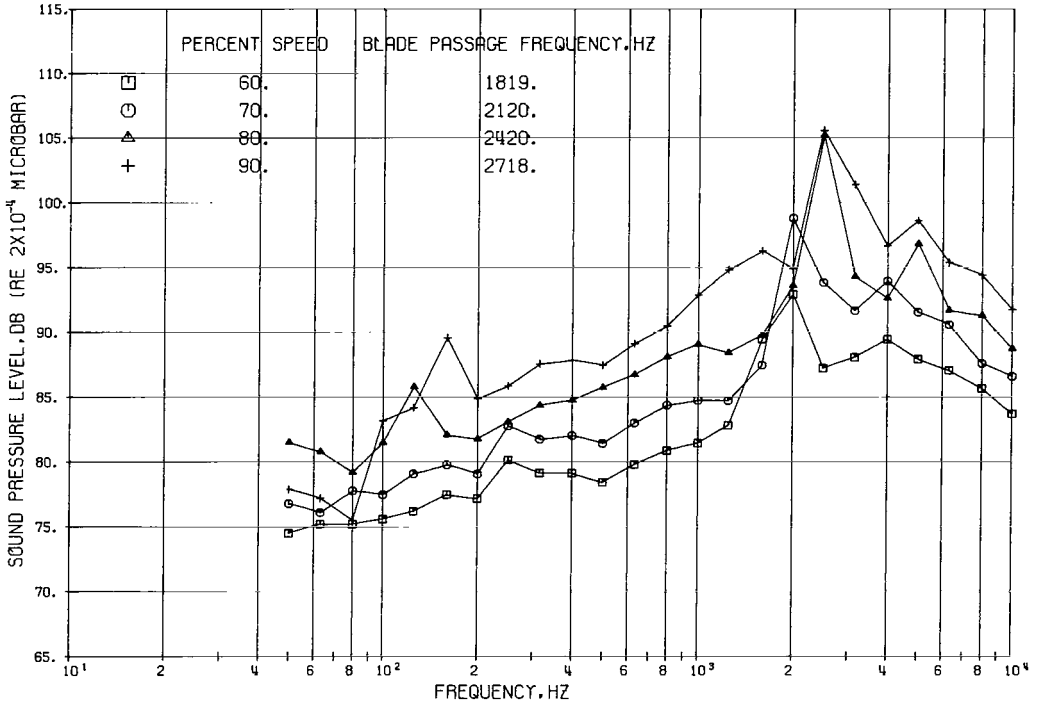

(e) Microphone location, 50°.

Figure 22. - Continued.

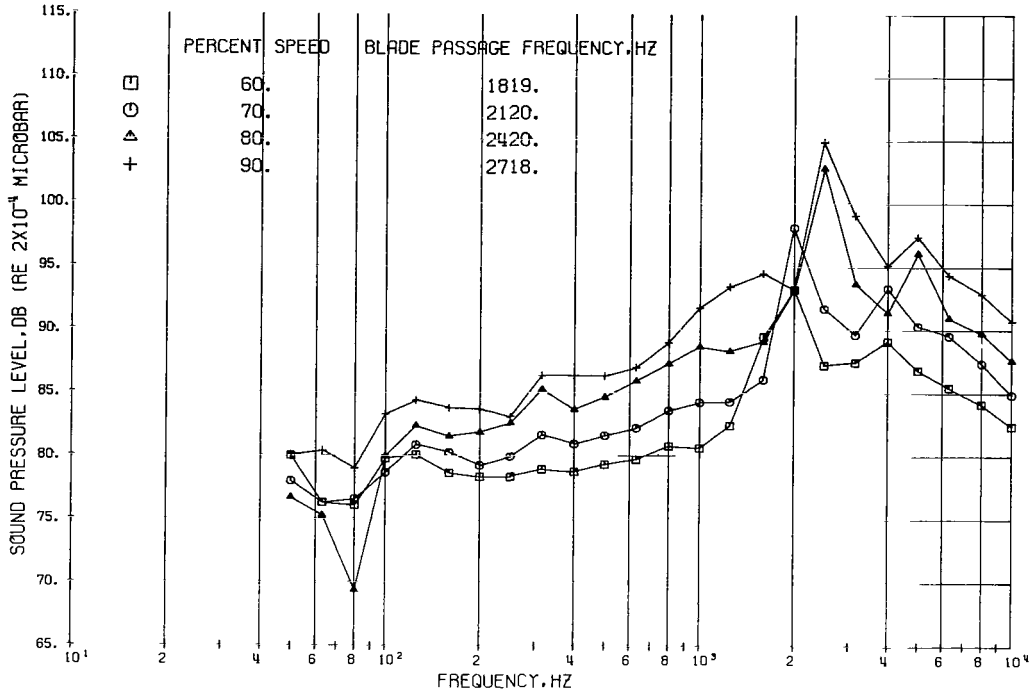

(f) Microphone location, 60°.

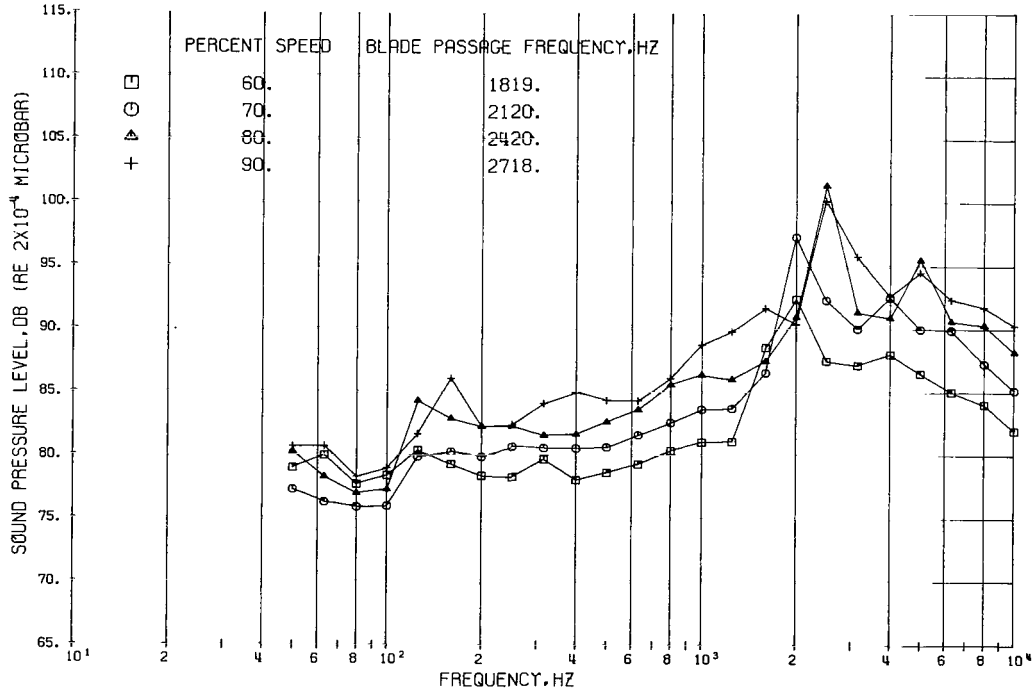

(g) Microphone location, 70°.

Figure 22. - Continued.

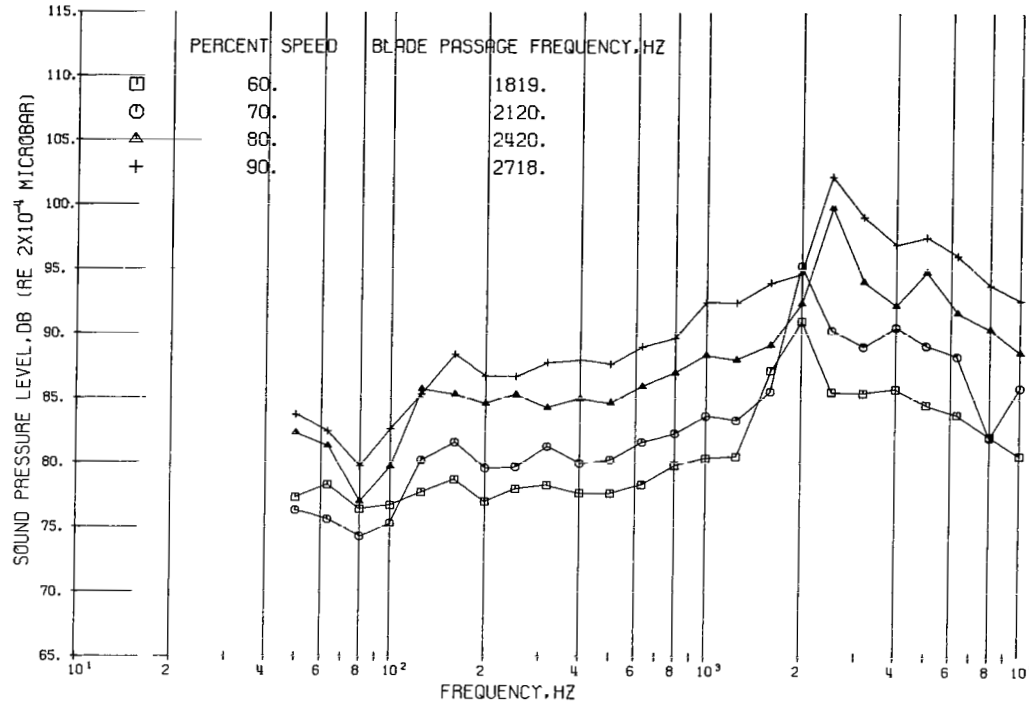

(h) Microphone location, 80°.

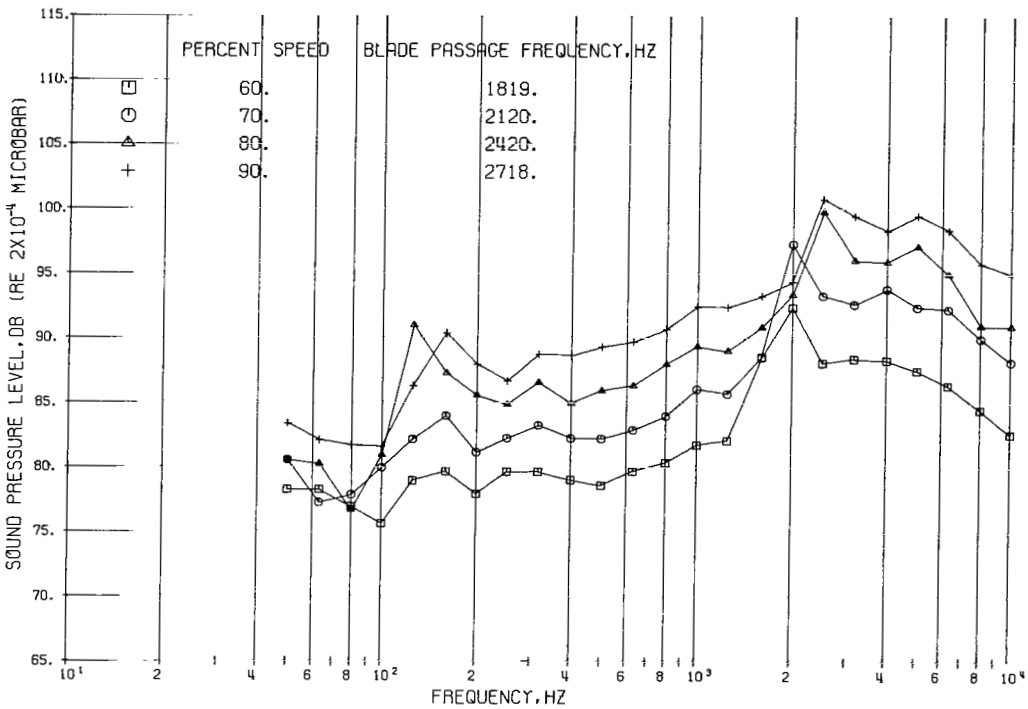

(i) Microphone location, 90°.

Figure 22. - Continued.

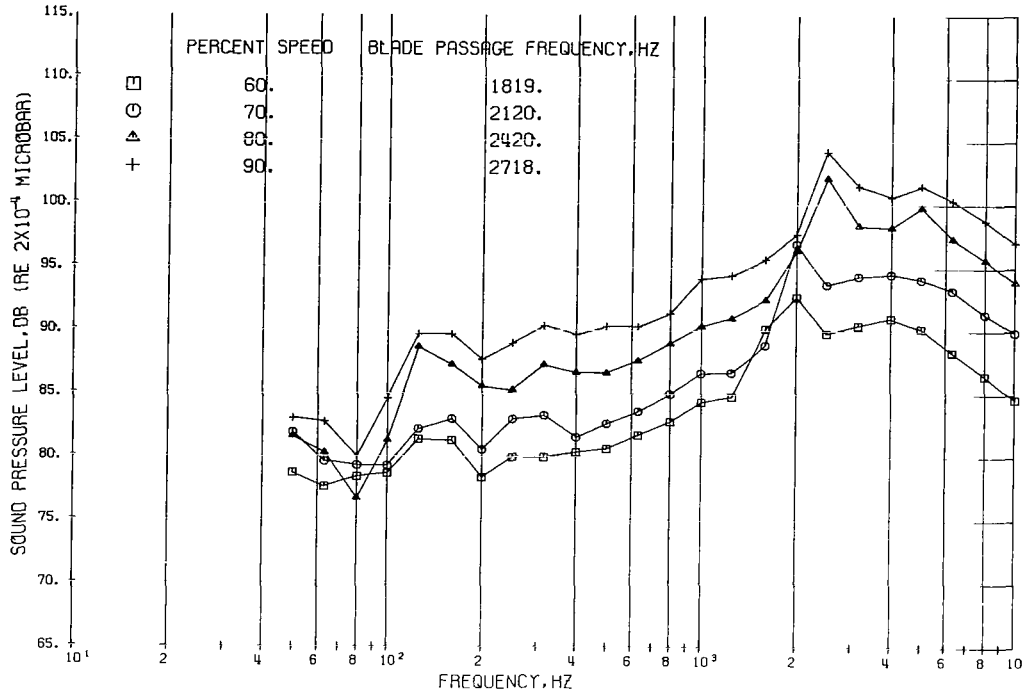

(j) Microphone location, 100°.

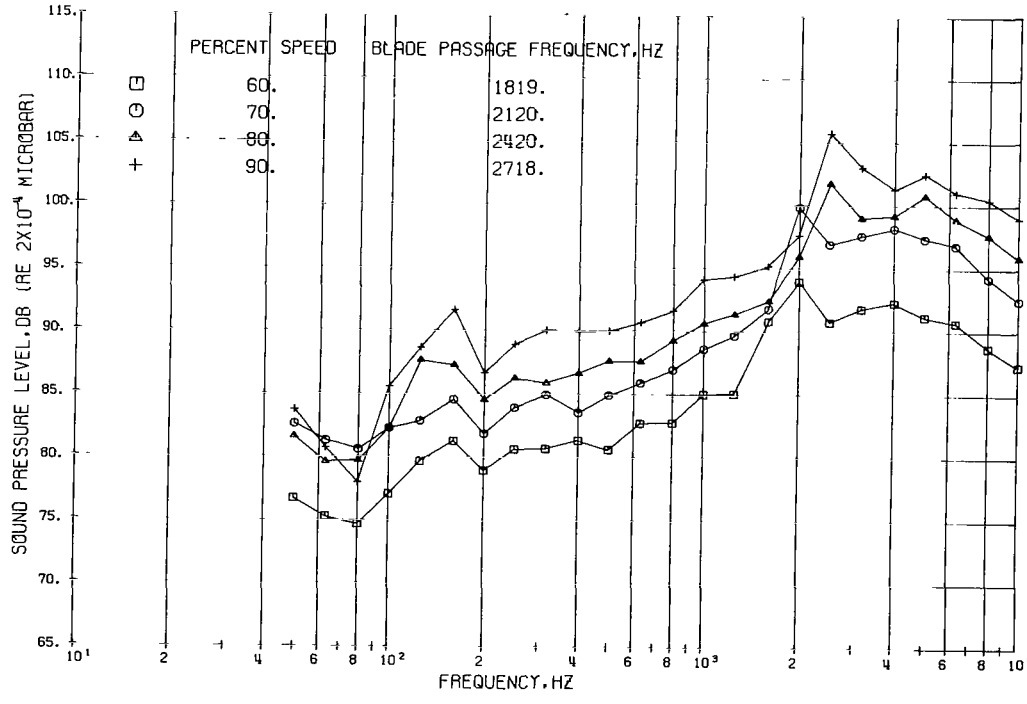

(k) Microphone location, 110°.

Figure 22. - Continued.

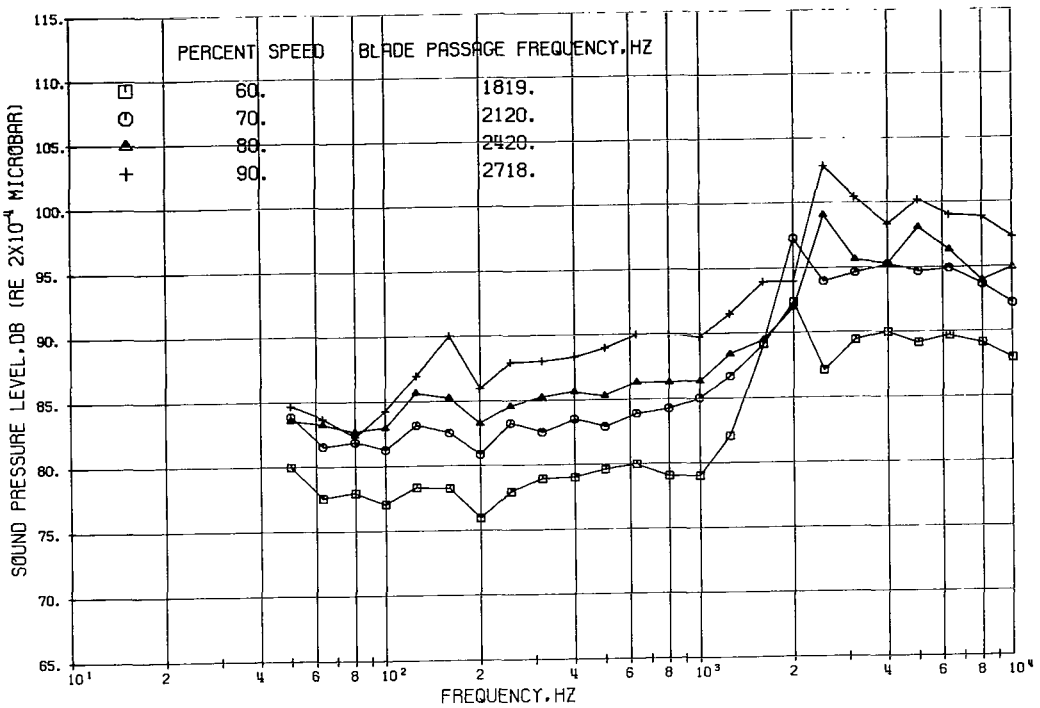

(l) Microphone location, 120°.

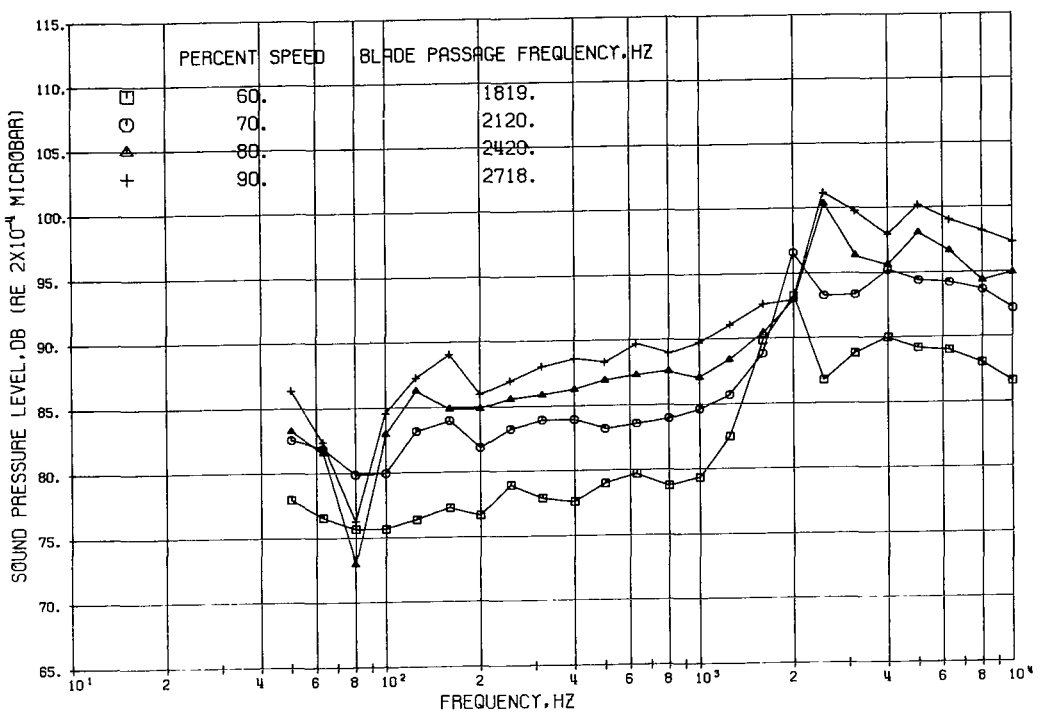

(m) Microphone location, 130°.

Figure 22. - Continued.

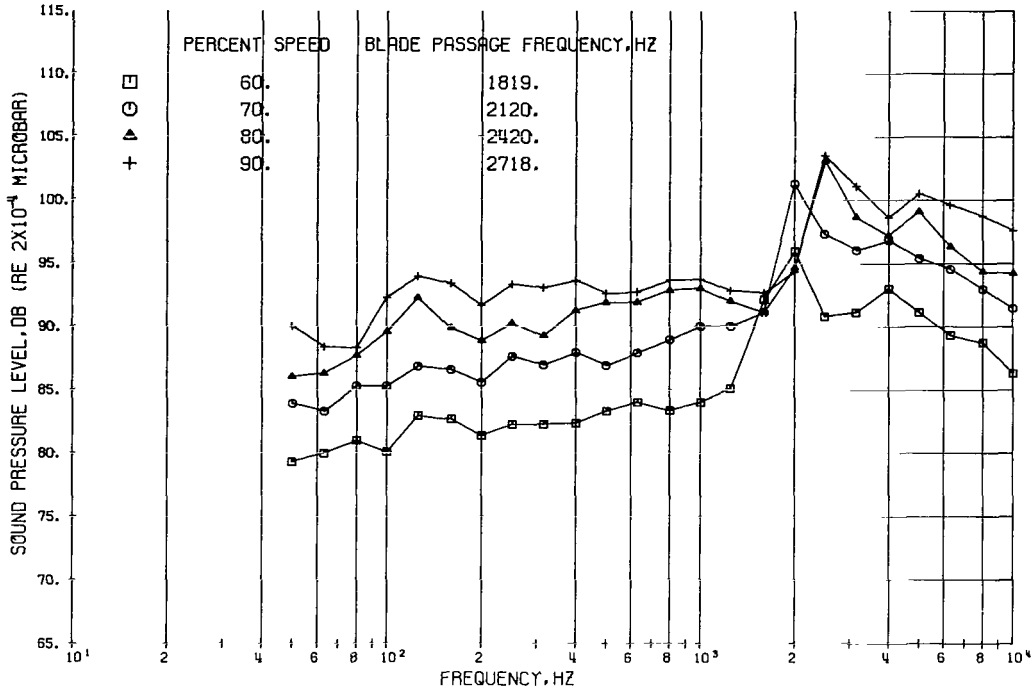

(n) Microphone location, 140°.

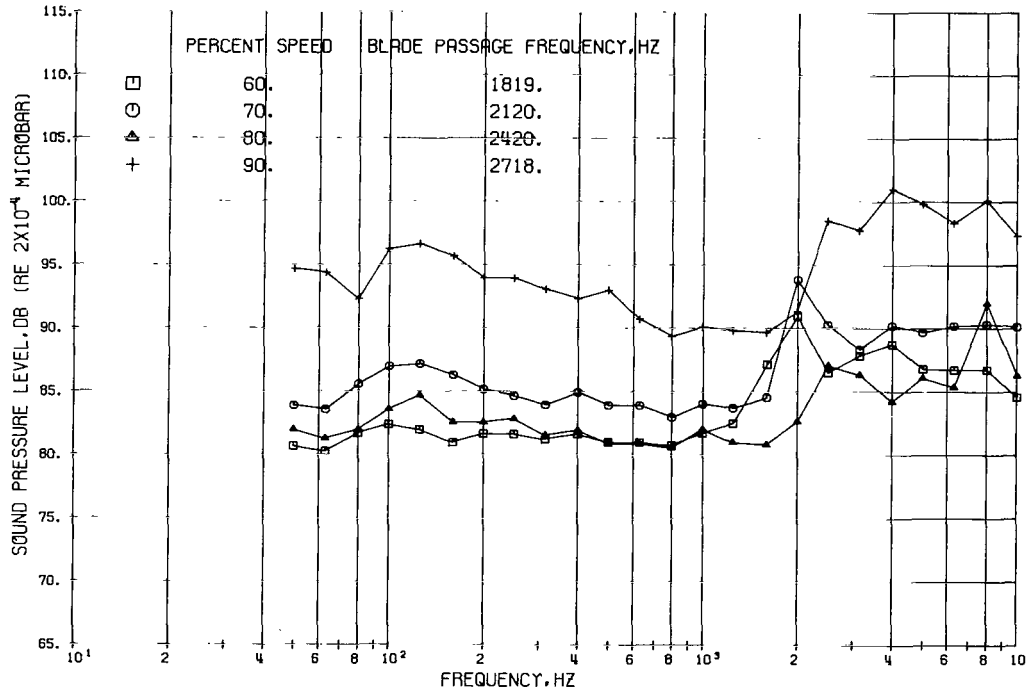

(o) Microphone location, 150°.

Figure 22. - Continued.

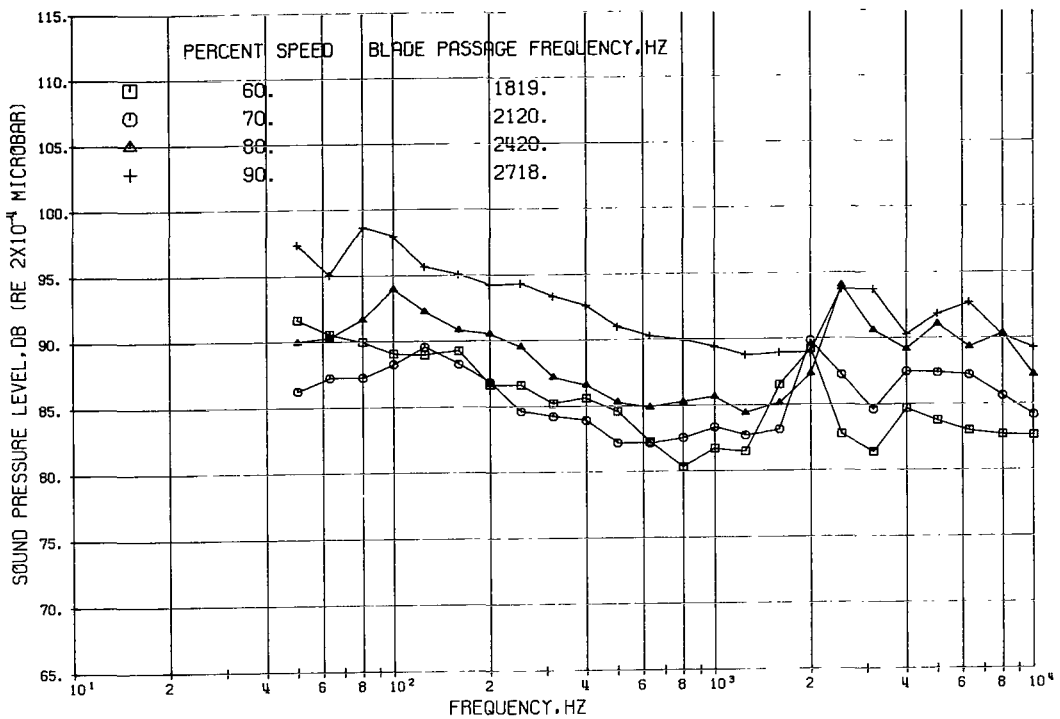

(p) Microphone location, 160°.

Figure 22. - Concluded.

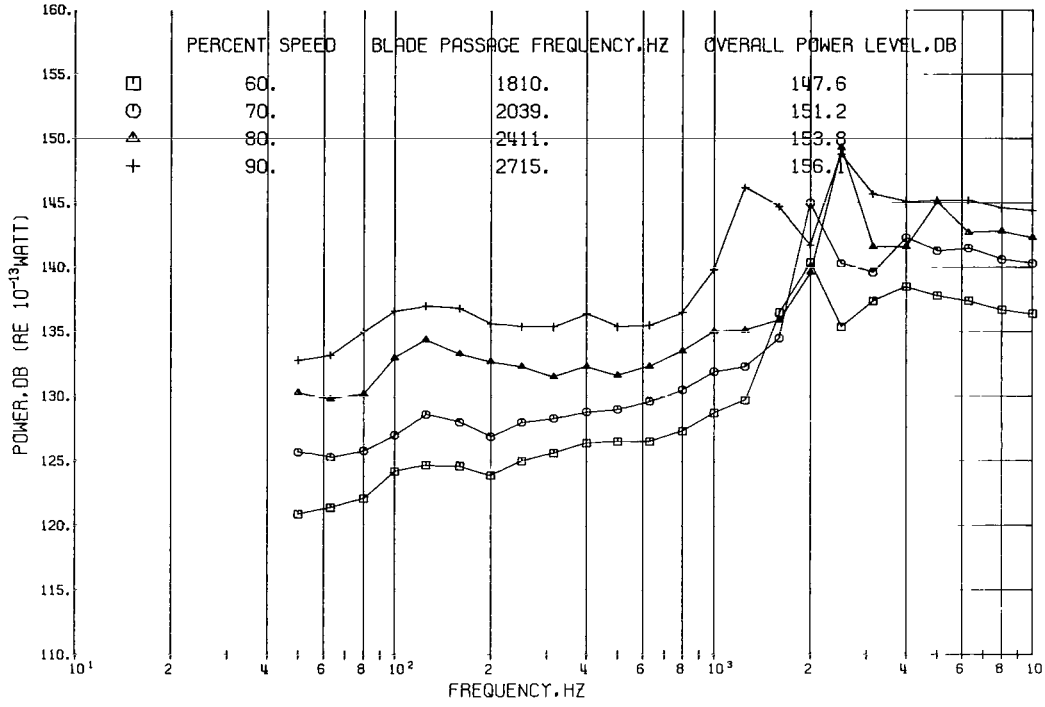

(a) Configuration 1: inlet cowl length, 86 inches (2.18 m); nozzle size, 110 percent of design area.

Figure 23. - Power spectra.

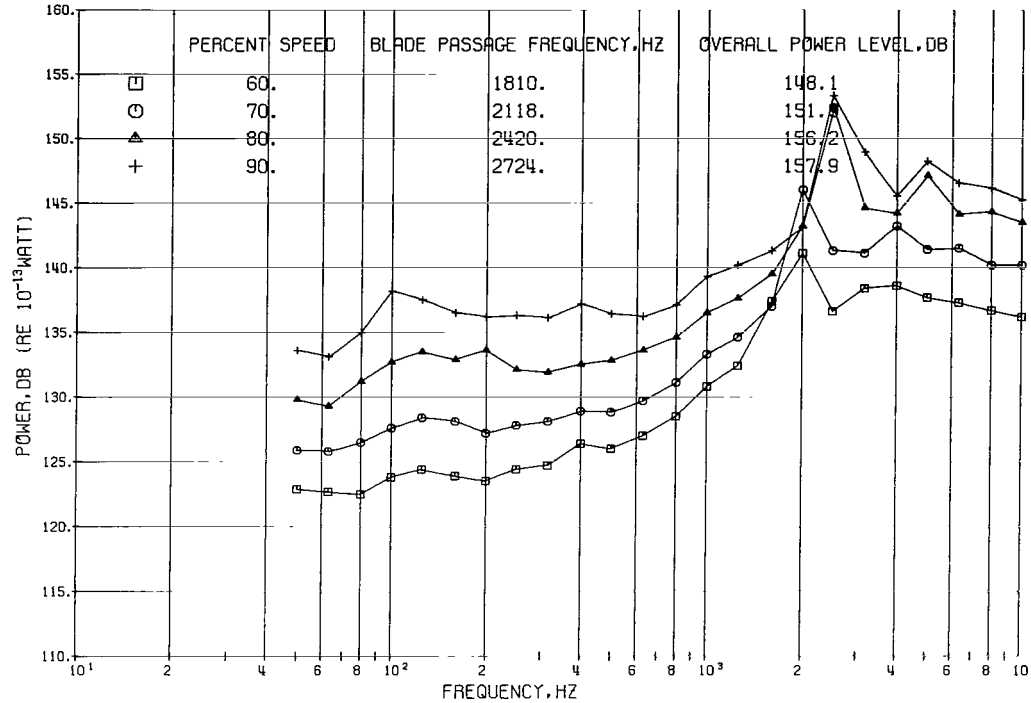

(b) Configuration 2: inlet cowl length, 86 inches (2.18 m); nozzle size, 97 percent of design area.

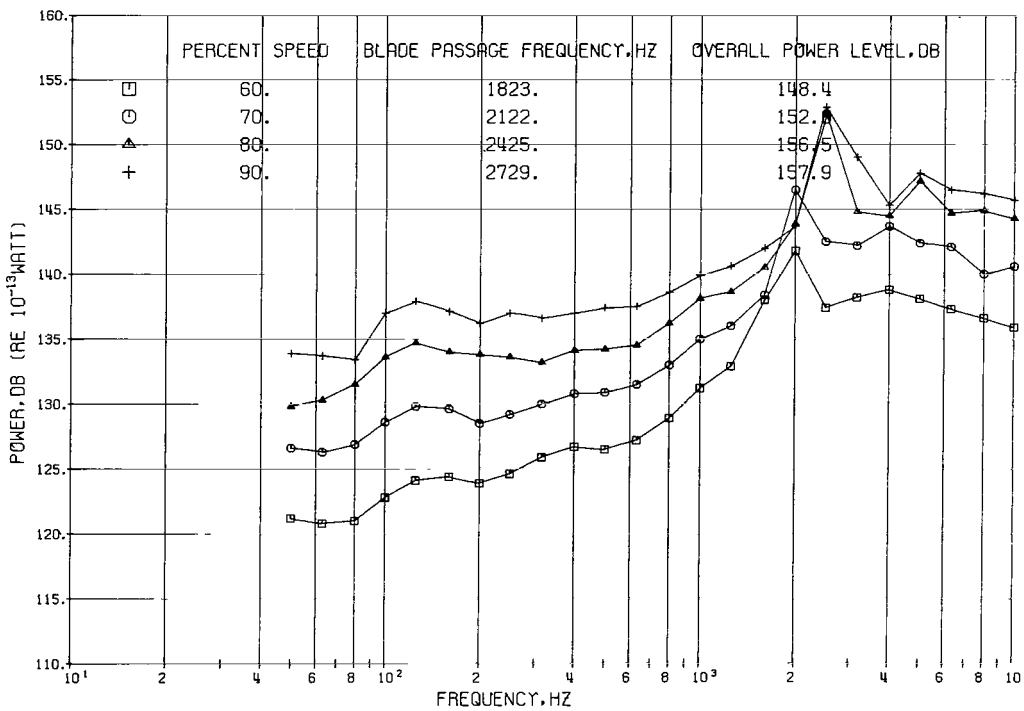

(c) Configuration 3: inlet cowl length, 127 inches (3.23 m); nozzle size, 97 percent of design area.

Figure 23. - Continued.

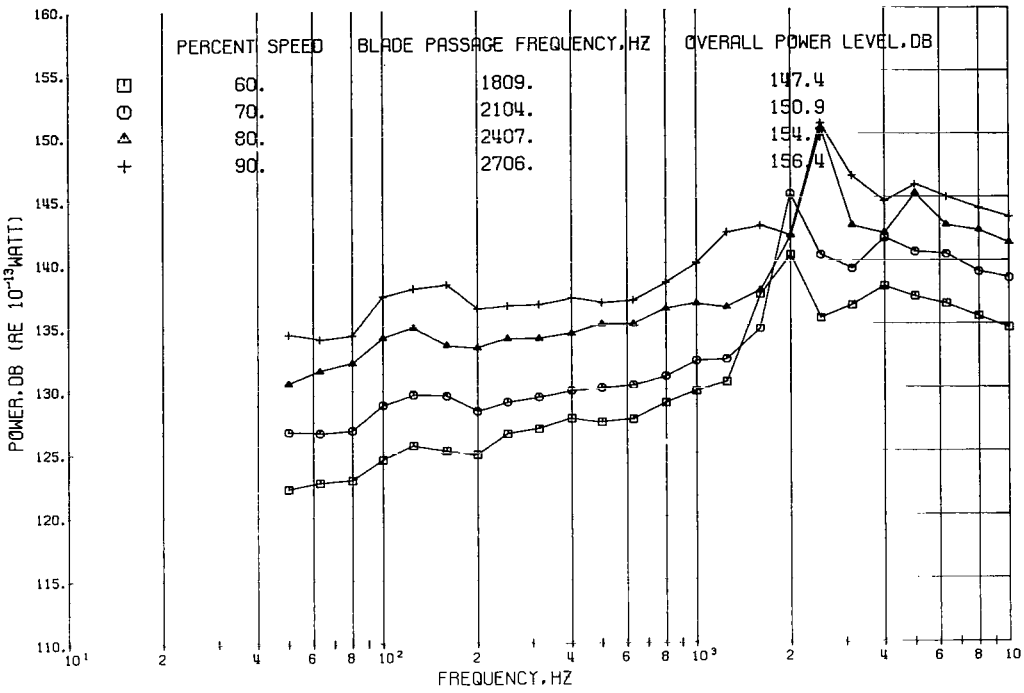

(d) Configuration 4: inlet cowl length, 127 inches (3.23 m); nozzle size, 110 percent of design area.

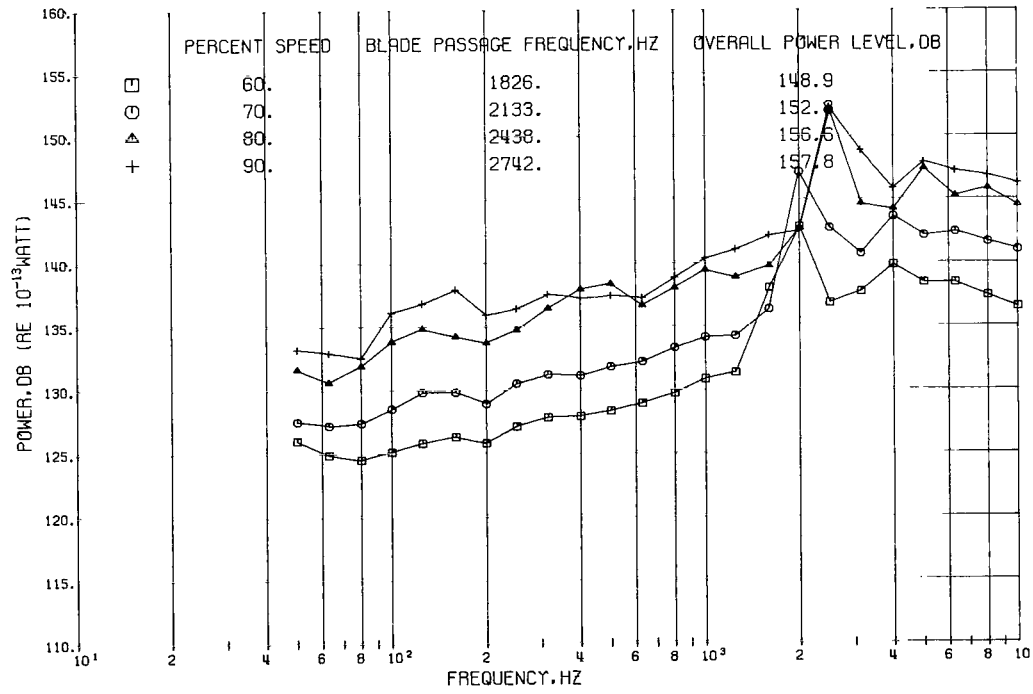

(e) Configuration 5: inlet cowl length, 86 inches (2.18 m); nozzle size, 124 percent of design.

Figure 23. - Continued.

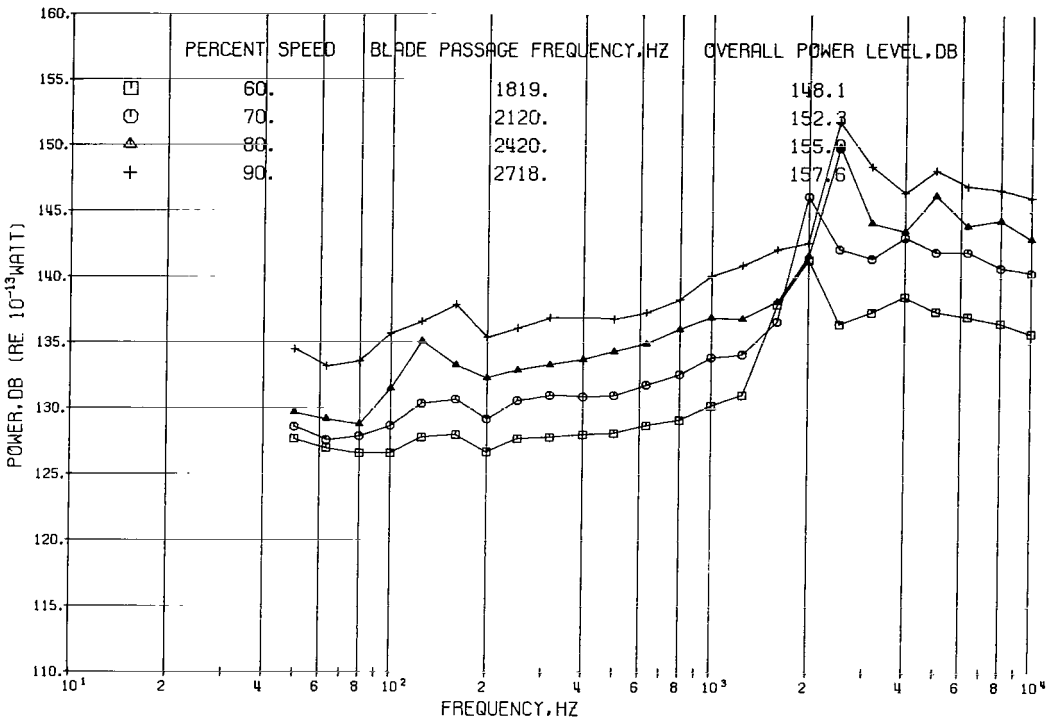

(f) Configuration 6: inlet cowl length, 127 inches (3.23 m); nozzle size, 124 percent of design.

Figure 23. - Concluded.

"The aeronautical and space activities of the United States shall be conducted so as to contribute . . . to the expansion of human knowledge of phenomena in the atmosphere and space. The Administration shall provide for the widest practicable and appropriate dissemination of information concerning its activities and the results thereof."

—NATIONAL AERONAUTICS AND SPACE ACT OF 1958

NASA SCIENTIFIC AND TECHNICAL PUBLICATIONS

TECHNICAL REPORTS: Scientific and technical information considered important, complete, and a lasting contribution to existing knowledge.

TECHNICAL NOTES: Information less broad in scope but nevertheless of importance as a contribution to existing knowledge.

TECHNICAL MEMORANDUMS: Information receiving limited distribution because of preliminary data, security classification, or other reasons.

CONTRACTOR REPORTS: Scientific and technical information generated under a NASA contract or grant and considered an important contribution to existing knowledge.

TECHNICAL TRANSLATIONS: Information published in a foreign language considered to merit NASA distribution in English.

SPECIAL PUBLICATIONS: Information derived from or of value to NASA activities. Publications include conference proceedings, monographs, data compilations, handbooks, sourcebooks, and special bibliographies.

TECHNOLOGY UTILIZATION PUBLICATIONS: Information on technology used by NASA that may be of particular interest in commercial and other non-aerospace applications. Publications include Tech Briefs, Technology Utilization Reports and Notes, and Technology Surveys.

Details on the availability of these publications may be obtained from:

SCIENTIFIC AND TECHNICAL INFORMATION DIVISION

NATIONAL AERONAUTICS AND SPACE ADMINISTRATION

Washington, D.C. 20546